REPORT DOCUMENTATION PAGE

Form Approved OMB NO. 0704-0188

1. REPORT DATE (DD-MM-YYYY)	2. REPORT TYPE	3. DATES COVERED (From - To)
25-08-2014	MS Thesis	-

4. TITLE AND SUBTITLE
Application of Weakest Link Probabilistic Framework for Fatigue Notch Factor to Aero Engine Materials

5a. CONTRACT NUMBER
W911NF-11-1-0141

5b. GRANT NUMBER

5c. PROGRAM ELEMENT NUMBER
206022

6. AUTHORS

5d. PROJECT NUMBER

5e. TASK NUMBER

5f. WORK UNIT NUMBER

7. PERFORMING ORGANIZATION NAMES AND ADDRESSES
Howard University
2400 Sixth Street N.W.

Washington, DC 20059 -1000

8. PERFORMING ORGANIZATION REPORT NUMBER

9. SPONSORING/MONITORING AGENCY NAME(S) AND ADDRESS (ES)
U.S. Army Research Office
P.O. Box 12211
Research Triangle Park, NC 27709-2211

10. SPONSOR/MONITOR'S ACRONYM(S)
ARO

11. SPONSOR/MONITOR'S REPORT NUMBER(S)
58941-EG-REP.13

12. DISTRIBUTION AVAILIBILITY STATEMENT
Approved for public release; distribution is unlimited.

13. SUPPLEMENTARY NOTES
The views, opinions and/or findings contained in this report are those of the author(s) and should not contrued as an official Department of the Army position, policy or decision, unless so designated by other documentation.

14. ABSTRACT
Nickel base super alloy and titanium alloy notched components are of utmost importance because of their application in the aero industry. Titanium alloy is used for airframe components and compressor blades application because of its high strength and fracture toughness at low temperatures and high strength and creep resistance at elevated temperature. Nickel base super alloy is used in hot sections of the gas turbine engine due to its high strength and good creep, fatigue, and corrosion resistance at high temperature. The microstructure features of these alloys are reviewed and crystal plasticity finite element modeling is presented. A new probabilistic approach based

15. SUBJECT TERMS
Probabilistic mesomechanics, titanium alloy, nickel base supperalloy, fatigue notch factor, crystal plasticity

16. SECURITY CLASSIFICATION OF:			17. LIMITATION OF ABSTRACT	15. NUMBER OF PAGES	19a. NAME OF RESPONSIBLE PERSON
a. REPORT	b. ABSTRACT	c. THIS PAGE			Gbadebo Owolabi
UU	UU	UU	UU		19b. TELEPHONE NUMBER: 202-806-6594

Report Title

Application of Weakest Link Probabilistic Framework for Fatigue Notch Factor to Aero Engine Materials

ABSTRACT

Nickel base super alloy and titanium alloy notched components are of utmost importance because of their application in the aero industry. Titanium alloy is used for airframe components and compressor blades application because of its high strength and fracture toughness at low temperatures and high strength and creep resistance at elevated temperature. Nickel base super alloy is used in hot sections of the gas turbine engine due to its high strength and good creep, fatigue, and corrosion resistance at high temperature. The microstructure features of these alloys are reviewed and crystal plasticity finite element modeling is presented. A new probabilistic approach based on weakest-link theory which captures both the essence of microstructure and the notch root stress gradient is described and applied to nickel base superalloy and titanium alloys to determine their microstructure sensitive fatigue notch factor and notch sensitivity index at varying notch root radii. The effects of the position and the orientations of inclusion on the fatigue notch factor of nickel base super alloy is also investigated. The fatigue notch factors obtained are in direct correlation with the experimentally obtained value for the different notch root radii.

HOWARD UNIVERSITY

Application of Weakest Link Probabilistic Framework for Fatigue Notch Factor to Aero Engine Materials

A Thesis
Submitted to the Faculty of the
Graduate School

of

HOWARD UNIVERSITY

in partial fulfillment of
the requirement for the
degree of

Master of Engineering

Department of Mechanical Engineering

by

Oluwamayowa Ayobami Okeyoyin

Washington, D.C.
December 2013.

HOWARD UNIVERISTY
GRADUATE SCHOOL

DEPARTMENT OF MECHANICAL ENGINEERING

THESIS COMMITTEE

_____

Mohsen Mosleh, Ph.D.
Chairperson

_____

Gbadebo M. Owolabi, Ph.D.

_____

Horace A. Whitworth, D.Sc.

_____

Gbadebo M. Owolabi, Ph.D.

Thesis Advisor

Candidate: Oluwamayowa A. Okeyoyin

Date of Defense: November 13, 2013

DEDICATION

I dedicate this work to my parents (Mrs Folasade Okeyoyin and HRH Jacob Okeyoyin), my siblings (Riike, Tosin and Tunrayo) and my uncles (Mr Dapo Oladeji and Dr George Okeyoyin) for their love and support during this work. I also dedicate this thesis to almighty God for His favor, mercy, grace and strength bestowed upon me for the successful completion of this work.

ACKNOWLEDGEMENTS

It is a great honor and privilege to work under the supervision of Dr. Gbadebo Moses Owolabi. I would like to thank him for the several selfless hours he has committed to make this work a successful one. Also, his guidance and encouragement throughout the completion of this work are greatly appreciated. I have greatly benefited from his helpful and insightful comments all through. I would also like to thank the other committee members, Dr. Mohsen Mosleh and Dr. Horace Whitworth for their time and patience in conducting a thorough review of this thesis. I will also like to extend my appreciation to the department's secretary Mrs. Eliza Gibson for her unwavering support and assistance on administrative challenges. I also express my profound gratitude to the Department of Defense for the financial support provided through research and educational program for the HBCU/MSI (contract # W911NF-11-1-041, Dr. Larry Russell and Dr. David Stargel, program Managers ARO and AFOSR respectively).

I owe my appreciation to my friends Odoh Daniel, Benedict Egboiyi, Olalekan Adewuyi, Alex Peterson, Aina Johnson, Efe Steve, and Ayotunde Igbalajobi who made my stay at Howard a memorable one and for their moral support from time to time. I would like to thank the Director of Computer Learning and Design Center, CLDC, (Dr. Sonya Smith) and Staffs (Ravindranath Jaglal and Ainsley Gibson) for support provided on ABAQUS installation and maintenance. I owe a big appreciation to Dr. Jiang (Leo) Li for his assistance with modification of some of the computer codes used during this work. Lastly, I would like to thank my parents, siblings and relatives for their patience, understanding and encouragement during my studies.

ABSTRACT

Nickel base super alloy and titanium alloy notched components are of utmost importance because of their application in the aero industry. Titanium alloy is used for airframe components and compressor blades application because of its high strength and fracture toughness at low temperatures and high strength and creep resistance at elevated temperature. Nickel base super alloy is used in hot sections of the gas turbine engine due to its high strength and good creep, fatigue, and corrosion resistance at high temperature. The microstructure features of these alloys are reviewed and crystal plasticity finite element modeling is presented. A new probabilistic approach based on weakest-link theory which captures both the essence of microstructure and the notch root stress gradient is described and applied to nickel base superalloy and titanium alloys to determine their microstructure sensitive fatigue notch factor and notch sensitivity index at varying notch root radii. The effects of the position and the orientations of inclusion on the fatigue notch factor of nickel base super alloy is also investigated. The fatigue notch factors obtained are in direct correlation with the experimentally obtained value for the different notch root radii.

TABLE OF CONTENTS

LIST OF TABLES

LIST OF FIGURES

CHAPTER 1

INTRODUCTION

1.1 Background

One of the pioneer researchers to address the topic of fatigue was WhÖler, who in 1870 gave a general law expressed as follows: “Rupture may be caused, not only by a steady load which exceeds the carrying strength but also by repeated application of stresses, none of which are equal to this carrying strength. The differences of these stresses are measures of the disturbance of the continuity, in so far as by their increase the minimum stress which is still necessary for rupture diminishes [1].”

Many engineering components and structures operate under fluctuating or cyclic loads. These loading conditions induce cyclic stresses that lead to fatigue failure. There are two major domains of cyclic stresses: low-cycle fatigue (LCF) and high-cycle fatigue (HCF). Different attempts have been made to distinguish between LCF and HCF. Cyclic plasticity and strain control conditions characterize LCF while HCF is associated with purely elastic behavior and it generally involves load control conditions [1]. In general, HCF is characterized by low amplitudes, high frequencies, large number of cycles and nominally elastic cyclic behavior.

Fatigue failure is progressive in nature and it involves the initiation and propagation of cracks. In HCF, a large fraction of life is required to produce inspectable size cracks while a small fraction of life is left for propagation to failure due to its high frequency and low stress amplitudes. Once the cracks attain a critical dimension, sudden

failure results from additional loading cycle. This phenomenon makes the early discovery and prediction of HCF related failure a cumbersome endeavor.

Numerous failures relating to fatigue have been recorded in the past; typical examples of the failures are presented in Table 1.1. One significant failure worth mentioning of the listed failures is the United Airlines DC 10 Flight No 232 which crashed at Sioux City, Iowa with 112 fatalities in the year 1989 (Figure 1.1). According to the investigation conducted by the National Transportation Safety Board, the cause of failure was attributed to the fatigue crack which originated from an undetected metallurgical defect located in a significant area of the aircraft engine [2].

Table 1.1 Historic fatigue failures [3]

Failure	Year	Reason for Failure
Comet aircraft failures	1950s	Fatigue crack initiation in pressurized skins due to high gross stresses and stress concentration effects from geometric features.
F-111 Aircraft No. 94 wing pivot fitting	1969	Fatigue failure due to material defect in high-strength steel.
Aloha Incident, Boeing 737	1988	Accelerated corrosion and multiple fatigue crack-initiation sites in riveted fuselage skin.
Sioux City incident	1989	Hard alpha case present in titanium fan disk resulted in fatigue crack initiation and catastrophic failure.

Fatigue failure is mostly dangerous as it occurs over time and at stress levels not only lower than the ultimate tensile strength but also the yield strength of the material.

Figure 1.1. United Airlines DC-10 Sioux City Incident **[4]**.

Most engineering components have structural discontinuities and imperfections. Discontinuities can be in the form of keyways, weld fillets, holes for bolts, and rivets. Other forms of discontinuities are caused by the ingestion of foreign objects during operation causing foreign object damage. Imperfections can be in the form of voids or inclusion of impurities during metal forming. These discontinuities and inclusions serve as stress concentration zones or stress raisers as they tend to change the stress field distribution in the region; the local stress in the vicinity of the discontinuities is usually higher than the net section stress in the component. This effect is quantified in linear

elastic material using the stress concentration factor, k_t which is the ratio of the maximum local stress at the notch root to the remotely applied stress. The regions of stress concentration are perfect sites for crack initiation for components under cyclic loading. These discontinuities are usually modeled as notches with a certain depth and notch root radius to investigate their effects on the fatigue life of components subjected to cyclic loading [5, 6]. The resulting notch effect is characterized using a fatigue strength reduction factor also known as fatigue notch factor, k_f. A good relationship has been determined for k_t and k_f which is called the fatigue notch sensitivity index, q, and is used to indicate materials sensitivity to notches. The value of q ranges from zero to one; zero indicates no notch sensitivity while one indicates full notch sensitivity.

1.2 Research Motivation and Objectives

Nickel base superalloy and titanium alloy find applications in aero engine components because of their unique properties and are thus referred to as aero engine materials. Titanium alloy Ti-6Al-4V offers a range of properties such as high strength and fracture toughness at low temperatures to high strength and creep resistance at elevated temperature. Thus, they are widely used in engineering applications from airframe components and fans to compressor blades of jet engines. Nickel based super alloy IN 100 is widely used in the hot sections of the gas turbine engine due to its superior strength, high creep and corrosion resistance at high temperatures [7]. A cross-section of a jet engine (PW2037) showing different components of the aircraft engine and the alloys used in making them is shown in Figure 1.2.

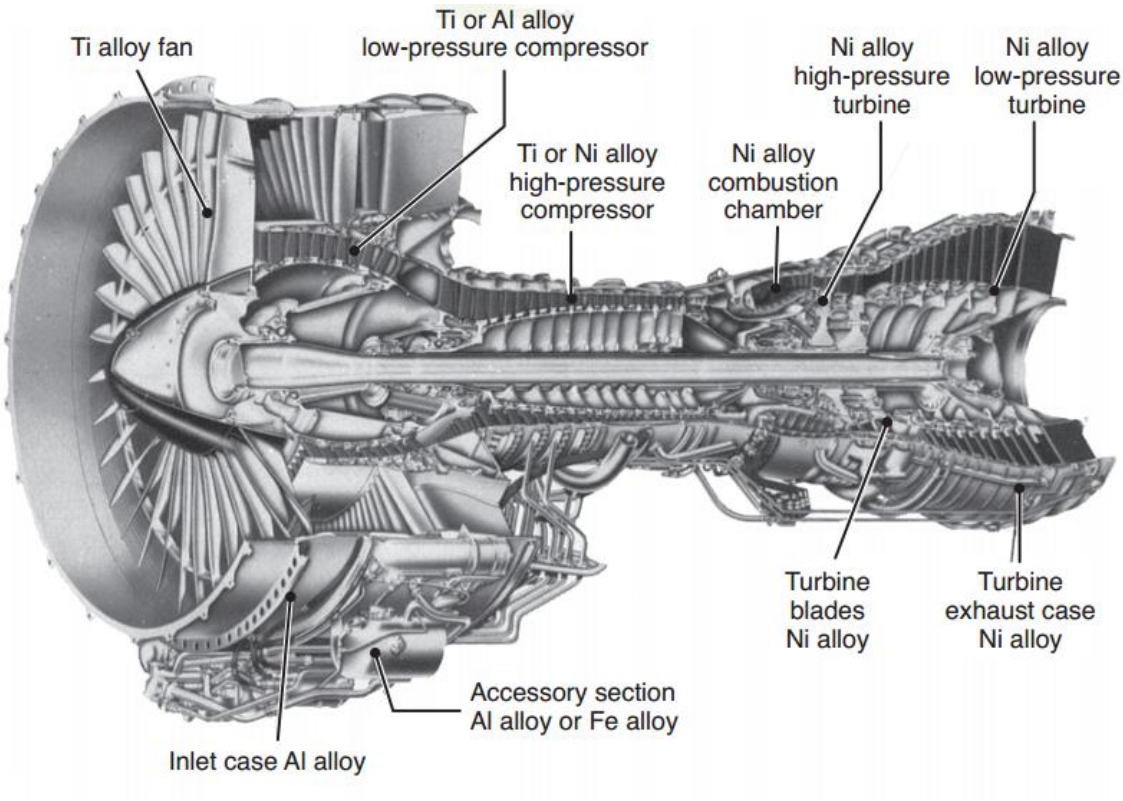

Figure 1.2. Cross section of a jet engine(PW2037) **[8]**

Ingestion of debris into the engine of aircraft during takeoff and landing causes nicks and dents to form on the leading and trailing edge of turbine blades (Figures 1.3 and 1.4). These dents and nicks can be treated as small notches and thus serve as stress raiser and favorable zones for crack initiation therefore reducing the fatigue strength of the material. This phenomenon is referred to as foreign object damage (FOD) and can be modeled as small notches with notch root radius and notch depth [5, 6].

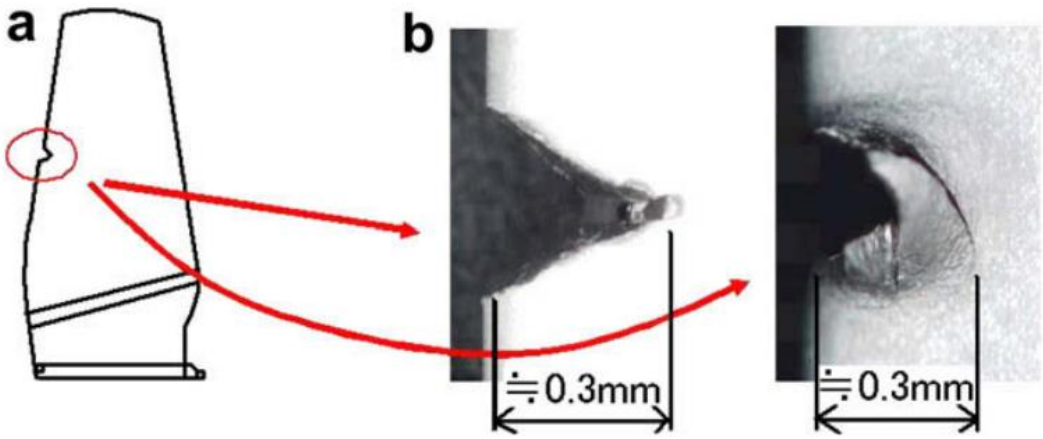

Figure 1.3. Image of FOD damage; (a) Fan blade schematics (b) FOD damage example on edges of airfoil **[6]**

Figure 1.4. Nicks and dents caused by ingested foreign materials on the leading edge of compressor blade **[9]**

Inclusions play a major role in the fatigue strength reduction of multiphase alloys such as nickel base superalloys as the inclusions serve as zones of crack nucleation [10]. Popular inclusions commonly found in nickel base superalloy are carbides close to the grain boundaries or within a grain and pores within the polycrystal which results in

incompatible deformation between the inclusions and the neighboring materials leading to localized plasticity when subjected to cyclic loading.

The turbine engine operates at very high temperature and thus the blades have tiny pores for cooling purposes as shown in Figure 1.5. The coolants are forced through the pores at high pressure for cooling of the system [11]. These pores serve as areas of stress concentration and are typical locations for localized micro-plasticity thus reducing the fatigue strength of the material when subjected to cyclic loading. The holes also serve as favorable zones for crack initiation leading to early retirement of the turbine blade and engine (Figure 1.6). Notches and inclusions form part of the major factors that dictate the fatigue strength of structures.

The fatigue strength reduction factor otherwise known as the fatigue notch factor, kf, is used in the estimation of fatigue life and strength of structures. Hence, it becomes of ultimate importance to develop more accurate methods of estimating fatigue notch factor of aero engine materials for reliable fatigue life assessment and prevention of disastrous and calamitous fatigue failure of aero engines in service.

Figure 1.5. Leading edge of turbine blade showing tiny cooling holes [12]

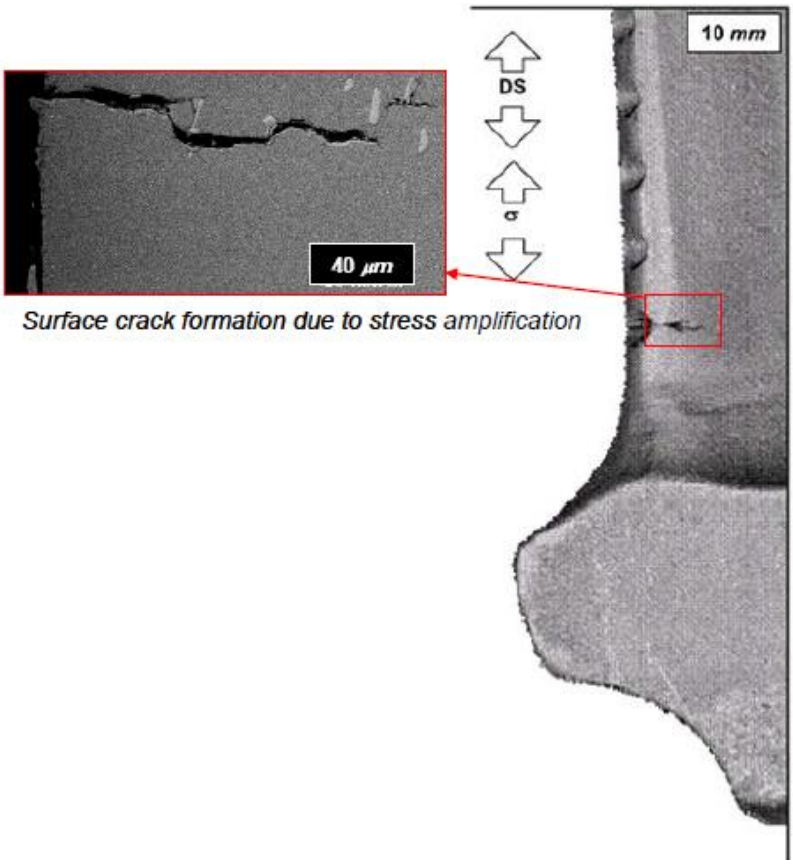

Figure 1.6. Crack Initiation at cooling hole of turbine blade **[13]**

Untill now, finding a brief and economical derivation for k_f remains an unsolved problem as there is yet to be a commonly accepted expression for k_f for different conditions. This is because the fatigue notch factor is synonymous to a black box whose output is dependent on several input factors such as the material properties, stress gradient around the notch root, material imperfections or inherent defects, size and geometry of specimen, loading type and the number of loading cycles. However, k_f is generally defined as the ratio of fatigue strength of a smooth specimen, $S_{S,}$ to that of a notched specimen, S_N, under the same experimental conditions and same number of cycles.

Different expressions based on different assumptions have been developed for k_f in the past. The Neuber [14], Kuhn et al. [15], Peterson [16], Heywood [17, 18], Buch [19, 20], and Siebel et al. [21] expressions are all based on average stress assumptions. The average stress assumption stipulates that fatigue failure will occur given that the average stress over a length A, as shown in Figure 1.7, in the vicinity of the notch root is equal to a smooth specimen fatigue limit σ_e in the normal tensile direction σ_y while R is the notch root radius also represented as "ρ". Other existing expressions for k_f include: Ting et al. [22] and Yu et al. [23] which are based on fracture mechanics models and lastly Sheppard [24] which is based on stress field intensity models.

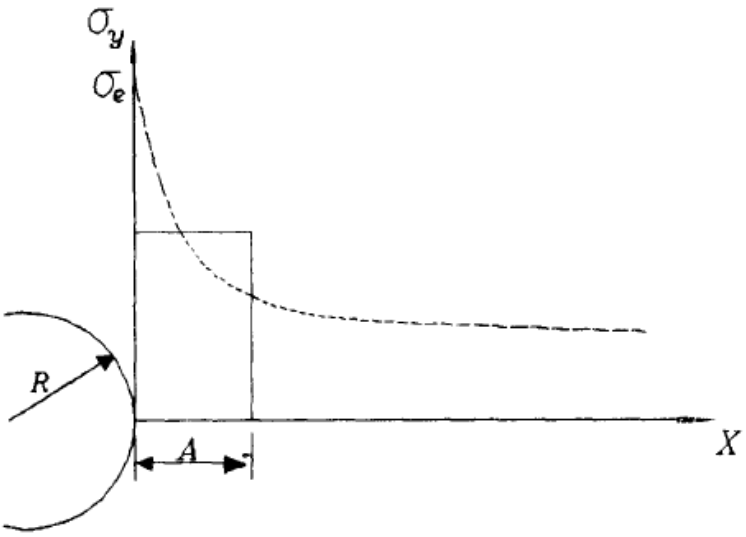

Figure 1.7. Average stress model

The problems with these models are some fundamental drawbacks commonly encountered at the design stage. One of these drawbacks is that the fatigue notch factors are obtained by conducting series of time consuming and costly experiments on notched and smooth specimens. At present, there is no simulation-based methodology for modeling the interactive effects of stress/strain field gradients at the notch-root and microstructure-scale behavior in predicting notch-root fatigue failure in service loads where performance outweighs other considerations. The usual fatigue life prediction methods for notches via the fatigue notch factor account for combined effects of notch size and notch root plasticity in a relatively primitive fashion and do not incorporate explicit sensitivity to the combined effects of microstructure and strength of the notch root stress field gradient. The relationship of microstructure to k_f, via a constant in Peterson's classical equation [16], has proven to be elusive, while the former issue (finite volume for damage process zone) addresses a key physical aspect of the problem, namely comparative scales of notch root gradients to characteristic scales of microstructure and

distributed cyclic microplasticity. Recent approaches have been developed to incorporate these finite process zone effects at notches [25, 26], but are deterministic and do not address the role of microstructure explicitly. It is therefore very difficult to link the k_f obtained using these methods to the realistic microstructure of the material such as grain size, grain orientation, presence of inclusion, and the notch root geometry.

A predictive basis for nucleation and propagation of small crack dependency on notch size effects which can only be possible by the holistic treatment of the plastic strain field gradients, notch root stress and intrinsic scales of grains and other material attributes is yet to be developed. Owolabi et al. [27, 28] recently developed a probabilistic framework based on weakest link and extreme-value statistics where elements of crystal plasticity were combined with new probabilistic methods for notch sensitivity based on computed slip at the notch root within a well-defined fatigue damage process zone for homogenous oxygen free high conductivity copper (OFHC).

The purpose of this work is to extend the recently developed probabilistic framework based on weakest link and extreme-value statistics to heterogeneous multiphase aero-engine materials such as titanium alloy and nickel-base superalloy. The concept of fatigue notch factor, the ratio of unnotched to notched specimen fatigue strength in the HCF regime (or equivalently the notch sensitivity index), will effectively be extended to incorporate microstructure sensitivity via probabilistic arguments. The approach to be used in this work will combine elements of crystal plasticity with new probabilistic approaches for notch sensitivity based on slip distributions in the microstructure at the notch root. The framework to be developed will incorporate information regarding not only the peak stress but also the stress gradient relative to

microstructure length scales for turbine engine materials. It will also account for other competing damage mechanisms such as inclusion in aero-engine materials. This approach can reduce the amount of testing required to make design decisions on material or component reliability by systematically estimating the scatter of fatigue life associated with microstructure variations through the use of simulations.

It is significant to note that fatigue notch factor and associated notch sensitivity index are not well quantified beyond the level of the ratio of average remote applied stress amplitudes corresponding to unnotched and notched specimens at a given HCF life, requiring the designer to apply a safety factor to account for uncertainty associated with material condition or microstructure variability. However, using an exorbitant factor of safety to account for uncertainties for fatigue design of engineering components under service loads is no longer an acceptable approach in many safety-critical applications. The uniqueness of this task is that it will combine elements from microstructure-sensitive crystal plasticity models for alloys used in safety critical components with a nonlocal probabilistic mesomechanics framework for fatigue strength reduction and the probabilities of formation and growth of small cracks at notches that depends on microstructure features (i.e., grain size, phase distribution, composition, pores, inclusions, etc.). To this point, most traditional fatigue design tools for components with notches have only implicitly reflected the role of materials microstructures.

The resulting methods will be of significant utility to large scale industries such as the aerospace industry in fatigue life prediction strategies and assessment of alloys in notch resistance.

1.3 Thesis Outline

To accomplish the objectives of this thesis, the following tasks were carried out:

1. Chapter 2 gives a literature review to the thesis. An overview of fatigue, fatigue notch factor and different stages and regimes of fatigue are presented. The various existing expressions for fatigue notch factor are also examined and analyzed for their limitations.

2. In Chapter 3, the material structures of IN100 nickel base super alloy and Ti-6Al-4V titanium alloy are discussed. Crystal plasticity constitutive models and finite element implementation for the two materials are also discussed.

3. Chapter 4 describes the finite element models, the probabilistic framework developed, and the associated fatigue notch factor based on probabilistic arguments.

4. Chapter 5 presents the result and discussion

5. Chapter 6 gives a general summary of the thesis and offers recommendations for future work

CHAPTER 2

LITERATURE REVIEW

2.1 Stress Concentration Factor

Notches and discontinuities in materials serve as areas of stress concentration which make the local stress in the vicinity of the notch root to be higher than the applied remote stress (Figure 2.1).

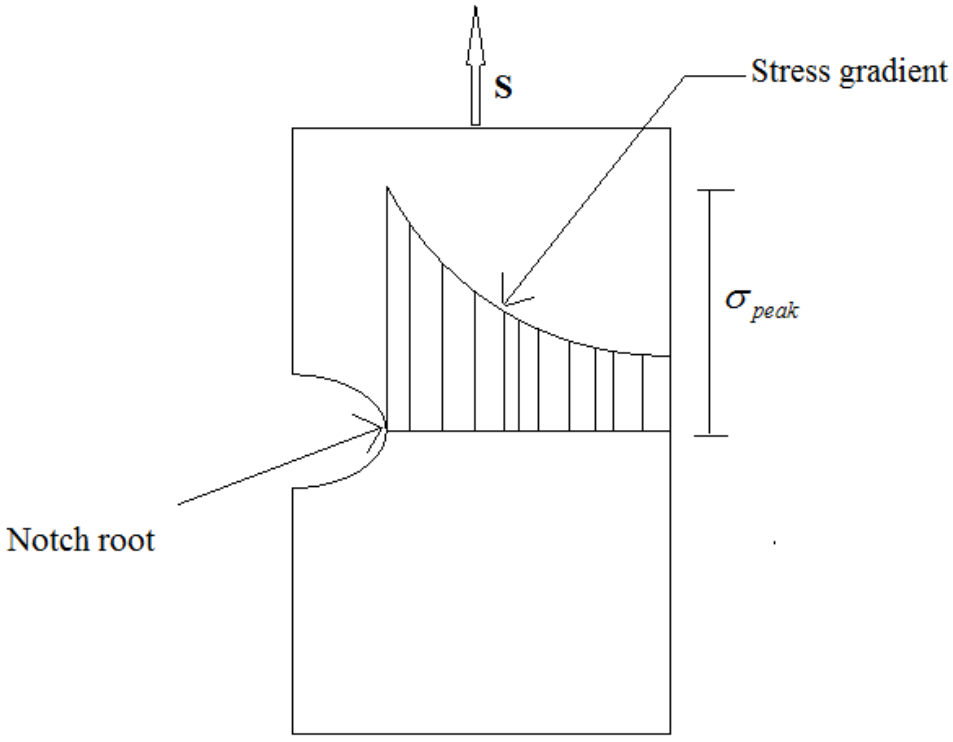

Figure 2.1. Stress distributions in a notched specimen.

The ratio of the peak stress at the notch root to the remotely applied stress is referred to as stress concentration factor (k_t) in linear elastic material and it is used to characterize notch severity.

$$k_t = \frac{\sigma_{peak}}{S} \tag{2.1}$$

k_t is dependent on the mode of loading (tensile, bending, torsional, etc.) and the geometry of the component. Neuber [29] determined the theoretical stress concentration factors for deep hyperbolic notch and shallow elliptical notch in infinitely wide material under bending, shear and tension mode of loading. A comprehensive list of experimentally determined stress concentration factors for different geometries and loading can be found in Peterson's stress concentration factor book [30].

Although, it is very simple to obtain the maximum stress and fatigue life of notched components using k_t, it is well known that k_t under-estimates the fatigue life and thus fatigue notch factor k_f is generally used in predicting fatigue life of notched components as it gives more accurate result.

2.2 Fatigue Notch Factor

The peak stress at the notch root of a notched component is not solely responsible for the fatigue behavior of the component. In general, if only the peak stress at the notch root is considered, then the fatigue strength of a notched component is greater than that of a smooth specimen with the same stress uniformly distributed across the cross section [1]. In the past, researchers have attributed this phenomenon to the fact that the stresses and strains distribution over a critical volume in a material dictates the fatigue behavior of the

material. Based on experimental data accumulated over years, expression for predicting the fatigue behavior of notched component based on smooth component fatigue behavior was developed. In general, the fatigue notch factor, k_f is defined as the ratio of fatigue strength of a smooth specimen, S_S, to that of a notched specimen, S_N, under the same number of cycles and experimental conditions; generally a fully reversed loading condition with load ratio R= -1, given as:

$$k_f = \frac{\textit{fatigue}\ \text{strength of smooth specimen, } S_S}{\text{fatigue stength of notched specimen, } S_N} \qquad 2.2$$

The range of value for the fatigue notch factor k_f is usually given as $1 < k_f < k_t$ indicating the over conservative nature of k_t when used in fatigue life prediction or notch sensitivity description. Another quantity used for describing the behavior of notched component is the notch sensitivity index, q, which indicates sensitivity of materials to notches. The notch sensitivity index, q, which also gives the relationship between the fatigue notch factor k_f and the elastic stress concentration factor k_t is given as:

$$q = \frac{k_f - 1}{k_t - 1} \qquad 2.3$$

The range of value for notch sensitivity index q is $0 < q < 1$. When $q = 0$, this implies that the material is not sensitive to notch and $k_f = 1$. When $q = 1$, i.e $k_f = k_t$, this implies that the material is fully notch sensitive and that the behavior is dictated solely by the local notch root stress.

2.3 Factors Affecting Fatigue Strength of Materials

Different factors have been identified to affect the fatigue strength or fatigue notch factor of a material [31]. Some of these factors include: material inherent defects

[32], loading type [32], material properties, geometry of specimen, number of loading cycles, size of notch and notch root stress gradient [19, 33, 34], etc. Dabayeh et al. [32] investigated the effect of flaw at the notch root on the fatigue life of a material. Notched cast aluminum alloy 319 of notch sizes 1.0 mm, 3.0 mm, and 6.0 mm having natural flaw at the center of the notch root were subjected to constant and variable amplitude loading to determine their fatigue strength. Dabayeh et al. concluded that the presence of flaws at the notch root of cast Al 319 resulted in reduction of the fatigue strength of the aluminum alloy. Dabayeh et al. also investigated the effects of constant amplitude loading and variable amplitude loading on the fatigue life of the same material. The result of their experiment shows that material subjected to constant amplitude loading can withstand more strain amplitude than a material subjected to variable amplitude loading at the same number of cycles to failure as depicted in Figure 2.2.

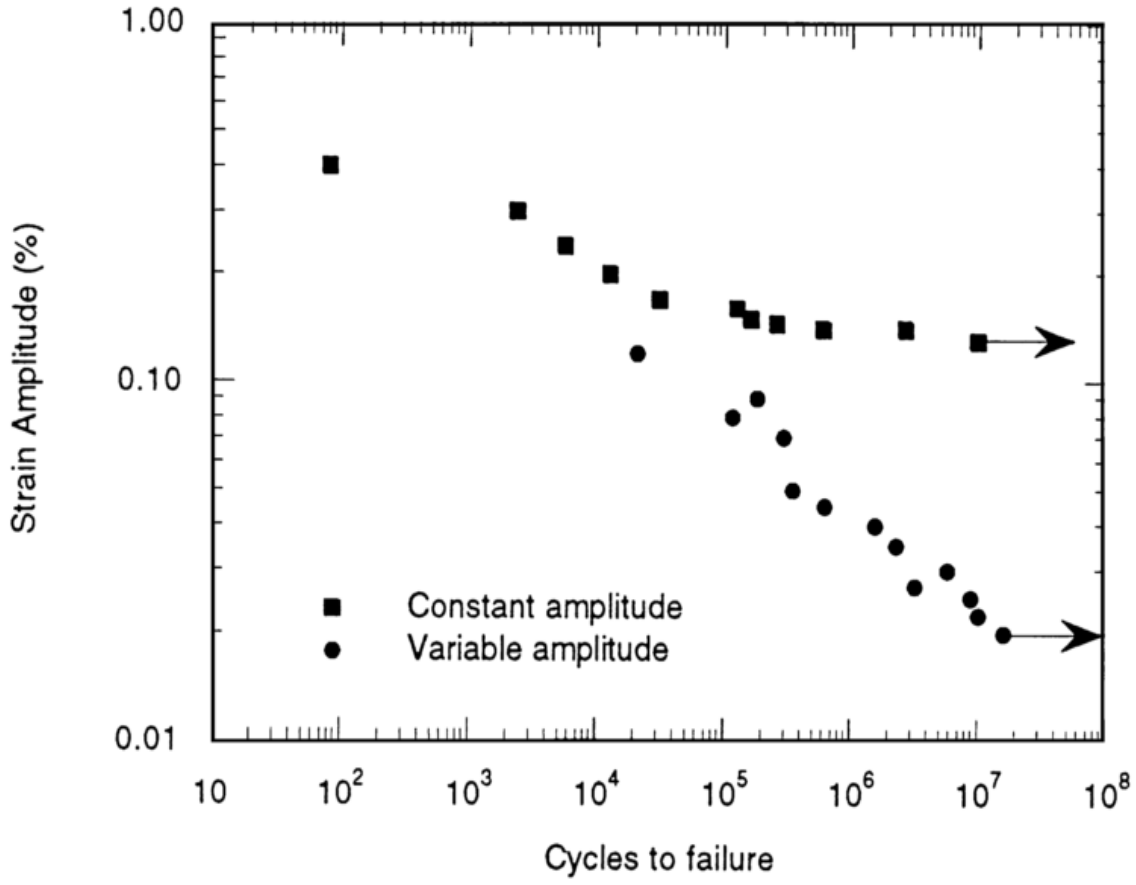

Figure 2.2.Constant and variable amplitude strain-life curves for hipped Al319 **[32]**

Kristoffer et al. [35] investigated the effect of random defects on the fatigue notch factor of at different stress ratios. Here, fatigue crack growth simulations were performed for defects, treated as cracks, of different sizes randomly distributed in the specimen. The conclusion reached by Kristoffer et al. is that the defect size distribution couple with the defect density has influence on the fatigue limit distribution and consequently the fatigue notch factor distribution.

Neuber [29] has shown that notches in material serves as areas of stress concentration causing high localized stress at the notch root thus leading to reduced

fatigue strength when such material is subjected to fatigue loading. George et al. [5], Weiju et al. [26] and Cheng et al. [36] have all investigated notch size effects on fatigue behavior of notched component subjected to fatigue loading. Past researches by Benedetti et al. [37] and Teh et al. [38] have established that the fatigue strength of a notched component depends on the stress distribution in the vicinity of the notch. Other researchers who have also suggested that the stress gradient in a notched component plays a significant role in the fatigue process of the component include: Buch [19], Neuber [29] and Peterson [16].

2.4 Existing Expressions for Fatigue Notch Factor

Different expressions for the fatigue notch factor have been developed by researchers based on certain assumptions. Some of the most popular expressions include: the stress field intensity (SFI) model, the average stress (AS) model, and the fracture mechanics (FM) model.

The average stress model is based on the assumption that fatigue failure will occur when the average stress over a length A measured from the notch root of a notched specimen is the same as the fatigue limit σ_e of a smooth specimen. Based on this assumption, Kuhn and Hardraht [39] give the expression (KH model) for K_f as:

$$K_f = 1 + \frac{K_T - 1}{1 + \frac{\pi}{\pi - \omega}\sqrt{\frac{A}{\rho}}} \qquad 2.4$$

Where ρ is the notch root radius, ω is the notch angle, and A is a material constant.

Neuber [40] modified the KH model to give the NKH model expressed as

$$K_f = 1 + \frac{K_T - 1}{1 + \sqrt{\frac{a}{\rho}}} \qquad 2.5$$

Here $a = f(\sigma_b)$ and is a material constant, σ_b is the material tensile strength.

Peterson [16] developed a special type of the average stress model called a point stress model with the assumption that the stress field around the notch root drops linearly and expressed K_f as following:

$$K_f = 1 + \frac{K_T - 1}{1 + \left(\frac{a}{\rho}\right)} \qquad 2.6$$

where ρ is the notch root radius and "a" is a material constant.

Heywood [18] developed another expression for K_f based on intrinsic defects given as:

$$K_f = \frac{K_T}{1 + 2\sqrt{\frac{a}{\rho}}} \qquad 2.7$$

where a is material dependent (material constant).

Buch [19, 20] based on the consideration of stress gradient developed a two parameters expression for K_f given as:

$$K_f = K_T \frac{\left(1 - \frac{2.1h}{\rho_0 + \rho}\right)}{A} \qquad 2.8$$

where A and h are dependent on the material and type of specimen while ρ_0 is a function of A and h. The shortcoming of the average stress models for predicting fatigue notch factor is that they fail to explicitly account for notch size effects, stress/strain gradient and also microstructural inhomogeneity of the material [27, 35].

Stress field intensity model is based on the assumption that the fatigue strength of a material does not depend only on the peak stress at the notch root but also on the stress-field intensity in the damaged zone shown in Figure 2.3.

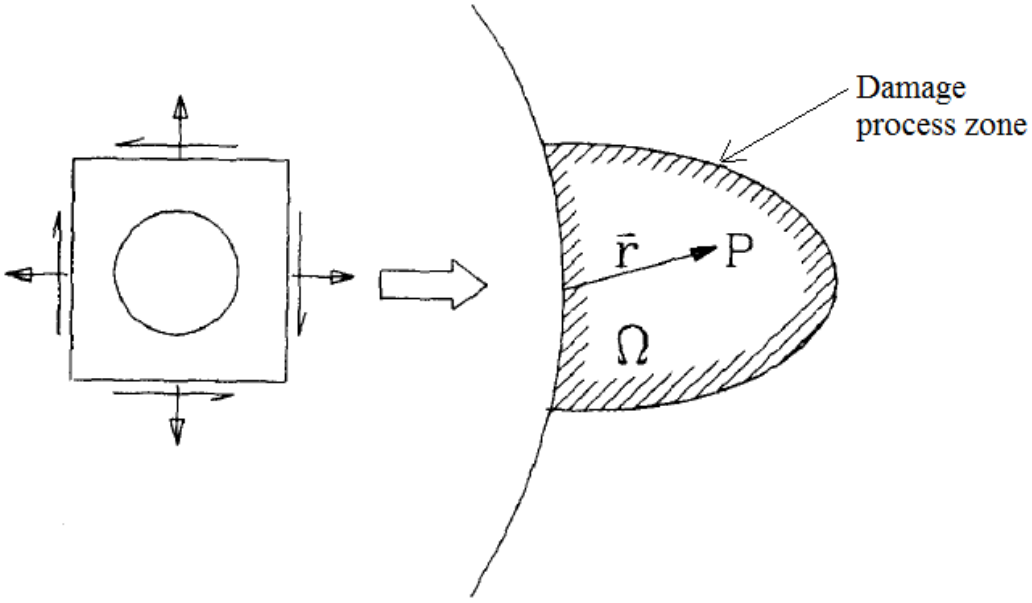

Figure 2.3. Stress Field Intensity Model **[31]**

The stress field intensity approach deals with stress field intensity function σ_{FI} defined according to Yao [41, 31] as follows:

$$\sigma_{FI} = \frac{1}{V}\int_{\Omega} f\left(\sigma_{ij}\right)\varphi(\overrightarrow{r})dv \qquad 2.9$$

where Ω is the fatigue damage zone, V is the volume of the fatigue damage zone, $f\left(\sigma_{ij}\right)$ is the equivalent stress function, and $\varphi\left(\vec{r}\right)$ is the weight function. According to the stress field intensity approach assumption, the stress field intensity in an un-notched specimen is the same as its fatigue strength namely:

$$\sigma_{FI}^{0} = S_e \tag{2.10}$$

where S_e is the endurance limit of the material

The stress field intensity for notched specimen is given as:

$$\sigma_{FI}^{N} = \frac{1}{V}\int_{\Omega} f\left(\sigma_{ij}\right)\varphi\left(\vec{r}\right)dv \tag{2.11}$$

Given the stress tensor σ_{ij} as a function of applied stress, i.e

$$\sigma_{ij} = \sigma_{ij}\left(S_N\right) \tag{2.12}$$

and the equivalent stress function as

$$f\left(\vec{\sigma}_{ij}\right) = {f\left(\sigma_{ij}\right)}\Big/{S_N} \tag{2.13}$$

Substituting Equations (2.16) and (2.17) into Equation (2.15) yields:

$$\sigma_{FI}^{N} = \frac{S_N}{V}\int_{\Omega} f\left(\vec{\sigma}_{ij}\right)\varphi\left(\vec{r}\right)dv \tag{2.14}$$

The fatigue notch factor is thus calculated using:

$$k_f = \frac{S_e}{S_N} = \frac{1}{V}\int_{\Omega} f\left(\vec{\sigma}_{ij}\right)\varphi\left(\vec{r}\right)dv \tag{2.15}$$

This method offers improvement over the local hot spot method of determining fatigue notch factor as it captures the effect of the stress/strain gradient at the notch root. However, it has the short coming of not clearly defining the fatigue damage zone Ω.

The fracture mechanics model operates on the assumption that crack initiates at the notch but becomes non-propagating at length a_{th} (Figure 2.4). Frost and Phillips [39] pioneered the application of fracture mechanics to study notched specimens fatigue strength.

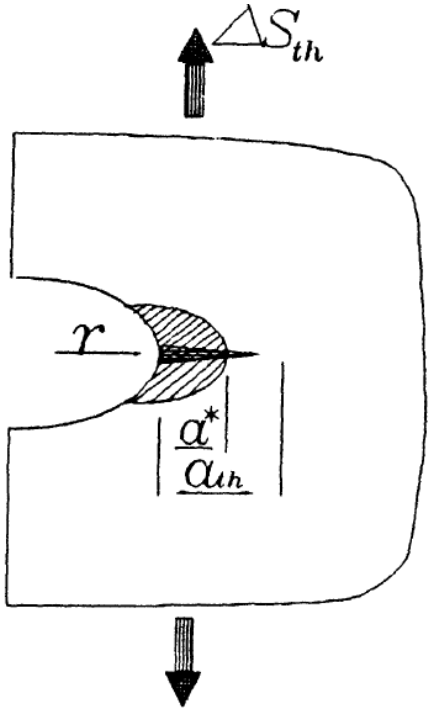

Figure 2.4. Fracture Mechanics Model **[31]**

Ting and Lawrence [42] developed a crack closure at a notch (CCN) model given as

$$K_f = \frac{\Delta S_c}{\Delta S_{th}} \qquad 2.16$$

where ΔS_c is a smooth specimen fatigue limit stress range and ΔS_{th} is the threshold stress range.

For smooth specimen and notched specimen, the effective threshold stress intensity factor range $\Delta K_{eff,th0}$ is given respectively as:

$$\Delta K_{eff,th0} = U_{th0}\Delta S_c\sqrt{\pi l_0} \tag{2.17}$$

$$\Delta K_{eff,th0} = U_{th}Y(a_{th})\Delta S_{th}\sqrt{\pi\left(D + a_{th}\right)} \tag{2.18}$$

where U_{th0} is the effective threshold stress intensity factor for a long crack, U_{th} is the effective threshold stress intensity for a_{th} crack length, and $Y(a_{th})$ represents the geometry factor for the stress intensity factor. Equating Equation (2.21) to (2.22) which is the assumption for fatigue failure to occur, we have the following expression for K_f:

$$K_f = \frac{\Delta S_c}{\Delta S_{th}} = \frac{U_{th}Y(a_{th})}{U_{th0}}\sqrt{\frac{D + a_{th}}{l_0}} \tag{2.19}$$

where l_0 is the smooth specimen intrinsic crack length, D is the notch depth, and a_{th} is the maximum length of non-propagating (short) crack.

The FM model is best suited for predicting K_f at infinite fatigue life thus it becomes difficult to use since K_f is not limited only to infinite fatigue life. Also, the FM model uses stress field intensity factors estimates which might be difficult to obtain for complicated geometries.

A comprehensive summary of the different existing model for fatigue notch factor is presented in Table 2.1 as obtained from Yao et al. [31]

Table 2.1

Comprehensive summary of existing expressions for Kf [31]

Authors	Abbreviation	Expression	Material Parameters
Average stress models			
Neuber, Kuhn and Hardraht	NKH	$K_f = 1 + \frac{K_T - 1}{1 + \sqrt{\frac{a}{\rho}}}$	$a = f(\sigma_b)$ is the function of ultimate stress
Peterson	P	$K_f = 1 + \frac{K_T - 1}{1 + \frac{a}{\rho}}$	a is a material constant
Heywood	H	$K_f = \frac{K_T}{1 + 2\sqrt{\frac{a}{\rho}}}$	$a = f(\sigma_b)$ depends on material and specimen
Buch	B	$K_f = K_T\left(\frac{1 - 2.1\frac{h}{\rho + \rho_0}}{A}\right)$	A, h depend on materials and specimen, ρ_0 is a function of A and h
Stieler and Siebel	SS	$K_f = \frac{K_T}{1 + \sqrt{1 + a\chi}}$	$a = f(\sigma_{0.2})$ is a material constant
Wang and Zhao	WZ	$K_f = \frac{K_T}{0.88 + A\chi^b}$	A, b are material constants
Fracture mechanics models			
Ting and Lawrence	TL	$K_f = Y(a_{th})\left(1 + \sqrt{\frac{D_{eff}}{l_0}}\right) a_{th} > a^*$ $K_f = \frac{U_{th}^* Y(a^*)}{U_{th0}} \sqrt{\frac{D + a^*}{l_0}} a_{th} \le a^*$	l_0 is the intrinsic crack length, U_{th0} is effective threshold stress intensity ratio for a long crack
Yu, DuQuesnay and Topper	YDT	For sharp notch: $K_f = \frac{1}{F}\left(1 + \sqrt{\frac{D}{l_0}}\right)$	$\Delta\sigma$ and $\Delta\varepsilon$ are the local stress and strain range at notch root

CONTINUED

Table 2.1 (Continued)

		For blunt notch : $K_f = \frac{K_T \Delta S_c}{\sqrt{\Delta\sigma \Delta\varepsilon E}}$	
Zu, Huang and Chen	ZHC	$K_f = K_T \Big/ \sqrt{1+4.4C_c/\rho}\left(\frac{b}{a}=1.0\right)$ $K_f = K_T \Big/ \sqrt{1+3.5C_c/\rho}\left(\frac{b}{a}=0.05\right)$	C_c is critical crack length, a and b are semi-axle of an ellipse
Stress field intensity models			
Yao Weixing and Gu Yi	YG	$K_f = \frac{1}{V}\int_\Omega f\left(\vec{\sigma}_{ij}\right).\varphi\left(\vec{r}\right)dv$	Stress field domain Ω is a material constant
Sheppard	S	$K_f = \frac{\sigma_{ave}\big\vert_M}{S_N}$	M is stress field domain

2.5 Probabilistic Framework

One major problem common with fatigue research is the scatter in fatigue life or fatigue strength for similar experiments conducted under the same operating conditions. To account for scatters commonly encountered in HCF, various probabilistic methods have been developed. Weakest link theory, first proposed by Weibull in 1939 [43, 44] remains one of the most widely used probabilistic approaches in fatigue. Subsequent works on the theory include Bomas et al. [45] on a bearing steel and Hild and Roux [46] on a nodular cast iron. They both used the probabilistic approach to explain the effect of defect distribution on fatigue strength. The weakest-link theory basic assumption is the existence of statistically distributed defects at the surface or in the material volume and the occurrence of crack initiation at the largest defect. The defects can be in the form of inclusions, voids, or microcracks which contribute to fatigue failure [47, 48, 49]. Furthermore, this theory is based on a number of hypotheses [45]: the entire material is considered as a combination of links, formation of crack in a link induces the crack of the

entire structure, it is assumed that there are no interaction between defects i.e the defects size is very small compared to inter-defect distance. The model hypothesis assuming no inter-defect interaction is reasonable only if we consider the initiation of fatigue crack and not crack propagation and this buttress the second hypothesis.

2.5.1 Probabilistic Framework without Inclusion

As discussed in the preceding section, most probabilistic approaches already developed by researchers consider the physical defect distribution such as inclusions, pores or microcracks that contribute to failure [48, 47, 49]. However, there are other approaches which consider the distribution of microvoids [50] or microplasticity [51]. According to the hypotheses on which the weakest link theory is based, given a structure with volume V, the probability of success, P_S, of the structure under uniaxial stress σ can be expressed as a function of probabilities of success of all the elementary/individual volumes of material $V_{e,i}$ making up the structure and it is given as:

$$P_s\left(V,\sigma\right)=\prod_{i=1}^{i=k}P_s\left(V_{e,i},\sigma\right) \tag{2.20}$$

The weakest link theory assumes that the probabilities of success of two separate sub volumes, $V_{e,1}$ and $V_{e,2}$, are independent, that is, there are no interaction between critically-stressed elementary volumes. In other words, it is assumed that there are no interaction between defects i.e the defects size is very small compared to inter-defect distance. This assumption is best suited for high cycle fatigue regime, where scatter of heterogeneous microplasticity in the fatigue specimen is a common occurrence. The probability of success of the two sub volumes is thus given as:

$$P_s\left(V_{e,1}+V_{e,2}\right)=P_s\left(V_{e,1}\right)*P_s\left(V_{e,2}\right) \tag{2.21}$$

If the sizes of the elementary volume or sub volumes tend to zero, the weakest link theory holds that the probability of failure of a series of links with random threshold stresses can be expressed as [52]:

$$P_f\left(V\right)=1-P_s\left(V\right)=1-\exp\left[\sum_i \varphi_i V_{e,i}\right] \tag{2.22}$$

$$P_f\left(V\right)=1-\exp\left\{-\int_v \varphi\left(x,y,z\right)dV\right\} \tag{2.23}$$

where φ_i characterizes the probability of failure of each sub volume $V_{e,i}$, and $\varphi\left(x,y,z\right)$ is the density function of the probability of failure of the material which is dependent on the stress σ. The analytic expression for the density factor was introduced by Weibull for three-parameter weibull distribution as [53]:

$$\varphi\left(x,y,z\right)=\frac{1}{V_0}\left(\frac{\left\langle\sigma-\sigma_0\right\rangle}{\sigma_u}\right)^m \tag{2.24}$$

where V_0 is the reference volume, σ_0 is the location parameter or a threshold stress below which damage does not occur, m is the shape parameter or Weibull slope, σ_u is the scale parameter and the Macaulay brackets $\left\langle\bullet\right\rangle$ indicate that $\left\langle a\right\rangle=a$ if $a>0$ and $\left\langle a\right\rangle=0$ if $a\le 0$.

According to Weibull [43, 44], the probability of failure is given as:

$$P_f\left(V,\sigma\right)=1-\exp\left[-\frac{1}{V_0}\int_v\left(\frac{\left\langle\sigma-\sigma_0\right\rangle}{\sigma_u}\right)^m dV\right] \tag{2.25}$$

Equivalent stress, such as Von Mises or Tresca, or maximum principal stress can be used as the value of σ in the equation. Different variations of Equation 2.25 have been used extensively by various researchers to model the variability of fatigue strength.

Doudard et al. [51], based on the approach proposed by Lemaitre et al. [54, 55], developed a probabilistic two-scale model for high cycle fatigue that not only account for failure of material but also the thermal effects during cyclic loadings. The approach assumes that microscopic yield stress is a probabilistic variable and defined the failure probability of a domain, Ω, of volume, V_Ω, subjected to homogeneous stress amplitude $\sum$ as equal to the likelihood of finding at least one active inclusion within the volume V_Ω and is expressed as:

$$P_f = 1 - \exp\left[-\frac{V_\Omega H_m}{V_0} \left(\frac{\sum_F}{S_0} \right)^m \right] \tag{2.26}$$

where m and $V_0 S_0^m$ are Weibull parameter, $\sum_F = \max_\Omega \left(\sum \right)$ and H_m is the stress heterogeneity factor and it is given as:

$$H_m = \frac{1}{V_\Omega} \int \left(\frac{\sum}{\sum_F} \right)^m dV \tag{2.27}$$

Different S/N curves prediction by the model for different effective volumes corresponding to bending and axial fatigue tests have been validated.

Wormsen et al. [56, 57], adopted a two-parameter Weibull distribution and based on a defect-tolerant-approach, developed an expression for probability of failure given as:

$$P_f = 1 - \exp\left\{ -\left(K_w \frac{S_{net}}{S_0^*} \right)^{b_s} \frac{V}{V_0} \right\} \tag{2.28}$$

where S_0^* and b_s are the Weibull scale and shape parameters, S_{net} is the net nominal stress, V_0 is the gauge volume, and K_w is the Weibull stress factor given as:

$$K_w = \left\{ \frac{1}{V} \int_V \left(\frac{S}{S_{net}} \right)^{b_s} dV \right\}^{1/b_s} \tag{2.29}$$

Wormsen et al. [56] also developed an expression for the fatigue notch factor of a component by comparing the fatigue strength S_{net}, of the an arbitrary component of volume V with the fatigue strength of a standard specimen $S_{net,0}$ of volume V_0 at the same number of cycles and probability of survival and is given as:

$$S_{net} = \frac{S_{net,0}}{K_w \left(V/V_0 \right)^{1/b_s}} \tag{2.30}$$

The denominator of the expression in Equation 2.30 is referred to as the fatigue notch factor of the component, i.e.:

$$K_f = K_W \left(V/V_0 \right)^{1/b_s} \tag{2.31}$$

The new approach was applied to three materials; forged steel, cast steel and aluminum alloys and parameter estimation was carried out using large quantity of experimental high cycle fatigue data. It was noticed that the estimated shape parameter b_s for cast steels is less than that of forged steels. This is attributed to the greater probability of finding larger defect in a cast steel.

Owolabi et al. [27] employed statistical distribution of the nonlocal Fatemi-Socie critical plane fatigue indicator parameter within a well-defined damage process zone as a basis of comparison for the fatigue susceptibility of various microstructure and a means of predicting the probability of failure over polycrystalline oxygen-free high thermal

conductivity (OFHC) copper ensemble of grains. The proposed probabilistic framework focused on the formation of fatigue crack at a single grain scale and thus most suited for high cycle fatigue and very high cycle fatigue where crack formation nearly solely account for the total fatigue life. Using Weibull weakest link theory, the resulting probability of failure based on statistical distribution of fatigue indicator parameter is given as:

$$P_f = 1 - \exp\left\{ -\frac{1}{V_0} \int_{V_d} \left(\frac{\Delta\Gamma - \Delta\Gamma_{th}}{\Delta\Gamma_0} \right)^{b_\Gamma} dV \right\} \tag{2.32}$$

where V_0 is the reference smooth specimen volume, V_d is the volume of the damage process zone, $\Delta\Gamma_0$ and b_Γ are the Weibull scale and shape parameters, $\Delta\Gamma_{th}$ is the threshold fatigue indicator parameter below which no microdamage will occur, and $\Delta\Gamma$ is the Fatemi-Socie critical plane fatigue indicator parameter expressed as:

$$\Delta\Gamma = \frac{\Delta\gamma_{\max}^{p^*}}{2} \left(1 + k \frac{\sigma_n^{\max^*}}{\sigma_y} \right) \tag{2.33}$$

where k is a coefficient that moderates the effect of normal stress to the plane of maximum plastic shear strain, $\Delta\gamma_{\max}^{p^*}$ is the nonlocal plastic shear strain amplitude, σ_y is the cyclic yield strength, and $\sigma_n^{\max^*}$ is the nonlocal peak stress acting perpendicular to the plane of the maximum plastic shear strain range.

Based on the proposed probabilistic framework, Owolabi et al. [27] also developed a microstructure sensitive fatigue notch factor expressed as:

$$K_f^\mu = \frac{\Delta\Gamma_{reference(ave)}}{\Delta\Gamma_{notch(net\ ave)}} = K_\Gamma^\mu \left(\frac{V_d}{V_0} \right)^{1/b_\Gamma} \tag{2.34}$$

where K_{Γ}^{μ} is a new microscopic concentration factor which is dependent on the microstructure introduced by Owolabi et al. and expressed as:

$$K_{\Gamma}^{\mu} = \left\{ \frac{1}{V_d} \int_{V_d} \left(\frac{\Delta\Gamma - \Delta\Gamma_{th}}{\Delta\Gamma_{net(ave)}} \right)^{b_{\Gamma}} dV \right\}^{1/b_{\Gamma}} \qquad 2.35$$

The fatigue notch factor developed is thus identical to the conventional fatigue notch factor, which is the ratio of unnotched to notched values of the identified driving force for a given high cycle fatigue life. However, a probabilistic argument based on the distribution of the fatigue indicator parameter in the damage process zone is assumed here. The trend of the notch sensitivity index determined for OFHC copper using the new microscopic concentration factor and the newly developed microstructure sensitive fatigue notch factor are similar to the trend in notch sensitivity index based on experimentally measured fatigue notch factor.

De Jesus et al. [58] proposed a probabilistic strain-life based Weibull model where the total strain amplitude , ε_a, for a given lifetime and the fatigue life, N_f, for a given strain amplitude, are the statistically distributed variables. The model assumed crack initiation as the dominating fatigue damaging process in riveted connections investigated which is in agreement with earlier findings by Iman B. [59]. Based on the application of the Weibull weakest link theory, the proposed probability of failure is given as:

$$P_f = 1 - \exp\left\{ -\left[\frac{\log\left(N_f / N_0\right)\log\left(\varepsilon_a / \varepsilon_{a0}\right) - \lambda}{\delta} \right]^{\beta} \right\} \qquad 2.36$$

where N_0 is the threshold value of lifetime, ε_{a0} is the endurance limit of ε_a, λ is a parameter defining the position of the corresponding zero percentile curve, δ is the scale parameter, and β is the shape parameter. De Jesus et al. [58] employed Neuber [60] and Molski and Glinka [61] rules in determining the local stresses and strains in the vicinity of the notch root and modeled the elastoplastic response as a Simple Ramberg-Osgood [62] stress-strain response.

Kristoffer et al. [35] investigated the effects of random defects on fatigue notch factor of a notched member. To get accurate fatigue predictions, the authors describe defect size distributions in the component using a generalized extreme value with the distribution given as:

$$F_{GEV}\left(a \le a_{\max}\right) = \exp\left(-\left(1+\xi\left(\frac{a_{\max}-a_0^*}{a_0}\right)^{-1/\xi}\right)\right) \tag{2.37}$$

where ξ is the shape parameter, a_0^* is the location parameter, and a_0 is the scale parameter. The randomly distributed defects are placed in the material and treated as cracks using software called P.FAT. The software is also used for post-processing. Among the methods of estimating fatigue notch factor considered by the authors is the Weibull weakest link method. The probability of failure based on the weakest link theory was given as:

$$P_f = 1-\exp\left(-\int_v\left(\frac{\sigma_{eff}-\sigma_{th}}{\sigma_u}\right)^m \frac{dV}{V_{ref}}\right) \tag{2.38}$$

where σ_{eff} is the effective fatigue stress using Crossland criterion [63], σ_{th} is a threshold stress, V_{ref} is the reference volume, m is a parameter describing the scatter, and σ_u is the

location parameter. The fatigue life of the components is determined using P.FAT at 50% probability of failure and the associated fatigue notch factor is determined using:

$$K_f = \frac{\sigma_{e,smooth}}{\sigma_{e,notched}} \tag{2.39}$$

where $\sigma_{e,smooth}$ is the fatigue is limit of a smooth specimen and $\sigma_{e,notched}$ is the fatigue limit for a notched specimen.

2.5.2 Probabilistic Framework with Inclusion

Investigating defect interaction is important in fatigue damage of components having significant defects in the form of pores or inclusions. Hild [64] and Chantier [65] have shown that presence of initial casting flaws that are more or less randomly distributed in cast component generally reduces the fatigue strength of the component as microcracks propagate from these initial flaws under cyclic loading. Also, Hyzak and Bernstein [66, 67] have established the important roles played by inclusion in the propagation and formation of fatigue crack in nickel base superalloys while considering two powder metallurgy (PM) nickel base superalloys. These inclusions can either be on the surface, called surface inclusions, or they can be in the material and referred to as bulk inclusions. Surface inclusions are more damaging and detrimental than bulk inclusions for a material subjected to low cycle fatigue [67, 66, 68]. It can therefore be said that the probability of failure of a nickel base superalloy and other materials containing inclusion will be largely dependent on the probability of initiating and propagating cracks due to surface and bulk inclusions.

Based on the known mechanism for microscopic initiation and propagation of cracks in direct-aged IN718 (DA 718), Deyber et al. [69] proposed a probabilistic framework using statistical distribution of particle size. The authors considered two different modes of fatigue crack initiation in the DA 718: Fatigue micro-crack formation on second phase particles (carbides and nitrides) of less than $10\,\mu m$ grain size and transgranular stage I initiation of fatigue crack along favorably oriented slip bands. The resulting probability of failure based on crack formation at particle interfaces is given as:

$$P_f\left(\sigma_d\right) = 1 - \exp\left(-\left[\frac{\Sigma_1 + \lambda\left\langle\sigma_{eq} - \sigma_y\right\rangle}{\sigma_0}\right]^m\right) \tag{2.40}$$

where Σ_1 is the maximum principal stress, λ is the particle shape factor, σ_{eq} is the equivalent Mises stress, σ_y is the yield stress, σ_0 is the scaling parameter, and the Macaulay brackets $\langle\bullet\rangle$ indicate that $\langle a\rangle = a$ if $a > 0$ and $\langle a\rangle = 0$ if $a \le 0$. Deyber et al. [69] also proposed a model for crack propagation based on Tomkins model [70] i.e.

$$\frac{da}{dN} = \alpha \bullet a, \text{ where } \alpha = \frac{\pi^2}{8}\frac{\Delta\varepsilon_p \Delta\sigma^2}{\left(2T\right)^2}\left(1 + \frac{\pi^2}{8}\left(\frac{\Delta\sigma}{2T}\right)^2\right) \tag{2.41}$$

where T is the ultimate tensile stress in the damage process zone of the crack, $\Delta\varepsilon_p$ is the plastic strain amplitude, $\Delta\sigma$ is the maximum principal stress amplitude. Based on the model, the probability that a particle of diameter D_0 will propagate, in a potential number of cycles (N_0), was determined. The probability of failure is therefore equal to the probability of finding a particle of size greater that the potential particle size, D_0. The overall global probability of failure is thus the combined product of the probabilities of failure at the surface, subsurface and within the bulk of the material and it is given as:

$$P_f = 1 - \left\{ \begin{array}{l} \prod_{n=1}^{Nel,surf} \left[\left(1 - P_f\left(\sigma_d\right) P\left(D \geq D_0\right)\right)^{N_{p,surf}} \right] \\ * \prod_{n=1}^{Nel,subsurf} \left[\left(1 - P_f\left(\sigma_d\right) P\left(D \geq D_0\right)\right)^{N_{p,subsurf}} \right] \\ * \prod_{n=1}^{Nel,bulk} \left[\left(1 - P_f\left(\sigma_d\right) P\left(D \geq D_0\right)\right)^{N_{p,bulk}} \right] \end{array} \right\} \quad 2.42$$

where $P_f\left(\sigma_d\right)$ is given in Equation 2.35, N_P *and* N_{el} are the number of particles contained in the meshed elements in each location (surface, subsurface and bulk).

Also, based on known microstructure of PM nickel base superalloy, Pineau [71] proposed a probabilistic framework that employs the statistical distribution of inclusion sizes to determine probability of failure of different components. The proposed model considers both surface and volume defects and the propagation of defects to a critical size. The resulting probability that any one inclusion intercept a free surface for uniform size distribution of spherical inclusion is given as [71]:

$$P_{surf}\left(D, n, S, V\right) = 1 - \left(1 - \frac{DS}{V}\right)^{nV} \quad 2.43$$

where D is the inclusion diameter, S is the highly stressed surface area, V is the volume of the specimen, and n is the number of inclusions per unit volume. However, for varying inclusion sizes grouped into classes, the probability that inclusion of size class k intercept a free surface for distribution of inclusions sizes is given as:

$$P_{k,surf}\left(D_k, n_k, S, V\right) = 1 - \left(1 - \frac{D_k S}{V}\right)^{n_k V} \quad 2.44$$

Pineau [71] used the proposed approach to estimate the probability of failure of three different sized components made from Rene 95 and established that probability of failure is highly size dependent.

2.5.3 Probabilistic Framework under Multiaxial Loading

Based on the fact that fatigue crack initiates and propagate on favorable "critical" slip planes, different attempts have been made by researchers in developing and studying multiaxial theories. A comprehensive summary of the different existing multiaxial fatigue models is contained in Kallmeyer et al. [72]. Theoretically, crack opening is driven by the normal stress and thus reduces the friction between crack surfaces while crack propagation is driven by the resolved shear stress on the dominant slip plane under stage 1 propagation. Attempts have been made by researchers to estimate the failure probability of specimen under complex non-proportional and multiaxial loadings by incorporating these multiaxial fatigues models into the Weibull models.

Existing probabilistic framework models account for stress heterogeneity effect using the concept of effective volume. Doudard et al. [73] extended this concept to account for multiaxial loading histories in high cycle fatigue by introducing a factor to represent the distribution of activated slip directions and also captures the variability of the activation level. Here, it is assumed that the critical shear stress is a random variable. In this approach, it is assumed that slip directions become active when the shear stress amplitude T_a exceeds the critical yield strength. Doudard et al. used Poisson point process [74, 75] to describe the activation and the average density of active sites λ is given as:

$$\lambda = \frac{1}{V_0 S_0^m} \int \left(2T_a\right)^m d\Theta \qquad 2.45$$

where m and $V_0 S_0^m$ are material-dependent parameters.

Equation 2.45 is integrated over all possible angles to account for all the space directions defined by the solid angle Θ. This model is identical to the Weibull law. However, Weibull uses the normal stress instead of the shear amplitude in describing material

failure. Doudard et al. defined the probability $P_{k,}$ (within a domain Ω of volume V) of finding k active sites as;

$$P_k = \frac{\left[N(\Omega)\right]^k}{k!}\exp\left[-N(\Omega)\right] \tag{2.46}$$

where $N(\Omega)$ is the average number of active sites given as;

$$N(\Omega) = \lambda V \tag{2.47}$$

The resulting probability of failure P_f is given as;

$$P_f = 1-\exp\left[-\frac{1}{V_0}\int\left(\frac{2T_a}{S_0}\right)^m \cos(\zeta)\,d\Theta dV\right] \tag{2.48}$$

This probabilistic framework can be used for both non-proportional loadings and multiaxial loading. It also accounts for scatter in HCF fatigue data through the distribution of the slip system and the variability in the slip system activation level.

Flaceliere and Morel [76] developed on the endurance criterion proposed by Papadopoulos [77] and defined equivalent stress as a function of the quadratic mean value of resolved shear stress T_a and the maximum hydrostatic pressure as;

$$\sigma_{eq} = M_\sigma + p\sum\nolimits_{H,\max} \tag{2.49}$$

where M_σ is the quadratic mean value of resolved shear stress T_a, p is the coefficient reflecting the sensitivity to hydrostatic stress and $\sum_{H,\max}$ is the maximum hydrostatic pressure over a loading period. This equivalent stress is applicable to any complex stress states (in-phase or out of phase loading). Therefore, the probability of failure is given as;

$$P_f = 1-\exp\left[-\frac{1}{V_0}\int_v \frac{\sqrt{\langle T_a^2\rangle} + p\sigma_{H,\max}}{\sigma_0}\,dV\right] \tag{2.50}$$

where V_0 is the reference volume and σ_0 is the damage threshold stress level. Flaceliere and Morel [76] also investigated the stress gradient and surface effects in probabilistic fatigue failure. Based on Papadopoulos proposal [33], they used an equivalent stress function dependent on the normalized gradient of the maximum hydrostatic stress given as;

$$\sigma_{eq,S} = M_\sigma + p\left(1-\beta\left\langle\frac{G}{\sum_{H,\max}}\right\rangle^n\right)\sum_{H,\max} \tag{2.51}$$

with

$$G = \sqrt{\left(\frac{\partial\sum_{H,\max}}{\partial x}\right)^2+\left(\frac{\partial\sum_{H,\max}}{\partial y}\right)^2+\left(\frac{\partial\sum_{H,\max}}{\partial z}\right)^2} \tag{2.52}$$

n is a constant assumed to be 1 while β is a normalized hydrostatic stress intensity factor. The surface stress Weibull function is then defined as;

$$P_f(\sigma_{eq,S}) = 1-\exp\left[-\frac{1}{S_0}\int_s\frac{\sigma_{eq,S}\left(\sigma,G\left(\sigma_{H,\max}\right)\right)}{\sigma_0}dS\right] \tag{2.53}$$

where S_0 is the reference surface area and $\sigma_{eq,S}\left(\sigma,G\left(\sigma_{H,\max}\right)\right)$ is as given in Equation 2.26. The authors demonstrated a good correlation between the surface model approach and the experimentally determined failure probability for GS52 nodular cast iron and C36 mild steel. However, wide discrepancies were noted between the surface and volume approaches when applied to the nodular cast iron due to the presence of pores ranging in size from 50-1000 μm [76].

Thomas et al. [78] developed a probabilistic approach for high cycle multiaxial fatigue by the combination of a three- parameter Weibull distribution with the deterministic energy-based and volumetric high-cycle multiaxial fatigue criterion

proposed by Banvillet et al. [79, 80]. To account for the multiaxiality of the stresses, the Weibull stress is replaced by the strain work density per loading cycle. The resulting failure probability is given as;

$$P_f\left(V,\sigma\right)=1-\exp\left[-\frac{1}{V_0}\int_v\left(\frac{\left\langle W_g-W_g^*\right\rangle}{W_u}\right)^m dV\right] \tag{2.54}$$

where V_0 is the reference volume, W_g is the strain work density given to the material per loading period, W_g^* is the threshold value of W_g, W_u is a scale parameter and m is the Weibull slope. The predictions by the proposed probability framework are in good agreement with experimental probability distribution when applied to five materials investigated: the 30NiCrMo16 and 35CrMo4 quenched and tempered steels, the C20 annealed steel, the EN-GJS800-2 nodular cast iron and the Ti-6Al-4V titanium alloy. Thomas et al. [78] also investigated the size-effect which is usually linked to stress-strain gradient in high cycle fatigue as shown by Papadopoulos [34] and he gave the probability of failure in fully reversed tension for a smooth component as;

$$P_f\left(V,\sigma_a\right)=1-\exp\left[-\frac{V}{\varphi_u}\left\langle\frac{\left(\sigma_a\right)^2}{E}-W_g^*\right\rangle^m\right] \tag{2.55}$$

where V is the component volume, σ_a is the normal stress amplitude, E is the young modulus, and

$$\varphi_u=V_0W_u^m \tag{2.56}$$

2.6 Chapter Summary

This chapter presents a review of the existing probabilistic framework for probability of failure and their associated fatigue notch factor where applicable. A number of the statistically distributed variables used in constructing the probabilistic argument for failure include: distribution of microvoids [50], microplasticity [51], fatigue indicator parameter [27], total strain amplitude and fatigue life for a given strain amplitude [58] etc. Most of the frameworks considered were developed based on Weibull weakest link theory which assumes the existence of statistically distributed defects at the surface or in the bulk volume of the material and the occurrence of crack initiation at the largest defect. Other hypotheses on which the theory is based include: the material is considered as a combination of links, formation of crack in a link induces the crack of the entire structure, and lastly it is assumed that there are no interaction between defects. The probabilistic frameworks are adjudged more realistic than classical methods of determine fatigue notch factor because of their ability to capture the problem of scatter in fatigue failure.

CHAPTER 3

MATERIALS AND CRYSTAL PLASTICITY MODELING

3.1 Nickel Base Super Alloy

Nickel base superalloy has been identified as the most suitable material in high temperature applications requiring significant resistance to loading under fatigue, creep and static conditions [81, 82, 83]. Turbine engine discs are fabricated by machining of superalloys forging. The nickel base superalloy billets to be forged can be prepared by two different approaches: the conventional ingot metallurgy and the powder processing cast and wrought product. The ingot metallurgy procedure involves vacuum induction melting, followed by electro-slag refining and vacuum arc remelting; this is then followed by annealing to improve the compositional homogeneity of the billets. The billets are then thermal-mechanically worked before been subjected to different forging operations [84] (Figure 3.1). In general the choice of method to be used is dependent on a number of factors but largely on the chemistry of the chosen superalloy [85]. One common example of alloys processed by ingot metallurgy is IN718 because the levels of its strengthening elements Al, Ti and Nb are relatively low which renders additional cost associated with powder processing unjustifiable.

On the other hand, powder processing involves vacuum induction melting, followed by remelting and inert gas atomization to produce powder. Large non metallic inclusions are excluded by sieving the powder. The powder is then prepared in billets ready for forging by sealing it into a can. It is then degassed and sealed before extrusion

(Figure 3.2). When components made of various different chemical constituents are involved, powder metallurgy is preferred in order to reduce individual phase segregation. However, the presence of nonmetallic ceramic inclusions has been identified as limiting factor in the fatigue performance of powder metallurgy nickel base superalloy [66, 67]. These inclusions find their way into the molten metal due to spalling or erosion of the crucible prior to the gas atomization process for producing the powder [86, 87].

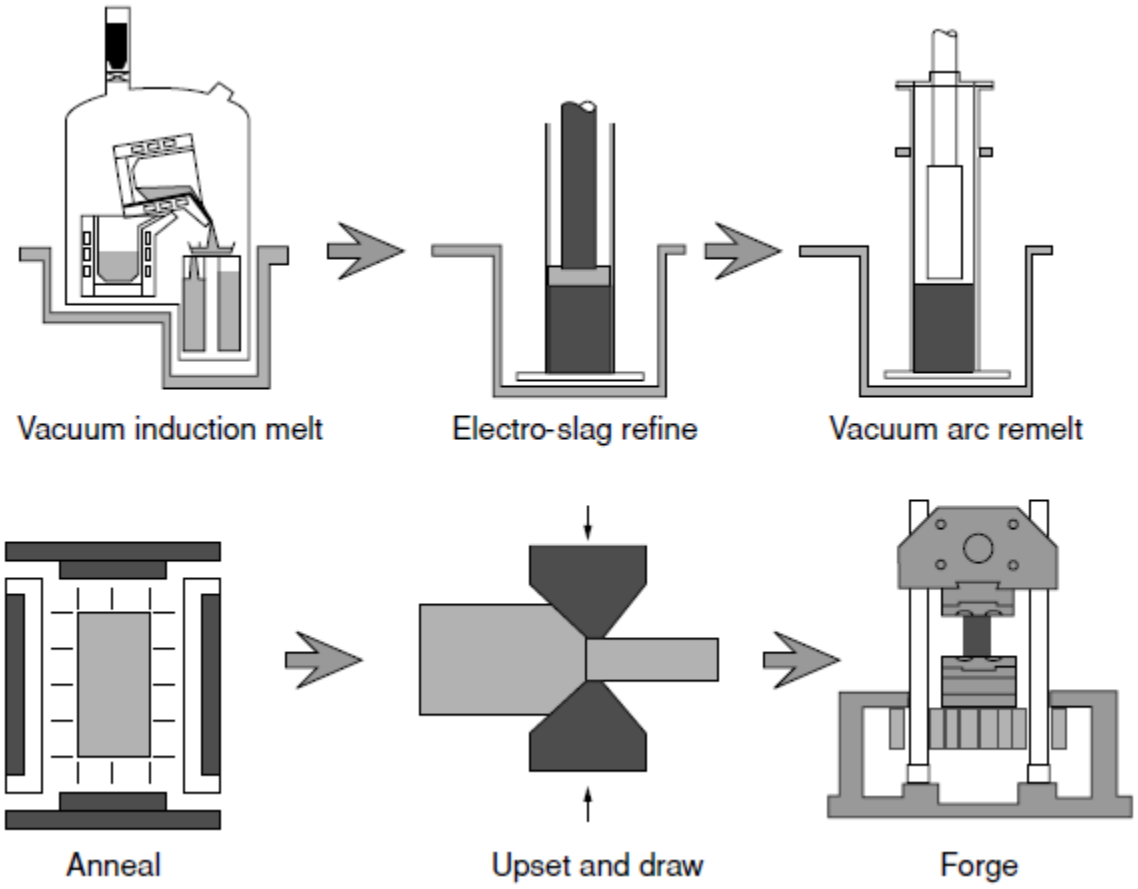

Figure 3.1. Procedural steps of producing turbine disc alloys by ingot metallurgy **[88]**.

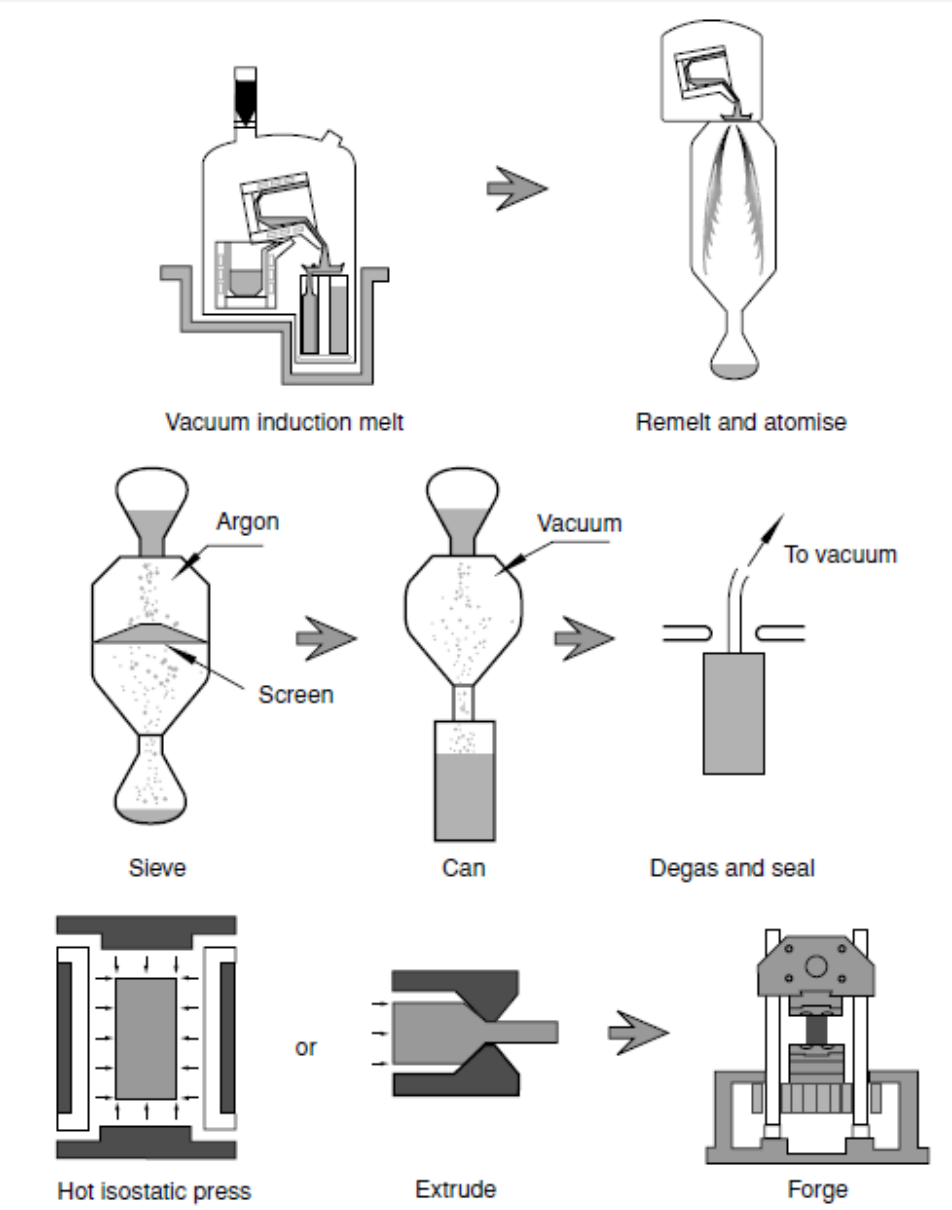

Figure 3.2. Procedural steps of producing turbine disc alloys by powder metallurgy techniques **[88]**.

3.1.1 The Physical Metallurgy of Nickel and Its Alloys

Nickel has atomic number of 28, atomic weight of 58.71 and five stable isotopes. It has a face-centered cubic (FCC) structure from room temperature to the melting point,

$1455\,^{0}C$, which is the absolute temperature capability of nickel-based superalloys and density of $8907\,kg/m^3$.

The microstructure of a typical superalloy comprises of different phases which include:

a. The gamma phase, which is denoted by γ. This forms the matrix phase in which other phases resides and it exhibits the FCC structure. It is made up of elements such as cobalt, chromium, molybdenum, ruthenium and rhenium since they prefer to reside in this phase.
b. The gamma prime precipitate, which is denoted by γ'. This is rich in elements such as titanium, tantalum and aluminum and it forms as a precipitate phase with a coherent structure with the $\gamma-$matrix.
c. Carbides and borides. Carbon and boron combine with reactive elements to form MC carbides and borides which prefer to reside on the $\gamma-$grain boundaries.

Strengthening of the superalloy can be achieved via different modes which include: solid solution strengthening of the γ matrix and γ' precipitates, grain size hardening of primary γ' precipitates and γ matrix and lastly strengthening due to dislocation interactions. γ' precipitates often have three different size distributions ($\approx 1.0,\ \approx 0.1$, and $\approx 0.01\,\mu m$ in diameter) and are referred to as primary, secondary and tertiary precipitates. These precipitates form at different stages of heat treatment; the primary γ' precipitates form at the first step of heat treatment (subsolvus heat treatment) while secondary and tertiary precipitates typically form during cooling and subsequent aging.

3.1.2 Grain Size Hardening

Grain size hardening is linked with variations in grain size and is the most commonly experienced hardening mechanism. In IN100, high-angle grain boundaries, which serve as sources of dislocation and deformation barriers, are present both between $\gamma - \gamma'$ grains and between the large primary γ' precipitates. Using Hall-Petch relation [89], the grain size hardening effect on a volume fraction occupied by the grain is given as:

$$\Delta\sigma = \frac{2}{3} f k_y d_m^{-1/2} \tag{3.1}$$

where $\Delta\sigma$ is the strengthening increment due to grain size hardening, d_m is the average grain size, f is the volume fraction occupied by the grain, and k_y is the Hall-petch constant. In IN100, only 2/3 of the primary γ' are in contact with adjacent primary γ' precipitate hence the 2/3 in Equation 3.1.

3.1.3 Solid-Solution Strengthening of γ Matrix

Gypen and Deruyttere [90] proposed a theory for solid solution strengthening of nickel matrix. The theory assumes a superposition of strengthening of individual solutes which exhibits individual differing potencies [91, 92, 93, 94]. Solute spacing is proportional to the square root of concentration. Hence, the strengthening is given as:

$$\Delta\sigma = \sum_i \left(\frac{d\sigma}{\sqrt{dC_i}} \sqrt{C_i} \right) \tag{3.2}$$

where $\frac{d\sigma}{\sqrt{dC_i}}$ is a constant that reflects the strengthening potency of each alloying element.

3.1.4 Strengthening Caused by Dislocation Interactions

When there is shearing of IN100 γ' precipitate, the dislocation has to move in pair to maintain the ordered $L1_2$ FCC structure of the γ' precipitate of IN100. Factors that determine the interaction dislocation with the γ' precipitate include the size of the precipitate and the antiphase boundary (APB) energy (i.e equilibrium spacing of the paired dislocations). When the pair of dislocation does not lie within the same precipitate, it is referred to as weak pair coupling (Figure 3.3a). When the pair of dislocation lie within the same precipitate (for large precipitates) it is referred to as strong pair coupling (Figure 3.3b). In both cases, the formation of APB is responsible for the strengthening increment. The schematic representation of the comparison of required stress to drive a pair of dislocation through the precipitate as a function of precipitate size for the two cases is presented in Figure 3.3c.

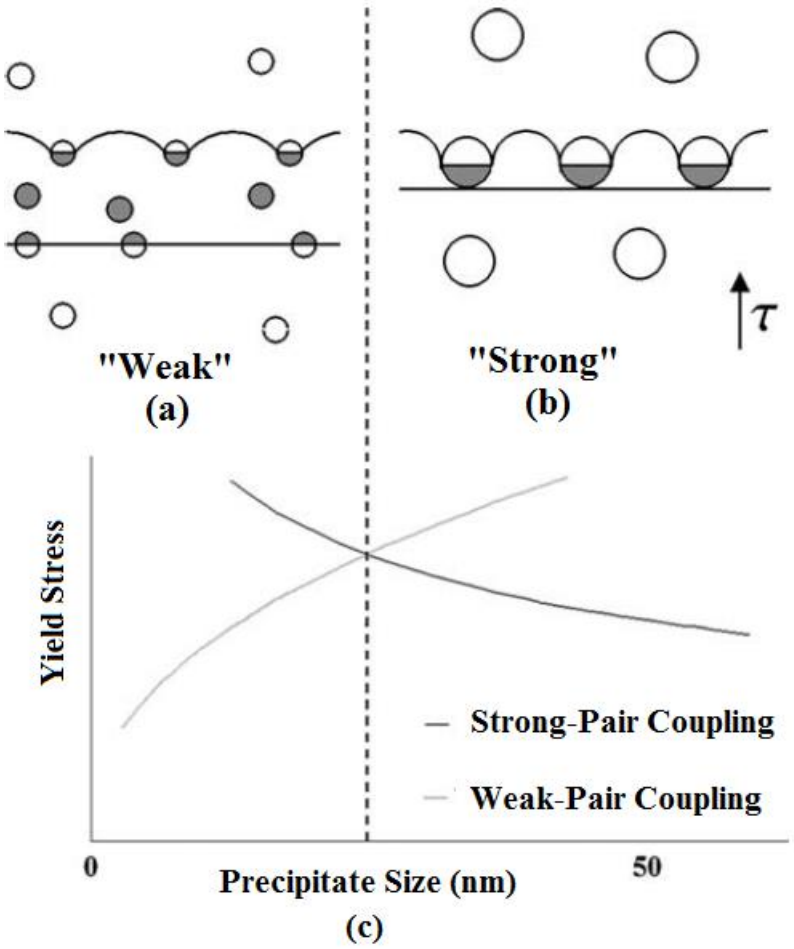

Figure 3.3. (a) weak pair coupling configuration of dislocations and precipitates, (b) strong pair coupling configuration of dislocations and precipitates, and (c) Stress required to drive dislocation as a function of the precipitate size **[95]**.

3.2 Key Material Microstructure and Composition of IN100

Over the years, attempts have been made to optimize the range of mechanical properties of polycrystalline superalloys of complex microstructure used for turbine disk applications [96, 97, 98, 99]. IN100 has a very complex microstructure, consisting of over ten constituent elements (Table 3.1) and is often developed using powder metallurgy techniques. The typical heat treatment procedure for IN100 is as given in Figure 3.4. The

heat treatment involve subsolvus or supersolvus heat treatment at $1185^{0}C$, this is followed by stabilization and aging heat treatment. The final microstructure of the alloy is established by these three heat treatments.

Table 3.1

Chemical Composition of IN100 and Its Phases [100]

Alloy/Phase	Ni	Al	Cr	Co	Mo	Ti	V	Fe	C	Zr	B
IN100	56.0	4.9	12.3	18.3	3.3	4.3	0.70	0.10	0.06	0.02	0.02
γ matrix	38.7	2.25	24.5	27.8	5.73	0.93	0.05	-	-	-	-
γ' ppt	71.8	7.06	2.59	8.94	1.42	6.97	1.23	-	-	-	-

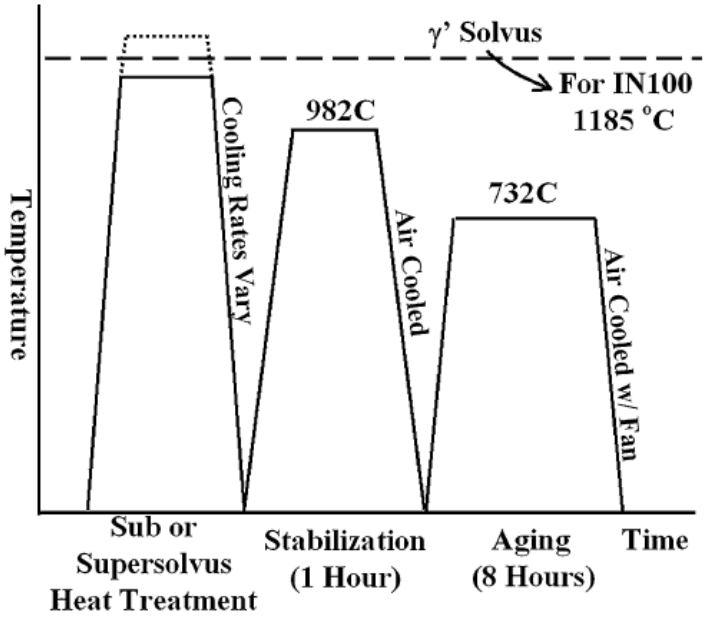

Figure 3.4. Typical heat treatment process for Nickel base Sueperalloy **[100]**.

The deformation mechanism for IN100 at the microstructure is similar for other nickel base superalloys and can be summarized as follows [101]:

1. As the temperature increases, the yield strength also increase for both tension and compression up to a peak temperature of $750\,^{0}C$, beyond which the yield strength decreases (Figure 3.5).

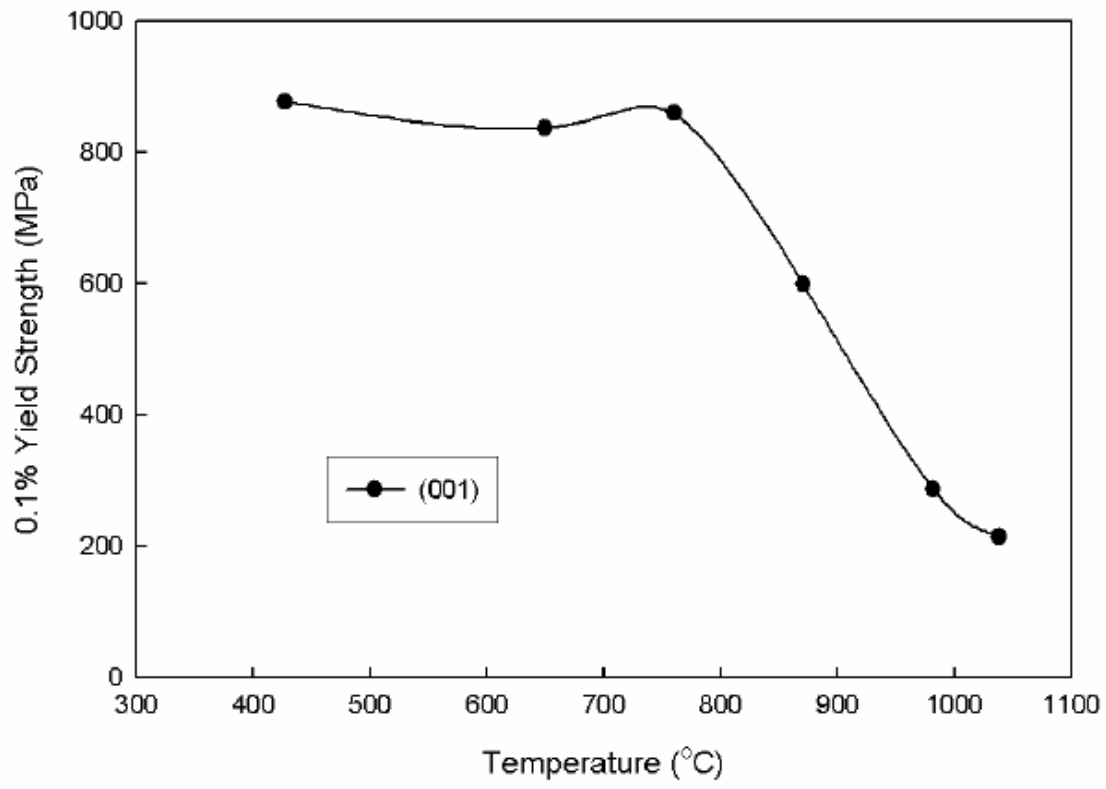

Figure 3.5. Variation of yield strength of Nickel base super alloy with temperature in the longitudnal (001) orientation **[102]**.

2. Generally, slip is dictated by the resolved shear stresses in the favorable crystallographic slip planes. However, Schmid's law is not obeyed in all orientations; orientations with similar Schmid factor (e.g <001> and <011>) have different yield strength. Also, slip on any plane can also be a function of the resolved stresses on other planes resulting from dislocation core propagating effects in the γ'.

3. For the different orientations (<001>, <011> and <111>), the yield strength differ at a given temperature in tension and compression over a certain temperature range. This asymmetry (magnitude and sense) depend on both temperature and orientation [103, 104, 105, 106, 107]. The <001> is stronger in tension compared to compression, while for <011> and <111> they are stronger in compression compared to tension. This tension- compression asymmetry is most conspicuous between room temperature and peak temperature range while it is less obvious at higher and lower temperatures.
4. Stress-strain curves exhibit a unique transition to plasticity especially at the two extreme temperatures (highest and lowest temperatures). The hardening effect on the yield strength is reversible with increasing temperature. A sample first deformed at high temperature with high yield strength and then deformed at low temperature will exhibit a material response similar to a virgin material deformed at the lower temperature [108].

All these mechanisms must be accounted for by the constitutive equations that will be used to model the deformation of the superalloy.

3.3 Crystal Plasticity Modeling of Nickel Base Super Alloy

A crystal plasticity constitutive model developed by Mahesh [102] is used in this work. The model captures the orientation dependent material response and it is rate dependent and microstructure sensitive. Rate dependent method is employed for the model because as the temperature increases, strain rate effects become increasingly important. Physically-based hardening models are employed on the basis of dislocation-

precipitate interactions already discussed under strengthening caused by dislocation interactions.

From a continuum mechanics point of view [109, 110, 111, 112, 113, 114, 115] and from a material science point of view [116, 117, 118], the deformation of the crystal is taken as the cumulative effect of two independent atomic mechanisms (Figure 3.6): (a) elastic distortion of the lattice denoted by F^e and (b) plastic deformation F^p which does not disturb the geometry of the lattice. The elastic portion accounts for both the reversible elastic stretch and the rigid body lattice rotation while the plastic portion accounts for dislocation glides along the crystallographic planes. The plastic deformation is associated with the change in grain shape but not its crystal lattice and it is formed due to dislocation motion.

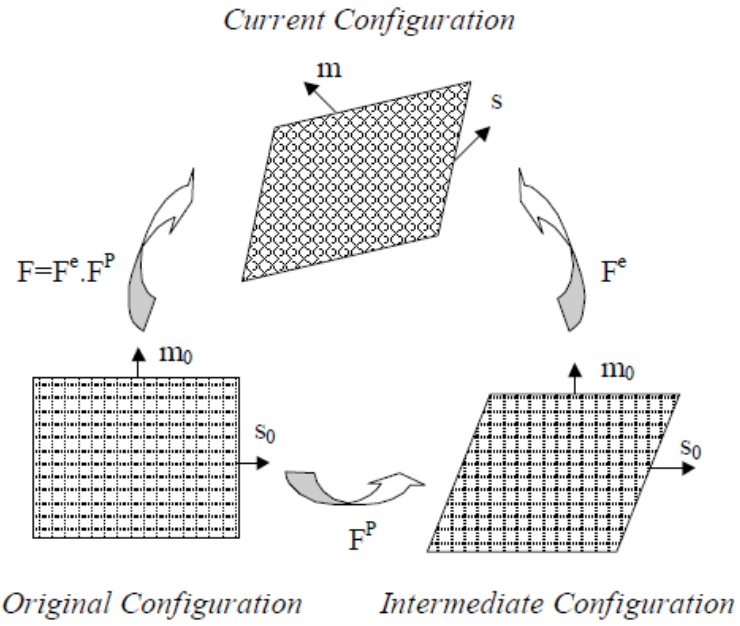

Figure 3.6. Elastic-plastic decomposition of the deformation gradient **[109, 119]**

The governing variables of the constitutive model are: (a) deformation gradient, F, (b) 2nd Piola Kirchhoff stress, σ^{pk2}, (c) crystal slip systems labeled by integers, α, (d) slip system unit normal, s^{α}, to the slip plane, (e) unit vector, m^{α}, which gives the slip direction, (f) plastic gradient of deformation, F^{p}, with $\det\left(\mathrm{F}^{p}\right)=1$, (g) slip resistance or threshold for slip system, K^{α}, with unit of stress, and (h) the back stress or slip system kinematic stress, χ^{α}.

A multiplicative rule is employed for the decomposition of the deformation gradient, F, and it is given as [109, 119]:

$$\mathrm{F}=\mathrm{F}^{e}\cdot\mathrm{F}^{p} \tag{3.3}$$

Since incompressibility is maintained in the dislocation glide (i.e $\det\left(\mathrm{F}^{p}\right)=1$), the stress power per unit reference volume of the isoclinic relaxed configuration determined by F^{p} is given as:

$$\dot{\omega}=\sigma^{pk1}:\dot{\mathrm{F}} \tag{3.4}$$

where σ^{pk1} is the first Piola-Kirchhoff stress and it is expressed as $\sigma^{pk1}=\det\left(\mathrm{F}\right)\sigma\cdot\mathrm{F}^{-T}$. The stress power may be decomposed into elastic and plastic component as:

$$\dot{\omega}=\dot{\omega}^{e}+\dot{\omega}^{p} \tag{3.5}$$

where $\dot{\omega}^{e}$ is the elastic stress power per unit volume of the intermediate configuration and it is expressed as $\dot{\omega}^{e}=\sigma^{pk2}:\dot{\varepsilon}^{e}$, with $\dot{\varepsilon}^{e}$ and σ^{pk2} being the Green elastic strain and the second Piola- Kirchhoff stress respectively and they are expressed as:

$$\varepsilon^{e}=\frac{1}{2}\left(F^{eT}\cdot F^{e}-1\right) \tag{3.6}$$

$$\sigma^{pk2}=\det\left(F^{e}\right)F^{e-1}\cdot\sigma\cdot F^{e-T} \tag{3.7}$$

Conversely, $\dot{\omega}^p$ is the plastic stress power per unit volume of the intermediate configuration and it is expressed as:

$$\dot{\omega}^p = \left(F^{eT} \cdot F^e \cdot \sigma^{pk2}\right) : \left(\dot{F}^p \cdot F^{p-1}\right) \tag{3.8}$$

For a linear elastic behavior with the assumption of small elastic strains i.e. $\varepsilon^e \approx E^e$, the constitutive equation (linear hyperelastic relation) is given as:

$$\sigma^{pk2} = C : \left(\varepsilon^e\right) \tag{3.9}$$

where C is ranked anisotropic elasticity tensor of fourth order.

Considering a slip plane with unit normal vector m_0^α and slip direction unit vector s_0^α for each of the slip systems (α) in the reference configuration, the plastic velocity gradient ($\hat{L}^p$) is obtained as the sum total of all the slip systems in the intermediate configuration and it is expresses as:

$$\hat{L}^p = \dot{F}^p \cdot F^{p-1} = \hat{D}^P + \hat{W}^p = \sum_{\alpha=1}^{N_{slip}} \dot{\gamma}^\alpha \left(s_0^\alpha \otimes m_0^\alpha\right) \tag{3.10}$$

where $\dot{\gamma}^\alpha$ is the shearing rate for each of the active slip system (α). $\hat{D}^p$ and $\hat{W}^p$ are the plastic rate of deformation and plastic spin respectively for the intermediate configuration and they are expressed as the symmetric and anti-symmetric parts of the plastic gradient:

$$\hat{D}_{ij}^p = \frac{1}{2}\left(\hat{L}_{ij}^p + \hat{L}_{ji}^p\right) \tag{3.11}$$

$$\hat{W}_{ij}^p = \frac{1}{2}\left(\hat{L}_{ij}^p - \hat{L}_{ji}^p\right) \tag{3.12}$$

Relationship exists between the slip system normals and directions in the current configuration and that of the reference configuration and it is given as $s^{\alpha} = F^{e} \cdot s_0^{e}$ and $m^{\alpha} = m_0^{\alpha} \cdot F^{e-1}$.

From Equation 3.10, the plastic shearing rate as given by Orowan [120] is expressed as:

$$\dot{\gamma}^{\alpha} = \rho_m^{\alpha} b \bar{v}^{\alpha} \tag{3.13}$$

where ρ_m^{α} is the density of mobile dislocation, b is the burgers vector and $\bar{v}^{\alpha}$ is the average velocity of the burgers vector.

Using Equations 3.8 and 3.10, the relation $\dot{\omega}^{p} = \sum_{\alpha} \tau^{\alpha} \dot{\gamma}^{\alpha}$ can be used to define the resolved shear stress, τ^{α}, for α slip system. Thus, the resulting resolved shear stress for each slip system is expressed as:

$$\tau^{\alpha} = \left(F^{eT} \cdot F^{e} \cdot \sigma^{pk2} \right) : \left(s_o^{\alpha} \otimes m_0^{\alpha} \right) \tag{3.14}$$

For material with a very small elastic strain, $F^{eT} \cdot F^{e} \approx 1$ and the second Piolar-Kirchhoff stress tensor, σ^{pk2}, can be replaced by the Cauchy stress tensor, σ. Thus Equation 3.14 becomes:

$$\tau^{\alpha} = \sigma : \left(s^{\alpha} \otimes m^{\alpha} \right) \tag{3.15}$$

The shearing rate on each slip system, using a two-term potential flow rule, is expressed as:

$$\dot{\gamma}^{\alpha} = \left[\dot{\gamma}_1 \left\langle \frac{\left| \tau^{\alpha} - \chi^{\alpha} \right| - \kappa^{\alpha}}{D^{\alpha}} \right\rangle^{n_1} + \dot{\gamma}_2 \left\langle \frac{\left| \tau^{\alpha} - \chi^{\alpha} \right|}{D^{\alpha}} \right\rangle^{n_2} \right] \operatorname{sgn}\left(\tau^{\alpha} - \chi^{\alpha} \right) \tag{3.16}$$

where $\dot{\gamma}_1$ and $\dot{\gamma}_2$ are constants, the flow exponents are represented as n_1 and n_2, κ^{α} is the slip resistance on each slip system and it is called the mechanical threshold [117], D^{α} is

the average drag resistance, χ^{α} is the back stress on each slip system. The back stress, unlike for pure single crystal, are very important component for two phase materials such as Nickel base superalloys and thus cannot be neglected [121]. It is also important to note that the back stress is subtracted from the applied shear stress to reflect the net force responsible for driving the dislocation. The threshold stress accounts for the anomalous yield behavior of the $\gamma - \gamma'$ nickel base superalloy, i.e, the increase in yield stress resulting from increase in temperature in the intermediate temperature range.

The first part of Equation 3.16 accounts for the dominant cyclic behavior where the threshold stress plays the role of the yield stress. Conversely, the second part of Equation 3.16 accounts for the effect of creep thermally activated at lower stresses. When the first term is not active, especially at lower stresses, matrix faulting and dissociation of heterogeneous plastic dislocation control the dominant flow mechanism. Complex cyclic stress – strain history like that of nickel base superalloy is best modeled by the two term flow rule presented in Equation 3.16.

A total of 18 slip systems are used to model dislocation motion within the matrix of nickel base super alloy; 12 octahedral slip systems and 6 cube slip systems. A list of the slip systems is provided in Table 3.2.

Table 3.2

Slip systems in nickel base superalloy [102]

Slip System	Octahedral Slip		Cube Slip	
∝	Slip Plane	Slip Direction	Slip Plane	Slip Direction
1	$\{111\}$	$\langle 01\bar{1}\rangle$	$\{100\}$	$\langle 011\rangle$
2	$\{111\}$	$\langle \bar{1}01\rangle$	$\{100\}$	$\langle 01\bar{1}\rangle$
3	$\{111\}$	$\langle 1\bar{1}0\rangle$	$\{010\}$	$\langle 101\rangle$
4	$\{1\bar{1}\bar{1}\}$	$\langle 0\bar{1}1\rangle$	$\{010\}$	$\langle 10\bar{1}\rangle$
5	$\{1\bar{1}\bar{1}\}$	$\langle \bar{1}0\bar{1}\rangle$	$\{001\}$	$\langle 110\rangle$
6	$\{1\bar{1}\bar{1}\}$	$\langle 110\rangle$	$\{001\}$	$\langle \bar{1}10\rangle$
7	$\{\bar{1}1\bar{1}\}$	$\langle 011\rangle$		
8	$\{\bar{1}1\bar{1}\}$	$\langle 10\bar{1}\rangle$		
9	$\{\bar{1}1\bar{1}\}$	$\langle \bar{1}\bar{1}0\rangle$		
10	$\{\bar{1}\bar{1}1\}$	$\langle 0\bar{1}\bar{1}\rangle$		
11	$\{\bar{1}\bar{1}1\}$	$\langle 101\rangle$		
12	$\{\bar{1}\bar{1}1\}$	$\langle \bar{1}10\rangle$		

The 12 octahedral slip systems are the active at lower temperatures within the γ matrix which is typical of a FCC lattice structure. However, at higher temperatures and higher resolved shear stresses, the 6 cube slip systems are activated in the γ' phase though their role is not yet well understood and characterized. The role of the cube slip system in the homogenized $\gamma-\gamma'$ single crystal is best appreciated by the inability of the octahedral slip in modeling the stress –strain – time behavior as a function of temperature. Two sources of cube slip have been indentified which include: (a) zig-zag octahedral slip formation in the γ - matrix at the $\gamma-\gamma'$ interface and (b) the manifestation

of actual cube slip at higher temperatures in the γ' precipitates along orientations close to $[111]$ [122]. Bettge and Osterle [123] have established that the cube slips are actually due to thermal activation of the zig-zag cross slip of screw dislocations. The screws dislocations are blocked at the $\gamma - \gamma'$ interface as they migrate through the γ' precipitate channels causing the zig-zag cross slip mechanism as shown in Figure 3.7. Hence, at elevated temperatures, there is complicated interaction of dislocations created by cross slip which result in an increased dislocation density and restricts the motion of mobile dislocations. Therefore, in this model, two internal state variables are employed to describe the nickel base superalloy microstructure namely dislocation density and the back stress. Based on the afore-discussed slip systems, 18 slip systems are modeled in IN100.

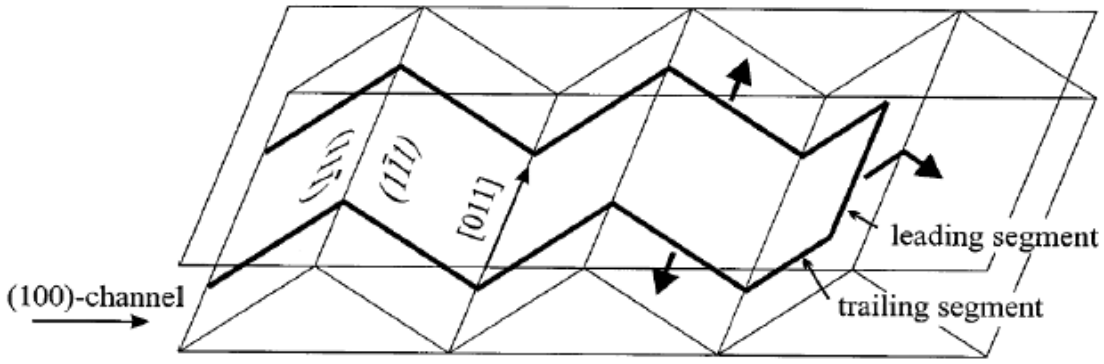

Figure 3.7. Schematic of interfacial zig-zag motion of screw dislocations **[123]**

Taylor relation is assumed for the hardening of the threshold stress on each of the slip system and it is expressed as:

$$\kappa^{\alpha} = \kappa_0^{\alpha} + \alpha_t \tilde{\mu} \tilde{b} \sqrt{\rho^{\alpha}} \qquad 3.17$$

where each slip system dislocation density is represented as ρ^{α} (for both cube and octahedral slip systems), $\tilde{\mu}$ is the shear modulus and it is govern by a rule of mixtures, $\tilde{b}$ is the effective burgers vector, α_t is a coefficient which accounts for the statistical arrangement of the dislocation population.

From Equation 3.17, the shear modulus is expressed as:

$$\tilde{\mu} = \left(f_{p1} + f_{p2} + f_{p3} \right) \mu_{\gamma'} + f_m \mu_m \tag{3.18}$$

where f_{p1}, f_{p2}, f_{p3} are the volume fractions of the three γ' matrix phases respectively i.e primary, secondary and tertiary while f_m is the volume fraction of the matrix phase. Also the effective burgers vector is expressed as:

$$\tilde{b} = \left(f_{p1} + f_{p2} + f_{p3} \right) b_{\gamma'} + f_m b_m \tag{3.19}$$

where $b_{\gamma'}$ is the burger vector of the γ' precipitates and b_m is the burger vector of the matrix.

The initial critical resolved shear stress (CRSS), $\kappa_{0,\lambda}^{\alpha}$, as given by Reppich et al. [124, 125] is expressed as:

$$\begin{aligned} \kappa_{0,oct}^{\alpha} &= \left[\left(\tau_{0,oct}^{\alpha} \right)^{n_\kappa} + \Psi_{oct} \left(f_{p1}, d_2, f_{p2}, d_3, f_{p3} \right)^{n_\kappa} \right]^{1/n_\kappa} + \left(f_{p1} + f_{p2} \right) \tau_{ns}^{\alpha} \\ \kappa_{0,cub}^{\alpha} &= \left[\left(\tau_{0,cub}^{\alpha} \right)^{n_\kappa} + \Psi_{cub} \left(f_{p1}, d_2, f_{p2}, d_3, f_{p3} \right)^{n_\kappa} \right]^{1/n_\kappa} \end{aligned} \tag{3.20}$$

where,

$$\Psi_{oct} = \Psi_{cub} = \left[c_{p1} \sqrt{\zeta \frac{f_{p1}^{'}}{d_1}} + c_{p2} \sqrt{\zeta \frac{f_{p2}^{'}}{d_2}} + c_{p3} \sqrt{\zeta f_{p3}^{'} d_3} + \frac{c_{gr}}{\sqrt{d_{gr}}} \right] \tag{3.21}$$

Here $\zeta = \frac{\Gamma_{APB}}{\Gamma_{APB,ref}}$ where Γ_{APB} is the anti-phase boundary energy. The primary, secondary and tertiary gamma prime precipitate sizes are represented by d_1, d_2 and d_3 respectively while the grain size is denoted as d_{grn}. $f_{p1}^{'}$, $f_{p2}^{'}$ and $f_{p3}^{'}$ are the normalized precipitate volume fractions. The value of exponent n_κ ranges from 1 – 1.2 and values of c_{p1}, c_{p2}, c_{p3} and c_{gr} are determined by curve fitting initial yield strength to the experimentally determined values.

Based on the work of Qin et al. [126, 127] and Shenoy et al. [128], the non-schmid stress, τ_{ns}^{α}, dependence of the octahedral slip systems is expressed as:

$$\tau_{ns}^{\alpha} = h_{pe}\tau_{pe}^{\alpha} + h_{cb}\left|\tau_{cb}^{\alpha}\right| + h_{se}\tau_{se}^{\alpha} \tag{3.22}$$

Here the resolved shear stress on the primary, secondary and cube slip systems are denoted by

$\tau_{pe}^{\alpha}, \tau_{se}^{\alpha}$ and τ_{cb}^{α} respectively while h_{pe}, h_{cb} and h_{se} are constants.

Feaugas et al. [129] have identified a direct proportionality between the rate of dislocation recovery and the dislocation density. Thus, the evolution of the dislocation density is expressed as [130]:

$$\dot{\rho}_{\lambda}^{\alpha} = h_0\left\{Z_0 + k_1\sqrt{\rho_{\lambda}^{\alpha}} - k_2\rho_{\lambda}^{\alpha}\right\}\left|\dot{\gamma}^{\alpha}\right| \tag{3.23}$$

and

$$Z_0 = \frac{k_\delta}{\tilde{b}d_{\delta eff}},\quad d_{\delta eff} \approx \left(\frac{2}{d_{2\delta}}\right)^{-1} \tag{3.24}$$

where $k_1\sqrt{\rho_\lambda^\alpha}$ is the dislocation storage and $k_2\rho_\lambda^\alpha$ is the dynamic recovery. k_1, k_2 and k_δ are constants, $d_{2\delta}$ is the secondary precipitate spacing and $d_{\delta eff}$ is the equivalent precipitate spacing. The hardening coefficient for cube and octahedral slip systems are given as $h_0 = 2.4$ and $h_0 = 4.8$ respectively.

Back stress is used to capture the effects of Bauschinger effect and it is expressed as [130]:

$$\dot{\chi}_\lambda^\alpha = C_\chi \left\{ \eta\tilde{\mu}\tilde{b}\sqrt{\rho_\lambda^\alpha}\,\mathrm{sgn}\left(\tau^\alpha - \chi_\lambda^\alpha\right) - \chi_\lambda^\alpha \right\} \left| \dot{\gamma}^\alpha \right| \tag{3.25}$$

and

$$\eta = \frac{\eta_0 Z_0}{Z_0 + k_1\sqrt{\rho_\lambda^\alpha}} \tag{3.26}$$

where C_χ is a fitting parameter and η reflects the relative proportion of geometrically necessary dislocations to total dislocation density.

3.4 Titanium Alloy

Titanium is widely known for its good resistance to corrosion and high strength to weight ratio. When alloyed with other metals and heat treated, it can achieve a wide range of attractive properties both at low and high temperatures. Titanium alloys exhibit high strength and creep resistance at high temperatures while at low temperatures, they exhibit high strength and fracture toughness.

At room temperature, an unalloyed titanium has hcp crystal structure but with increase temperature to the neighborhood of $882\,^0C$, it undergoes a change in phase from the hcp (α) phase to a bcc (β) phase. It is possible to produce a completely α- phase, β-phase, or a mixture of α and β phases by varying the alloying elements. In summary,

different microstructures can be realized for the same alloy by varying the processing parameters and heat treatment. Titanium is dual phase and it has the inherent problem of varying individual phases' properties due to different amount of alloying elements.

The hcp structure of titanium, unlike for fcc structured materials, has several planes which are favorable for occurrence of slip or twinning. In most hcp materials, basal (0001) and prismatic $\{10\bar{1}0\}$ have been identified as the primary slip planes with a closed packed direction $\langle 11\bar{2}0\rangle$ for the slip vector. Titanium has been identified to exhibit flow stress versus temperature anomaly as well as orientation dependent yielding according to the work of Naka et al. [131] . This phenomenon is modeled in the crystal plasticity codes presented in the following section.

3.5 Crystal Plasticity Modeling of Titanium Alloy

The crystal plasticity model used in this work follows the existing work of Mayeur et al. [132]. The framework is as described in Section 3.4 for nickel base superalloy. However, the flow rule and the hardening rule differ and these are presented in this section.

The relationship between the slip system shearing rate and the resolved shear stress of the α slip system is described by the power law flow rule given as:

$$\dot{\gamma}^{\alpha} = \dot{\gamma}_0 \left\langle \frac{\left|\tau^{\alpha} - \chi^{\alpha}\right| - \kappa^{\alpha}}{D^{\alpha}} \right\rangle^{M} \operatorname{sgn}\left(\tau^{\alpha} - \chi^{\alpha}\right) \qquad 3.27$$

Here, $\dot{\gamma}_0$ is the reference shearing rate, M is the inverse strain-rate sensitivity exponent which controls the rate sensitivity of flow, τ^{α} is the resolved shear stress, χ^{α} is the back

stress, κ^{α} is the length scale-dependent threshold stress and D^{α} is the drag stress. As developed by Zhang et al. [133], the drag stress is taken as a non-evolving constant, i.e. $D^{\alpha}=0$, while the back stress evolves according to an Armstrong-Frederick direct hardening/dynamic recovery type of equation, i.e.,

$$\dot{\chi}^{\alpha}=h\dot{\gamma}^{\alpha}-h_{D}\chi^{\alpha}\left|\dot{\gamma}^{\alpha}\right| \tag{3.28}$$

with $\chi^{\alpha}(0)=0$. The threshold stress is expressed as

$$\kappa^{\alpha}=\frac{\kappa_{y}}{\sqrt{d^{\alpha}}}+\kappa_{s}^{\alpha} \tag{3.29}$$

3.6 Three Dimensional Finite Element Implementation Procedure for Nickel Base Superalloy

The crystal plasticity model for nickel base superalloy presented in Section 3.3 is coded into ABAQUS 2006 UMAT based on the previous work by Mahesh [102]. The notched geometry modeled in this work is a v-notched cylindrical component schematically represented as shown in Figure 3.8. Different test cases are modeled which include: (a) nickel base specimen without inclusion (b) nickel base specimen with horizontal elliptical inclusion at varied distance from the notch root (c) nickel base specimen with inclusions at various orientations. Some of the material parameters for the nickel base superalloy in the crystal plasticity codes are obtained from Musinski [134] and Przybyla et al. [135] and are as presented in Table 3.3.

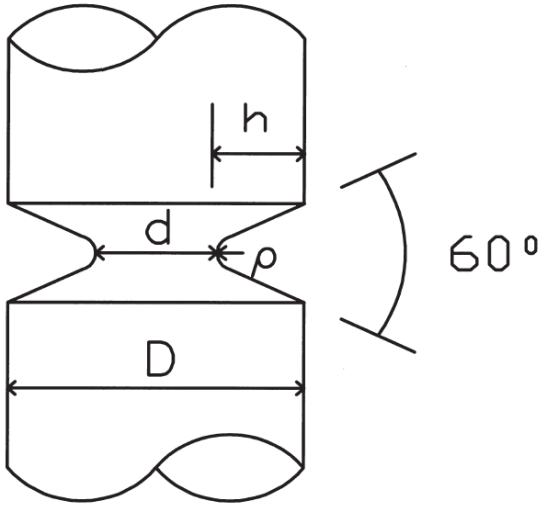

Figure 3.8. Gage section of the cylinderical specimen with a circumferential V-notch.

Table 3.3

Material parameter for nickel base superalloy constitutive model [134, 135]

$\tau^{\alpha}_{o,oct}$ (MPa)	$\tau^{\alpha}_{o,cub}$ (MPa)	c_{p1}	c_{p2}	c_{p3}	c_{gr}(MPa$\sqrt{\text{mm}}$	n_{κ}
85.1	170.2	1.351	1.351	$1.22*10^{22}$	9.432	1
$b_{\gamma'(nm)}$	$b_{\gamma(nm)}$	$\mu_{\gamma'(MPa)}$	$\mu_{\gamma(MPa)}$	$k_1(mm^{-1})$	k_2	$\rho^{\alpha}_{\lambda,o}(mm^{-2})$
0.25	0.41	81.515	130.150	$2.6*10^{5}$	8.2	10^{5}
h_o	h_{pc}	h_{cb}	h_{sc}	Γ_{APB}	η_o	k_{δ}
4.8 or 2.4	0.8	0	-0.4	$1.64*10^{-3}$	2.82	$2.5*10^{-3}$
$C_{11,\gamma'}$(MPa)	$C_{12,\gamma'}$(MPa)	$C_{44,\gamma'}$(MPa)	$C_{11,\gamma}$(MPa)	$C_{12,\gamma}$(MPa)	$C_{12,\gamma}$(MPa)	n_1
135,000	59,210	81,515	158,860	73,910	130,150	15
n_2	$\dot{\gamma}_1(s^{-1})$	$\dot{\gamma}_1(s^{-1})$	D^{α}(MPa)			
9	8.7	$3.9*10^{-11}$	150(oct) 180(cub)			

3.6.1 Nickel Base Specimen Without Inclusion

Due to symmetry in geometry and loading, only one-quarter of the notched cylindrical geometry is modeled. Three different notch root radii are modeled to investigate the effect of notch root radius on the fatigue notch factor of the notched specimens. The dimensions of the three test cases modeled are as given in Table 3.4.

Table 3.4

Dimensions of the notched specimens

Test Case	D (mm)	Notch radius, ρ (mm)	Notch depth, h (mm)	R-ratio
1	5	0.150	0.142	0.1
2	5	0.213	0.267	0.1
3	5	0.284	0.714	0.1

To determine the optimum element size to use for meshing the 3D model, mesh refinement study was conducted using a cube specimen and subjecting it to 568 MPa load which is one of the loads applied to the specimens according to the experimental data obtained from Weiju et al. [26]. The Von Mises stress converged at an element size of 64 μm and thus element size of 64 μm is used in meshing all nickel base superalloy specimens modeled. It is noted that the 64 μm falls within the range of grain size for nickel base superalloy which normally vary from 30 μm to 70 μm [136]. The model is meshed using 3D stress four-node linear tetrahedron element type (C3D4). The bottom of the model is encastre and symmetry boundary conditions are applied on the planes of symmetry of the geometry. Six steps are subsequently created for axial load application to form a 3 loading cycles. A complete model showing the applied boundary conditions and loading condition is as shown in Figure 3.9.

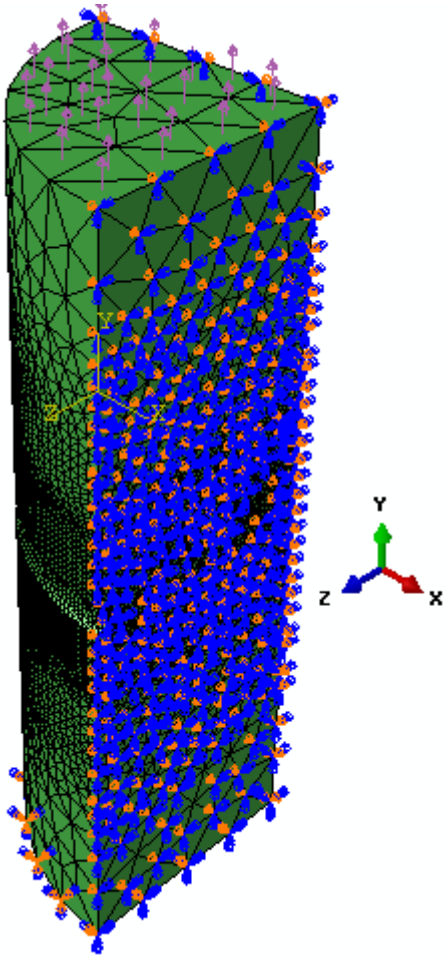

Figure 3.9. Model with notch root radius 0.150 mm and notch depth 0.142 mm showing load and boundary conditions application.

3.6.2 Nickel base specimen with horizontal elliptical inclusion at varied distance from the notch root

The metal carbide (MC) inclusions commonly found in nickel base superalloys are taken into consideration in this model. In this model, it is assumed that the shape of inclusions is elliptical with an aspect ratio, $A = a/b = 2$, where a and b are the major and minor axis of the ellipse respectively. Thus, the MC inclusions is modeled as horizontal inclusion of major axis 150 μm and minor axis 75 μm and assigned linear elastic material properties with Young's modulus 405 GPa and a Poisson's ratio of 0.14

[102] . Here, the full geometry is modeled because there is no symmetry in the geometry due to presence of inclusion though symmetry is still maintained in load application. The medium geometry is modeled and has diameter of 5 mm, notch root radius of 0.213 mm and notch depth of 0.267 mm with an applied stress of 568 MPa. The model is meshed using 3D stress four-node linear tetrahedron element type (C3D4) of size 64 μm as early established by the mesh refinement study conducted in the previous section. Four test cases (Table 3.5) are considered with the horizontal inclusion placed at different grain distances away from the notch root to investigate where the inclusion has maximum influence on the stress distribution in the vicinity of the notch root. The different test cases are as shown in Figure 3.10.

Table 3.5

Four test cases with inclusion at different distances from notch root radius

Test cases	Distance of Inclusion from Notch (grains)
1	10g
2	8g
3	6g
4	4g

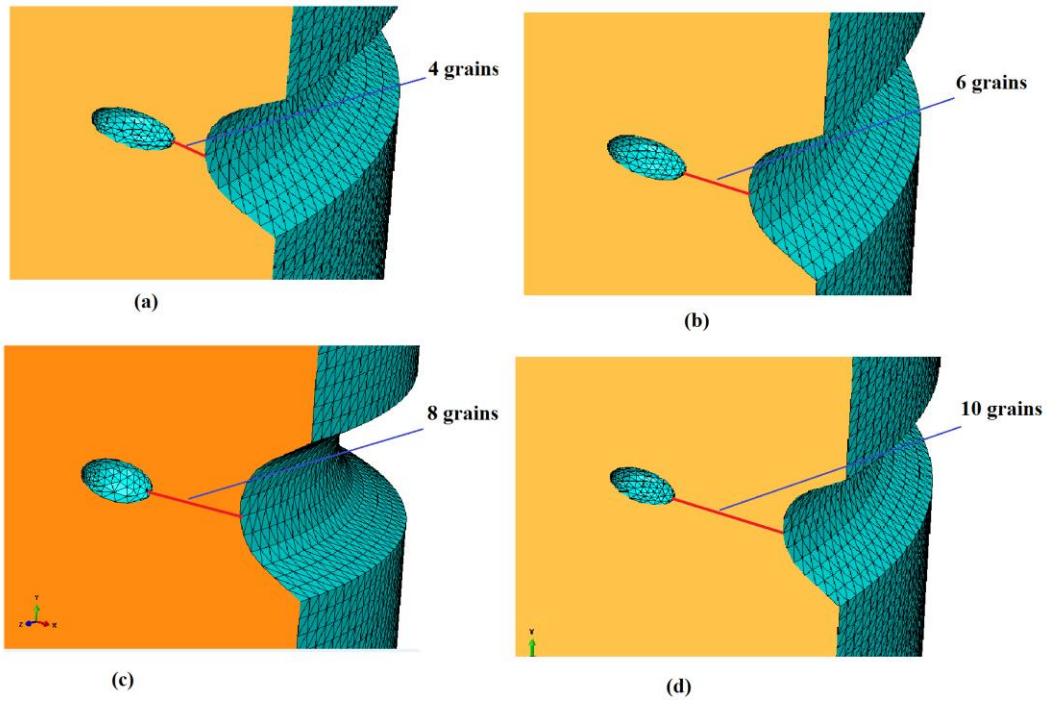

Figure 3.10. Inclusions at different grain distance from the notch root radius: (a) 4 grains, (b) 6 grains, (c) 8 grains, and (d) 10 grains.

3.6.3 Nickel base specimen with elliptical inclusion at various orientations

Here the effect of orientation of inclusion on probability of failure, fatigue notch factor and notch sensitivity index in nickel base superalloy is investigated. Three different orientations of inclusion are modeled, in the 3D matrix, which are horizontal, 45 degree rotation and 90 degree (vertical) rotation as shown in Figure 3.11. The inclusions for the three cases modeled are maintained at 8 grains distance from the notch root radius. This is because, from Section 3.6.2, 8 grain distance has been identified as the location where the inclusion has maximum influence on the stress distribution of the component. Linear elastic material properties are specified for the inclusion while the material parameters presented in the Section 3.6 were specified for the matrix. 3D stress four-

node linear tetrahedron element type is used in meshing the geometry and the bottom of the specimen is encastre and axial load of 568 MPa is applied at the top of the geometry.

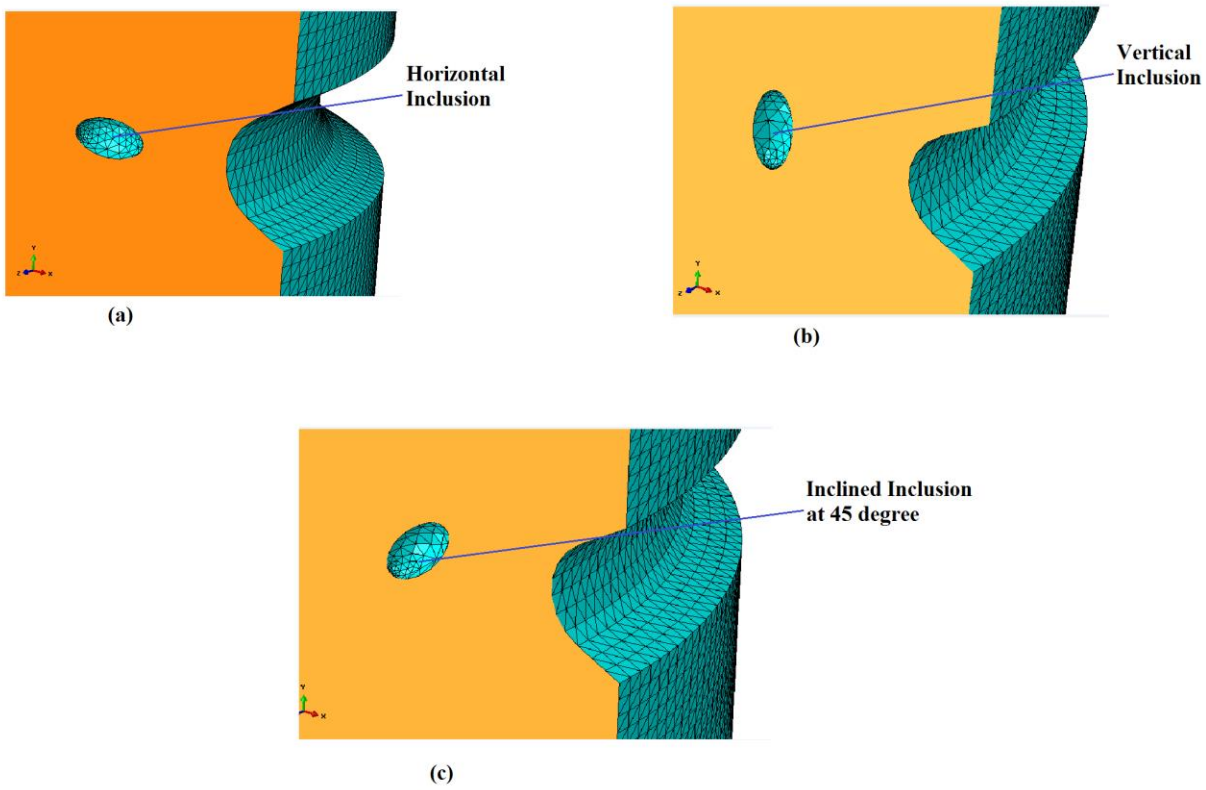

Figure 3.11. Different orientation of inclusion in the matrix: (a) horizontal (b) 90 degree rotation (vertical) and (c) 45 degree rotation.

3.7 Three Dimensional Finite Element Implementation Procedure for Titanium Alloy

The crystal plasticity model presented in Section 3.5 is coded into ABAQUS 2006 UMAT based on the previous work by Mayeur et al. [132] and Zhang et al. [133]. Some of the material parameters for the textured Ti-6Al-4V in the crystal plasticity codes are obtained from Brider et al. [137] and are as presented in Table 3.6. The elastic constants (c_{ij}) are obtained from the work of Simmons et al. [138] on single crystals and have been

adjusted based on the measurements by Larson et al. [139] on strongly textured Ti-6Al-4V alloy.

Table 3.6

Ti-6Al-4V crystal plasticity model parameters

Elastic stiffness	C_{11}	162,400 *MPa*
	C_{12}	92,000 *MPa*
	C_{13}	69,000 *MPa*
	C_{33}	180, 700 *MPa*
	C_{44}	49,700 *MPa*
Flow rule	γ_0	$0.001\, s^{-1}$
	M	15
Back stress	$\chi^{\alpha}(0)$	0
	h	40,000
	h_D	8000
Threshold stress	κ_y	17.3 *MPa* $mm^{-0.5}$
	$\kappa_s^{\alpha}(0)$	150 *MPa*
	μ	50

Finite element simulations were performed on three different geometries, meshed using 3D stress four-node linear tetrahedron element type (C3D4) and consisting of approximately 218940 elements to estimate the stress distribution and possible plastic straining that occur in the notched specimens. The dimensions of the specimens used and the different test cases are as given in Table 3.7.

Table 3.7

The seven different test cases

Test Case	K_t	Notch radius, ρ (mm)	Notch depth, h (mm)	R-ratio	Average alternating HCF strength at 10^6 cycles (MPa)
1	2.78	0.330	0.729	-1	173.6
2	2.78	0.330	0.729	0.1	158.9
3	2.78	0.330	0.729	0.5	104.6
4	2.78	0.203	0.254	0.1	167.2
5	2.78	0.203	0.254	0.5	105.2
6	2.78	0.127	0.127	0.1	144.7
7	2.78	0.127	0.127	0.5	111.0

To reduce computational time, two different simplifications were adopted;

(1) The notched specimen geometries are decomposed into three different regions: an outermost region, far from the notch root, where isotropic linear elasticity is used; an intermediate transition region where macroscopic J_2 cyclic plasticity theory is used; and finally the notch root region where crystal plasticity theory is used. The element size at the crystal plasticity region was chosen to coincide with the average grain size of Ti-6Al-4V which is 45 μm. The domain decomposition is as shown in Figure 3.12.

(2) One quarter of the cylindrical notched specimen was modeled because of the symmetry in loading and geometry of the specimen. Symmetry boundary conditions are applied at the planes of symmetry. The meshed specimen for the 0.33 mm notch root radius and $K_t = 2.78$ is as shown in Figure 3.13.

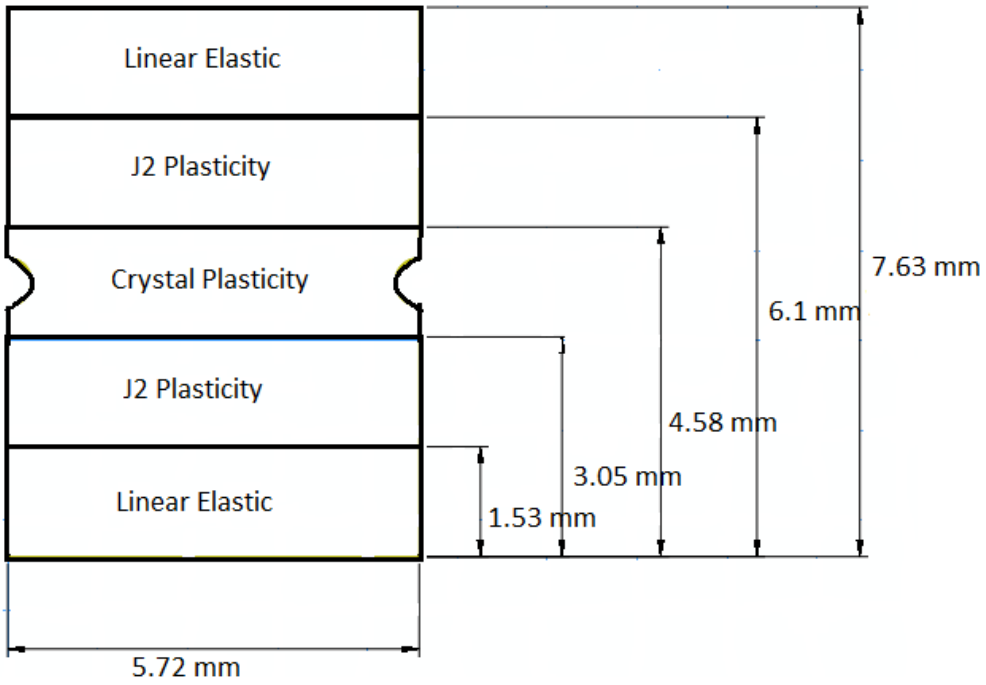

Figure 3.12. Domain decomposition of the cylindrical notched specimen geometry.

Figure 3.13. Finite element mesh for 0.33mm notch root radius and k_t= 2.78 consisting of four-node linear tetrahedron element type (C3D4).

The bottom of the notched specimen is encastre while symmetry boundary conditions are applied to the two planes of symmetry making up a total of 3 boundary conditions. A six step cyclic load involving three loading cycles are applied at the top of the specimen in the axial direction. The notched specimens were tested at three different load ratios; R=0.1, R=0.5, and R=-1. Average alternating HCF strength at 10^6 cylces, as determined by Naik et al. [140] are applied to the top of the specimen. Thus a load control constraint was used for the simulation. Figure 3.14 shows the ABAQUS 3D model of the notched geometry with the complete defined loading and boundary conditions.

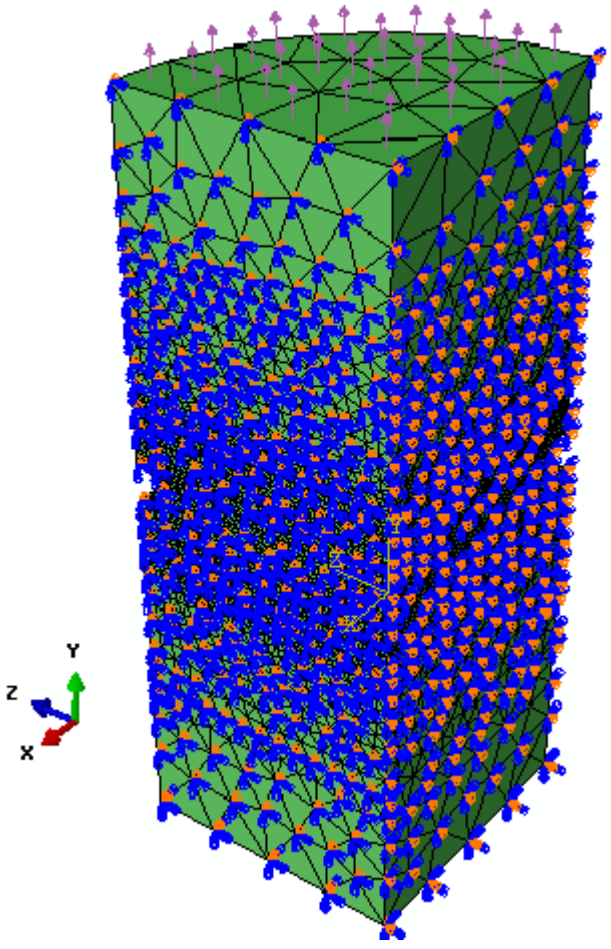

Figure 3.14. ABAQUS 3D view of the notched geometry with mesh, loading and boundary conditions.

3.8 Flow Chart of the Finite Element Modeling Strategy

The flow chart for the implementation of the finite element model is shown in Figure 3.15.

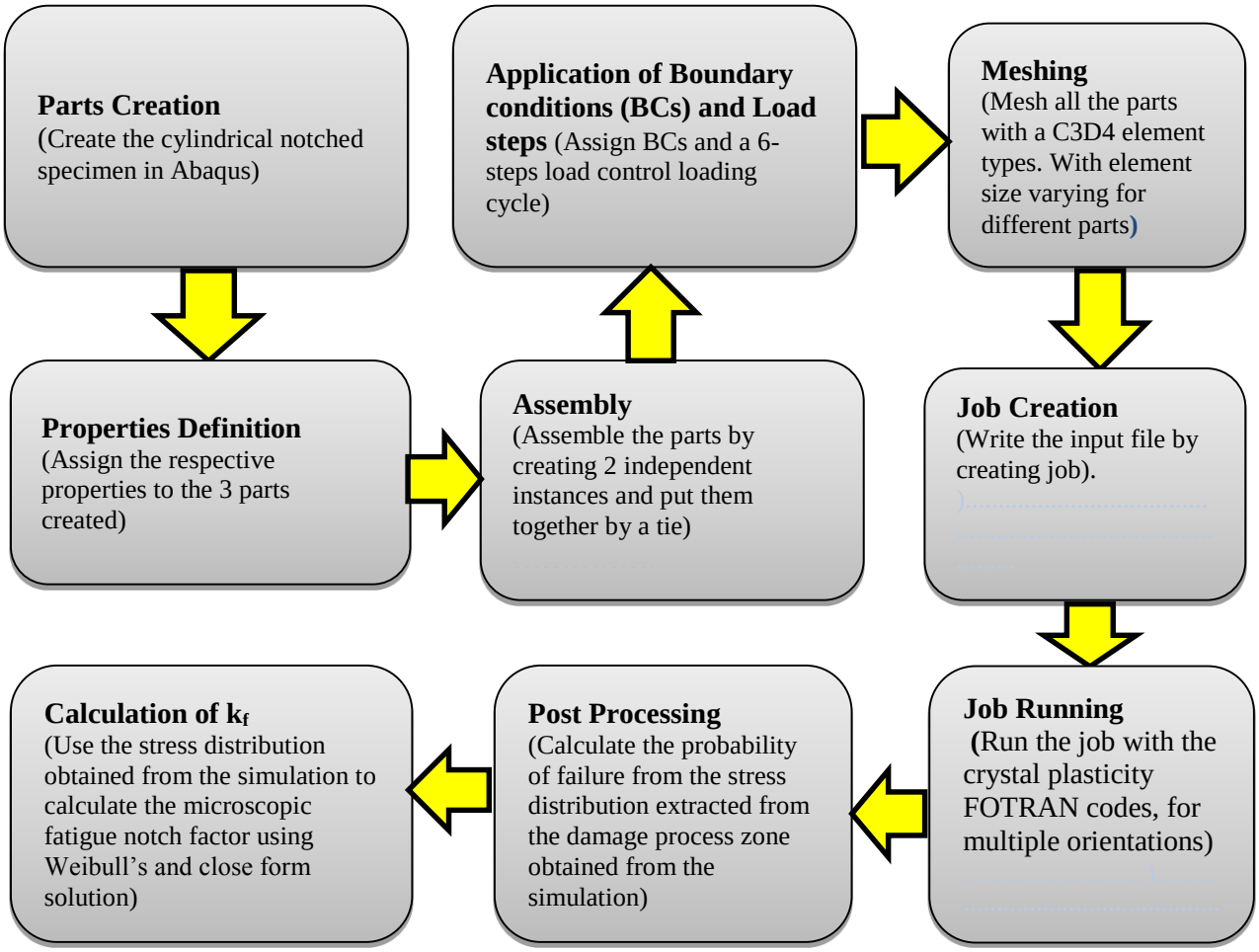

Figure 3.15. Flow chart of the finite element modeling and simulation strategy.

CHAPTER 4

WEAKEST LINK PROBABILISTIC FRAMEWORK FOR FATIGUE NOTCH FACTOR

4.1 Fatigue Damage Process Zone

Based on the stress/strain distributions extraction from finite element analysis for both elastic and elastic-plastic analysis, the concept of fatigue notch factor has been put forward and attempts have been made by different researchers to succinctly define the fatigue damage process zone [141, 142, 143, 73, 41, 31]. In general, the fatigue damage process zone is a volume comprising of pre-fracture zones in the vicinity of the notch, inclusion or any other stress raisers identified in the material. The pre-fracture zone is normally due to the detrimental effects of the stress raisers. To accurately predict life in HCF, it is of paramount importance to be able to define the fatigue damage process zone with some level of precision. However, it is difficult if not impossible a task to accomplish [141]. According to Ostash et al. [142], fatigue damage process zone is defined as some volume in the bulk material in which macro- and micro-plastic strains take place which also serve as source of initial damage of the material microstructure. Some of the factors that affect the size of the fatigue damage process zone include material properties, loading amplitude, and environment.

The fatigue damage process zone used in this work is an extension of the fatigue damage process zone as defined by Owolabi et al. [28, 144]. This new fatigue damage

process zone is defined based on the distribution of stress within the material. The statistical distribution of stress, σ, around the notch root and inclusion is used as a new criterion in defining the fatigue damage process zone. It is based on the assumption that the fatigue damage process zone is a region around the notches and inclusion having grains with σ values equal to or greater than a specified microscopic threshold value, σ_{th}, as shown in the Figure 4.1. Here, the yield stress of the material, σ_{yield}, is specified as the microscopic threshold value.

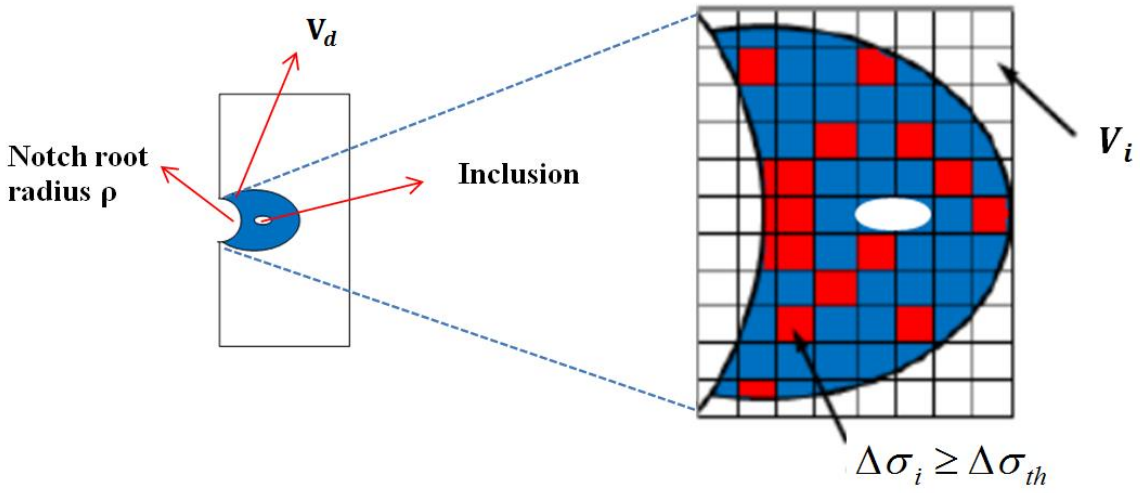

Figure 4.1. Schematic of fatigue damage process zone.

4.2 Probabilistic Framework for Fatigue Notch Factor (Weakest Link Thoery)

Due to inherent scatter involved in high cycle fatigue (HCF) lives of engineering materials, numerous probabilistic approaches have been developed in HCF lifing strategies [51]. These approaches can be used to predict scatter of fatigue data and the dependence of fatigue limits on fatigue damage process zone. The predictive capabilities of these models can be enhanced by incorporating information regarding the origin of the scatter such as due the presence of defects and micro-scale plastic deformation. The basic

assumption of the weakest link theory is the existence of statistically distributed defects at the surface or in the volume of the material and the occurrence of crack at the largest or most dangerous one when a certain critical stress level is reached.

The weakest link theory presented here to obtain the fatigue notch factor and associated notch sensitivity index follows the framework presented in [27, 145] with a few modifications based on the physical mechanisms of fatigue crack formation and growth for aero-engine materials with and without inclusions. IN 100 contain nonmetallic inclusions and pores that play a critical role in components failure. Fatigue is manifested by extremal microstructure attributes that promote slip intensification and hence does not conform to homogenization. Thus, a probabilistic formulation to determine the failure potency in heterogeneous materials should include a consideration for these defects. This task will combine the framework in [145] with other existing probabilistic formulations that consider the size distribution and proximity of defects and different competing damage mechanisms for IN 100. The applicability of the framework will also be investigated for materials containing more complex dual-phase microstructures such as Ti-6Al-4V with realistic texture.

For a smooth specimen having a fatigue damage process zone of volume V and containing defects, if the volume is divided into “m” small volume elements, dV, the probability of failure of a sufficiently small volume element is given as:

$$dP = \lambda dV \tag{4.1}$$

where, the critical defect density is denoted as λ and it is defined as the expected number of defects per unit volume of the smooth specimen. Invoking the weakest link theory, the

probability of survival of the entire volume can be obtained from the probability of survival of all "m" number of sub-volumes i.e.

$$P_s = \prod_{i=1}^{m}(1-dP_i) = \prod_{i=1}^{m}(1-\lambda dV) \tag{4.2}$$

Equation 4.2 is based on the assumption that the defects are randomly distributed within the volume and there is no any form of interaction between them. This assumption is only reasonable when considering the formation of a fatigue crack(s) in high cycle (HCF) and very high cycle fatigue (VHCF) regimes. Following the framework presented in [27], as the volume of each small element tends to zero, Equation 4.2 can be expressed as:

$$P_s = \exp\left(-\int_{V_d} \lambda dV\right) \tag{4.3}$$

Using the generalized extreme value (GEV) distribution function, the distribution of defects, *a*, that are above the threshold, a_{th}, is modeled by a power law of the form:

$$\lambda = \frac{1}{V_0}\left(1+\xi\left(\frac{a-a_{th}}{a_0}\right)\right)^{-1/\xi} \tag{4.4}$$

where scale and shape parameters are represented as a_0 and ξ respectively. Substituting Equation 4.4 into 4.3 becomes:

$$P_s = \exp\left\{-\frac{1}{V_0}\int_{V_d}\left(1+\xi\left(\frac{a-a_{th}}{a_0}\right)\right)^{-1/\xi} dv\right\} \tag{4.5}$$

if $a_{th} = a_0^*\xi$, re-arranging Equation 4.5 yields,

$$P_s = \exp\left\{-\frac{1}{V_0}\int_{V_d}\left(\frac{a}{a_0^*}\right)^{-1/\xi} dv\right\} \quad 4.6$$

where a_0^* is regarded as the mean defect size. Equation (4.6) is only valid if $\xi \neq 0$. The critical defect size is related to the microscopic stress (taking here as a random variable) through a power law relationship of the form

$$\sigma = \frac{A}{\sqrt[z]{a}} \quad 4.7$$

where A and z are materials constants. Similarly, the stress amplitude, σ_0 corresponding to the mean defect size a_0^* can be taken as the fatigue limit of the reference volume V_o for 50% failure probability. Thus we can have:

$$\sigma_0 = \frac{A}{\sqrt[z]{a_0^*}} \quad 4.8$$

Combining Equations 4.7 and 4.8 we have

$$\frac{a}{a_0^*} = \left(\frac{\sigma_0}{\sigma_a}\right)^z \quad 4.9$$

Substituting Equation 4.9 into Equation 4.6 yields

$$P_s = \exp\left[-\frac{1}{V_0}\int_{V_d}\left(\frac{\sigma_a}{\sigma_0}\right)^b dv\right] \quad 4.10$$

where $b=z/\xi$.

If $\sigma_a = \sigma - \sigma_{th}$, hence we have:

$$P_s = \exp\left[-\frac{1}{V_0} \int_{V_d} \left(\frac{\sigma - \sigma_{th}}{\sigma_0} \right)^b dv \right] \tag{4.11}$$

For ξ>0, b, σ_{th} and σ_0 represents a 3-parameter Weibull shape, location and scale parameters. The cumulative probability of HCF failure of the component, specifically defined can be obtained from Equation 4.11 as:

$$\mathrm{k}\, P_f = 1 - \exp\left[-\frac{1}{V_0} \int_{V_d} \left(\frac{\sigma - \sigma_{th}}{\sigma_0} \right)^b dv \right] \tag{4.12}$$

To facilitate development of the expression for fatigue notch factor from Equation 4.12, the concept of stress homogeneity factor that have been used in [27], is introduced here. Thus Equation 4.12 can be re-written as,

$$P_f = 1 - \exp\left[-\frac{kV_d}{V_0} \left(\frac{\sigma_{\max}}{\sigma_0} \right)^b \right] \tag{4.13}$$

where

$$k = \frac{1}{V_d} \int_{V_d} \left(\frac{\sigma - \sigma_{th}}{\sigma_{\max}} \right)^b dv \tag{4.14}$$

is regarded as the stress homogeneity factor. Conventionally, the fatigue notch factor is the ratio of unnotched to notched fatigue strength at the same probability of failure (usually 50%). Using Equation 4.11, the probability of failure of unotched specimen and a notched specimen will be the same when

$$\exp\left\{-\frac{k_s V_s}{V_o}\left(\frac{\sigma_{\max,s}}{\sigma_0}\right)^b\right\} = \exp\left\{-\frac{k_n V_n}{V_o}\left(\frac{\sigma_{\max,n}}{\sigma_0}\right)^b\right\} \quad 4.15$$

where the subscripts *n* and *s* represent the respective value of the variable for notched and smooth (unmatched) specimens respectively. The ratio of the smooth to notch fatigue driving force parameters (i.e., the stress amplitude) is used to define a new fatigue notch factor given as

$$k_f = \frac{\sigma_{\max,s}}{\sigma_{\max,n}} = \left(\frac{k_n}{k_s}\right)^{1/b}\left(\frac{V_n}{V_s}\right)^{1/b} \quad 4.16$$

For smooth specimen that is loaded at a very low stress or strain amplitude in the HCF regime, the number of critically stressed grains (or elements) is very small. Thus for the life limiting case in which only one grain or element is critically stressed above the threshold, $V_s = V_{et}$ (i.e. volume of element or grain) and $k_s = 1$; thus Equation (4.16) becomes

$$k_f = \frac{\sigma_{\max,s}}{\sigma_{\max,n}} = \left(k_n\right)^{1/b}\left(\frac{V_n}{V_e}\right)^{1/b} \quad 4.17$$

$$k_f = \left[\frac{1}{V_d}\int_{V_d}\left(\frac{\sigma-\sigma_{th}}{\sigma_{\max,n}}\right)^b dv\right]^{1/b}\left(\frac{V_n}{V_e}\right)^{1/b} \quad 4.18$$

However, if the materials contain some pores or inclusions, Equation 4.16 must be used. It is important to state that Eqs. 4.16 and 4.18 can be used only if subsurface crack initiation is the failure process, if crack originates from the surface, then the volume parameter in this equation should be replace with the surface area.

4.3 Closed Form Solution for Fatigue Notch Factor

To resolve inelastic deformation at the scale of microstructure to facilitate next generation microstructure-sensitive notch root analyses inherently requires mesh refinement to the scale of microstructure, which is often several orders of magnitude finer than the scale of the component. Moreover, the kind of constitutive equations that must be used are often of advanced form, for example, discrete dislocation mechanics, requiring rather sophisticated and time-consuming computational strategies to perform concurrent analyses at the component and notch root microstructure scales. Accordingly, direct application of multiscale finite element analysis is simply too computationally time consuming for practical microstructure-sensitive fatigue damage assessment of notched components under multiaxial loads. Thus, for practical engineering application, a more simplified and approximate model for fatigue notch factor is presented here based on closed form solution for stress distribution at the notch developed by Glinka using the Creager-Paris solutions of the stress field ahead of a crack. For a notch component with notch root radius ρ and stress concentration factor, k_t, the axial stress distribution along the notch root centre line is given as:

$$\sigma = \frac{1}{2}\left(\left(\frac{\rho}{x+\rho/2}\right)^{1/2} + \frac{1}{2}\left(\frac{\rho}{x+\rho/2}\right)^{3/2}\right) k_t S = \frac{1}{2}\left(\left(\frac{\rho}{x+\rho/2}\right)^{1/2} + \frac{1}{2}\left(\frac{\rho}{x+\rho/2}\right)^{3/2}\right) \sigma_{\max,n} \qquad 4.19$$

Finding the ratio of the stress amplitude to the maximum stress and substituting into Equation 4.18 at x = a_c (i.e., the critical distance) will allow the determination of an expression for the fatigue notch factor of the form

$$k_f = \left(\frac{1}{V} \int \left(\frac{1}{2} \left(\left(\frac{\rho}{a_c + \rho/2} \right)^{1/2} + \frac{1}{2} \left(\frac{\rho}{a_c + \rho/2} \right)^{3/2} \right) \right)^b dV \right)^{1/b} \left(\frac{V_n}{V_e} \right)^{1/b} \quad 4.20$$

Assuming that the critical distance is constant for the notched component with a notch root radius ρ, Equation 4.20 reduces to

$$k_f = \left(\frac{1}{2} \left(\left(\frac{\rho}{a_c + \rho/2} \right)^{1/2} + \frac{1}{2} \left(\frac{\rho}{a_c + \rho/2} \right)^{3/2} \right) \right) \left(\frac{V_n}{V_e} \right)^{1/b} \quad 4.21$$

The above equation for k_f was derived using the fatigue damage process zone based on critical distance, probabilistic framework based on the weakest link, and the Glinka's closed form solution based on the notch root stress distribution.

CHAPTER 5

RESULTS AND DISCUSSION

5.1 Determination of Parameter Values for the Weakest Link Probabilistic Framework

In Equation 4.12 there are three unknown parameters namely the shape, location and scale parameter. The location parameter otherwise called the threshold stress is taken as the yield stress of the material leaving us with two unknown parameters. The remaining two unknown parameters are estimated using the modified moment estimation (MME) technique [146]. Here, the first two sample moments are used i.e., the mean $\bar{\sigma}_m$ and the variance $\bar{\sigma}_m^2$ of the stress distribution σ. With modification of the expression obtained from Cohen and Whitten [146] to account for notch size effect, the mean and variance are given as:

$$\bar{\sigma}_m = \sigma_{th} + \sigma_0 \left(\frac{V_0}{V_d} \right)^b \zeta_1 \tag{5.1}$$

$$\bar{\sigma}_m^2 = \sigma_0^2 \left(\frac{V_0}{V_d} \right)^{2b} \left(\zeta_2 - \zeta_1^2 \right) \tag{5.2}$$

In Equations 5.1 and 5.2,

$$\zeta_k = \zeta(1+kb),\ k = 1,2 \tag{5.3}$$

And $\zeta(\ )$ is the gamma function defined by the integral

$$\zeta(s) = \int_0^{\infty} t^{s-1} e^{-t} dt \qquad 5.4$$

By solving Equations 5.1 and 5.2 simultaneously, the two parameters σ_0 and b are determined. The yield stress, σ_{th}, of the nickel base superalloy is 1045 MPa while for titanium alloy it is 990 MPa. From Equations 5.1 and 5.2, b is determined to be 15.6 and 7.7 for nickel base superalloy and titanium alloy respectively. While the scale parameter σ_0 is determined to be 2826.07 MPa and 3205.03 MPa for nickel base superalloy and titanium alloy respectively. From the geometry of the specimens, the reference volume V_0 is calculated to be 11.152 mm^3 and 16.96 mm^3 for nickel base superalloy and titanium alloy respectively.

5.2 Notch Size Effects on Fatigue Notch Factor, Notch Sensitivity Index, and Probability of Failure for Nickel Base Super Alloy without Inclusion.

Here, three different notch root radii are simulated in Abaqus but with ten different grain orientations for each of the notch root radius. The stress distribution from the simulation of the notched nickel based super alloy is extracted and it is used in Equation 4.12 to determine the probability of failure for each notch root radius and the associated fatigue notch factor. The notch sensitivity index q for each case is also computed using Equation 2.3. The stress distribution obtained from Abaqus for three different notch root radii is as shown in Figure 5.1 which shows the maximum principal stress in the y-direction (axial).

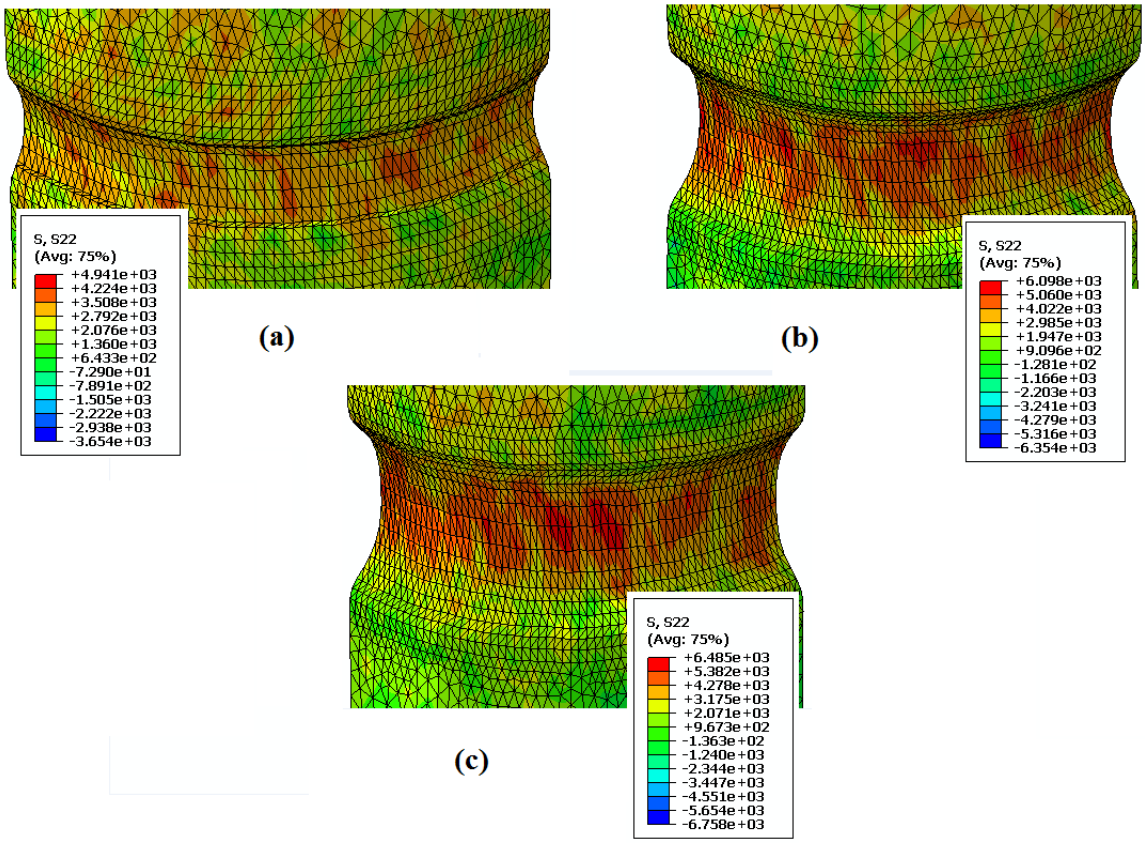

Figure 5.1. Stress distribution for nickel base notched specimen without inclusion: (a) notch radius ρ = 0.150 mm (b) notch radius ρ = 0.213 and (c) notch radius ρ = 0.284. (All results in MPa)

Using Equation 4.12, the probability of failure was computed for ten different grain orientations for each of the notch root radius and the results are as plotted in Figure 5.2.

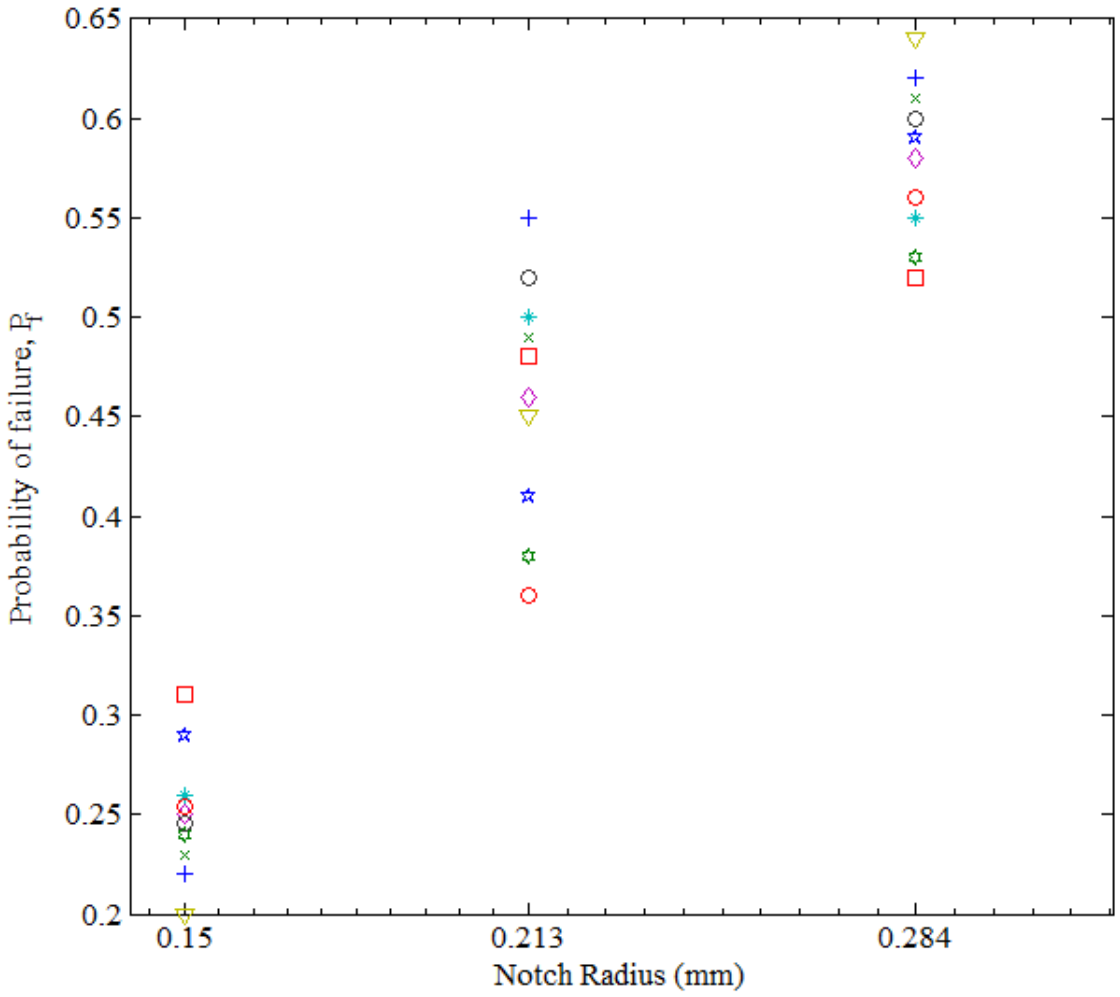

Figure 5.2. Probability of failure vs notch root radius for notched nickel base superalloy specimens without inclusion.

Figure 5.2, shows the combine effect of notch root radius and the grain orientation of nickel base superalloy on its probability of failure. It is observed that the probability of failure rapidly increases with increasing notch root radius. Also, it can be seen that the orientation of the nickel base superalloy grains plays a significant role in determining the probability of failure and susceptibility of the bulk material to fatigue failure. It is observed that the probability of failure for each notch root radius varies with grain orientation. For example, for nickel base superalloy with notch root of 0.284 mm, the

probability of failure varies from 0.52 to 0.64. Thus, notches with favorably oriented grains in the vicinity of the notch and inclusion exhibit higher probability of failure.

Using Equation 4.18, the associated microstructure dependent fatigue notch factors for the estimated probability of failures above are computed and the average fatigue notch factor for each notch root radius is plotted as shown in Figure 5.3. Also, experimentally obtained fatigue notched factor from Weiju et al. [26] for nickel base superalloy are plotted for comparison purpose (Figure 5.3). Table 5.1 shows both the experimentally obtained fatigue notch factor and that determined using the developed probabilistic framework.

Table 5.1

Experimental and Weibull fatigue notch factor for notched nickel base superalloy specimen without inclusion.

Notch Root Radius	Fatigue Notch Factor	
	Weibull	Experiment
0.150	1.54	1.56
0.213	1.70	1.73
0.284	1.74	1.73

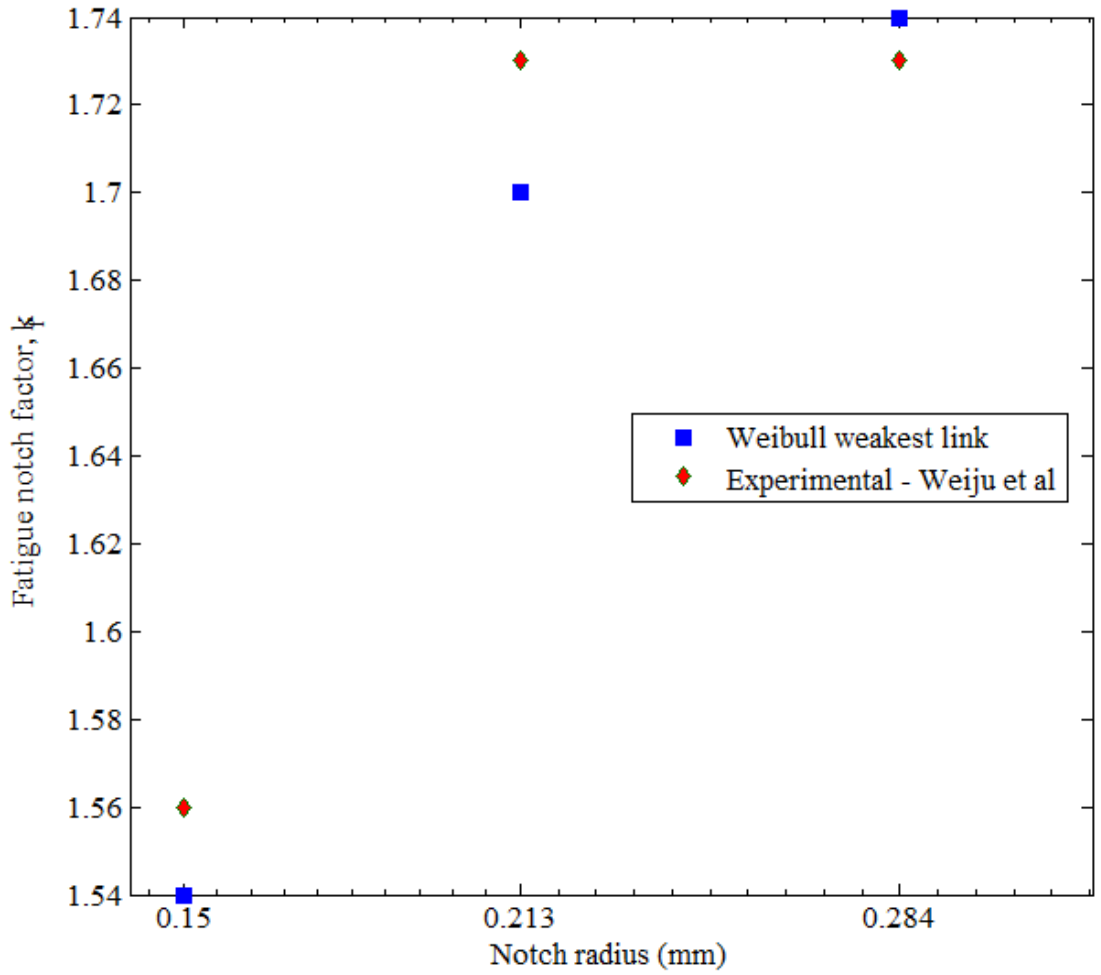

Figure 5.3. Comparison of experimentally determined kf with the determine kf using the developed probabilistic framework.

Figure 5.3 shows that the determined fatigue notch factor using the developed probabilistic framework follows the same trend as the experimentally obtained value. The result shows that the fatigue notch factor increases with increasing notch root radius. It can be inferred from the result that larger notch root radii are detrimental to fatigue failure of notched nickel base superalloy.

Using the expression for notch sensitivity index which is presented in Equation 2.3 of Chapter 2 of this thesis, the notch sensitivity index for both the experimentally

determined k_f and the k_f determined using the newly developed probabilistic framework are computed and plotted as given in Figure 5.4 below for comparison purpose.

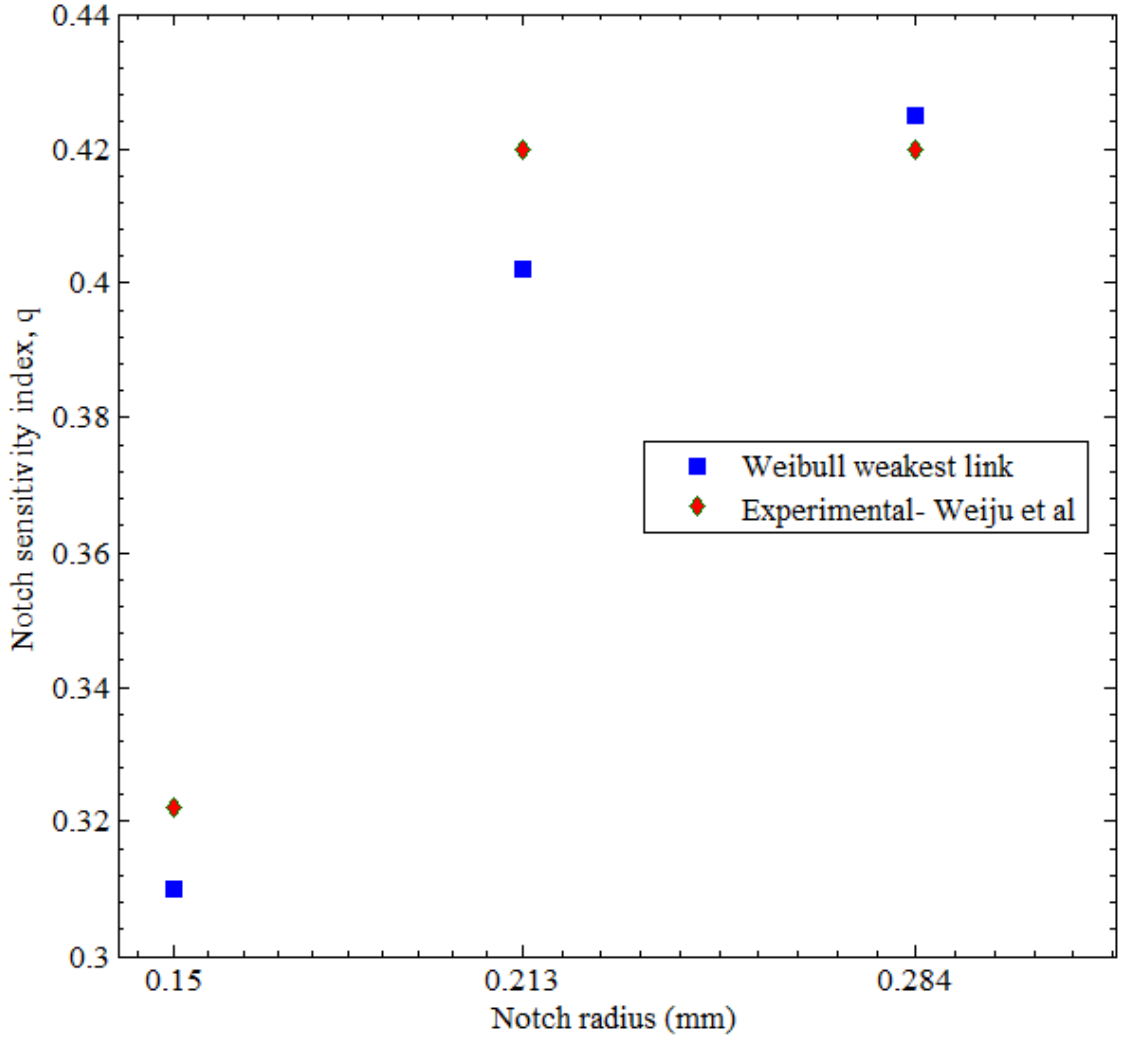

Figure 5.4. Comparison of notch sensitivity index obtained from experiment and that obtained from developed model.

Figure 5.4 shows that the Weibull notch sensitivity index follows the same trend as that of the experimentally determined value. It can be inferred from the result that the notch sensitivity of notched nickel base superalloy increases with increasing notch root radius.

To show the general performance of the newly developed model in accurately predicting fatigue notch factor, the determined fatigue notch factor using the new probabilistic framework and closed form solution are plotted against fatigue notch factor determined using existing conventional empirical methods like Neuber, Peterson and Heywood as shown in Figure 5.5.

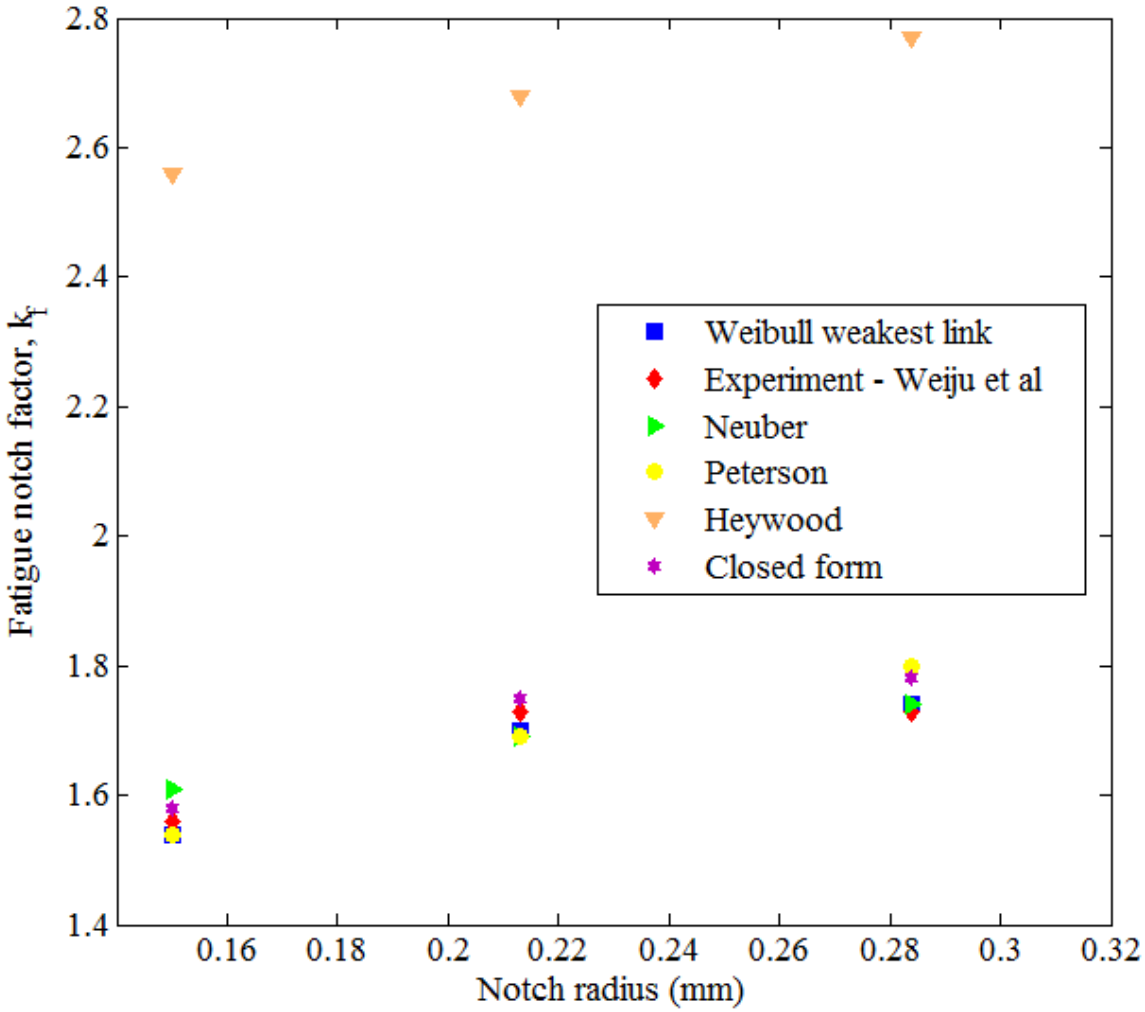

Figure 5.6. Comparison of k_f determined by the new model with existing conventional methods

The percentage variance/deviation of each method from the experimental value is presented in Table 5.2. The material constant for the empirical formulas Neuber (Equation 5.5), Peterson (Equation 5.6) and Heywood (Equation 5.7) are obtained from [26].

$$k_f = 1 + \frac{k_t - 1}{1 + \sqrt{\frac{a_n}{\rho}}} \tag{5.5}$$

$$k_f = 1 + \frac{k_t - 1}{1 + \frac{a}{\rho}} \tag{5.6}$$

$$k_f = 1 + \frac{k_t}{1 + 2\sqrt{\frac{a}{\rho}}} \tag{5.7}$$

Table 5.2

Fatigue notch factor % variance from experimental value for different methods

Radius	Experiment	Weibull		Neuber		Peterson		Heywood		Closed form sol.	
	K_f	K_f	% Var	K_f	% Var	K_f	% Var	K_f	% Var	K_f	% Var
0.150	1.56	1.54	1.28	1.61	-3.21	1.54	1.28	2.56	64.10	1.58	-1.28
0.213	1.73	1.70	1.73	1.69	2.31	1.69	2.31	2.68	54.91	1.75	-1.16
0.284	1.73	1.74	-0.58	1.74	-0.58	1.80	-4.05	2.77	60.12	1.78	-2.89

Table 5.2 shows that the Weibull fatigue notch factor exhibits relatively lower percentage variance from experimental values compared to other existing conventional methods. Also, the closed form solution is also observed to give relatively accurate prediction compared to the existing classical methods as it has lower percentage variance from experimental results. To a reasonable extent, it can be said that the newly developed probabilistic framework and the closed form solution more accurately predict fatigue

notch factor of notched nickel base superalloy compared to the existing conventional methods.

5.3 Notch Size Effects on Fatigue Notch Factor, Notch Sensitivity Index, and Probability of Failure for Titanium Alloy.

Here, seven different test cases were simulated in Abaqus with ten different grain orientations for each of the test case. The stress distribution for some of the test cases simulated in Abaqus is presented in Figure 5.6 showing the maximum principal stress in the y-direction (axial).

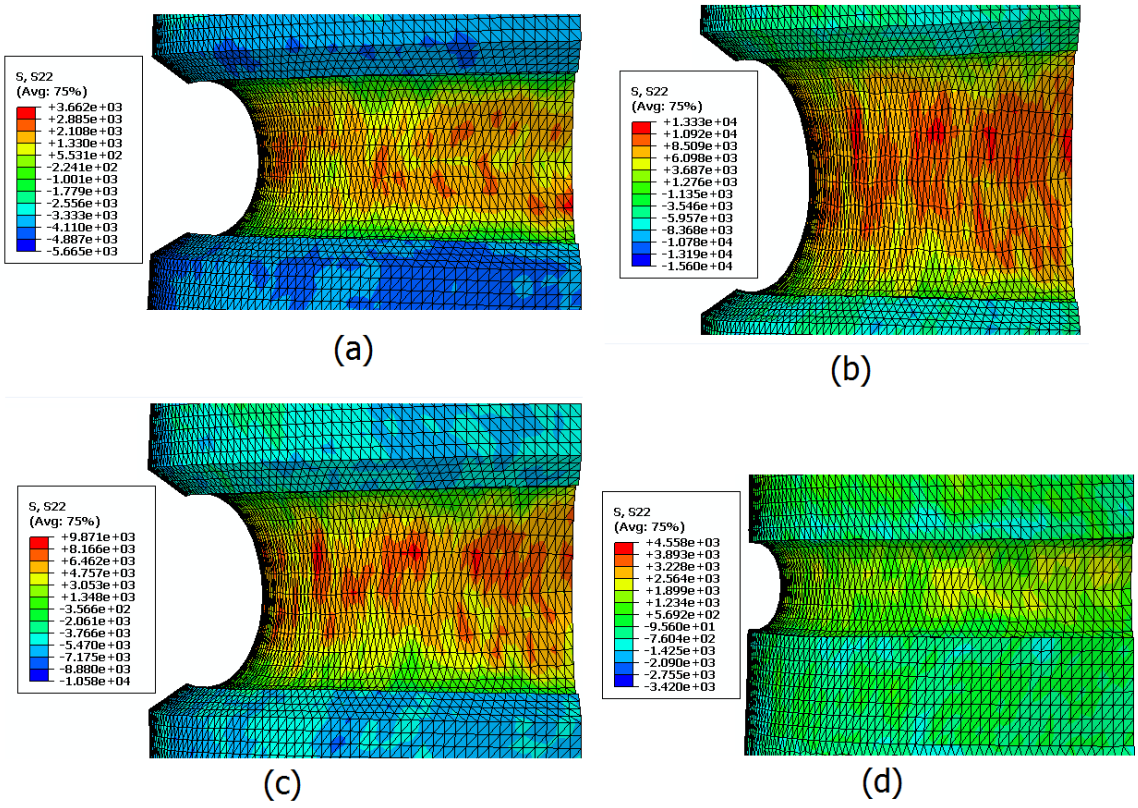

Figure 5.6. Stress distribution for notched titanium alloy: (a) ρ = 0.33, R = -1 and applied load P = 173.6 MPa (b) ρ = 0.33, R = 0.1 and P = 158.9 MPa (c) ρ = 0.33, R = 0.5 and P = 104.6 MPa (d) ρ = 0.203, R = 0.1 and P = 167.2 MPa. (All results in MPa)

The stress distribution obtained from the finite element analysis was used in the developed model for determining the probability of failure for each test case. Also, the average fatigue notch factor is computed for each test case using the developed probabilistic framework. Figure 5.7 shows probability of failure plotted against the notch root radii for ten different grain orientations.

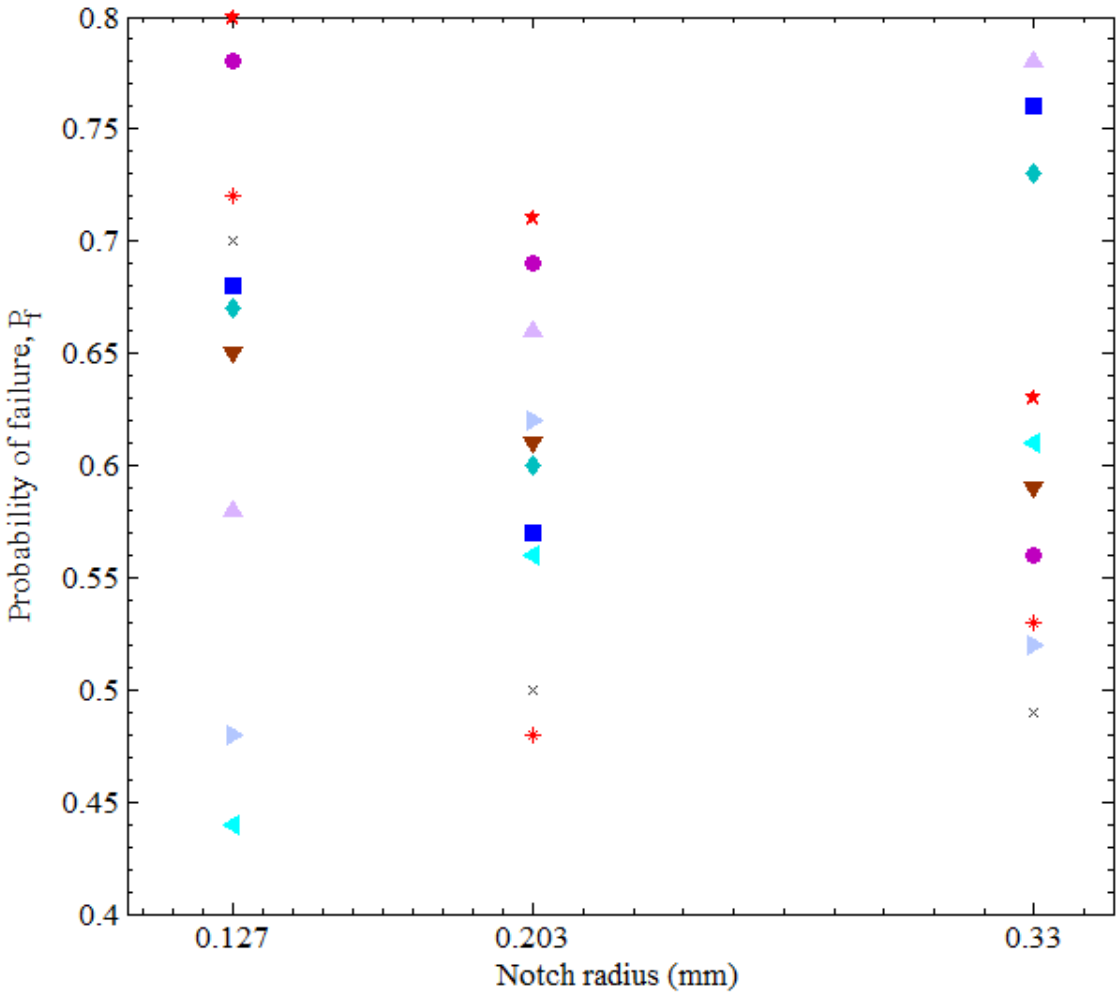

Figure 5.7. Probability of failure vs. notch radius for notched titanium alloy at load ratio R= 0.1.

Figure 5.7 shows that the probability of failure increases with increasing notch root radius. However, an exception is noted for titanium alloy specimen with 0.127 mm

notch root radius where some of the probabilities of failure for some of the grain orientations are higher than for the remaining notch root radii (0.203 mm and 0.33 mm). This is an indication that grain orientation also plays an equally important role in determining the occurrence of fatigue failure in notch titanium alloy specimen.

The effect of load ratio on the probability of failure of notched titanium alloy is also investigated by plotting probability of failure against notch root radii for two different load ratios R= 0.1 and R= 0.5 as shown in Figure 5.8.

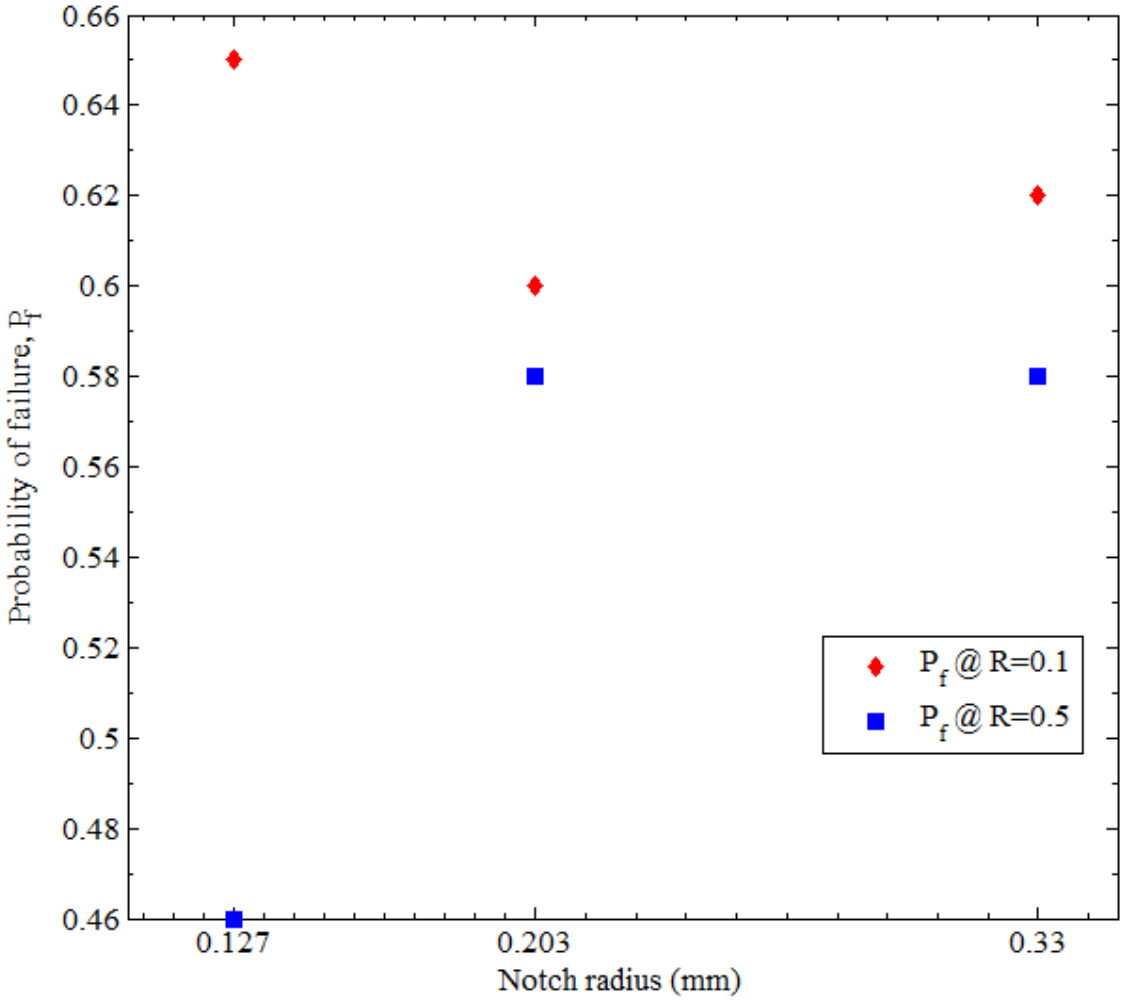

Figure 5.8. Probability of failure of notched titanium alloy vs. notch radius at two different load ratios R= 0.1 and R= 0.5.

Figure 5.8 shows the important role played by the load ratio on the susceptibility of notched titanium alloy to fatigue failure. The probability of failure are higher at load ratio of R= 0.1 than at R = 0.5 which implies that components operating at load ratio of 0.5 will have better fatigue life compared to components operating at load ratio of 0.1. This is an important observation to note while designing components that will be subjected or exposed to fatigue loading.

The fatigue notch factor determined using the developed method is compared to experimentally obtained values from Naik et al. [140], the close from solution developed and other existing conventional method such as Neuber as shown in Figure 5.9 and Table 5.3.

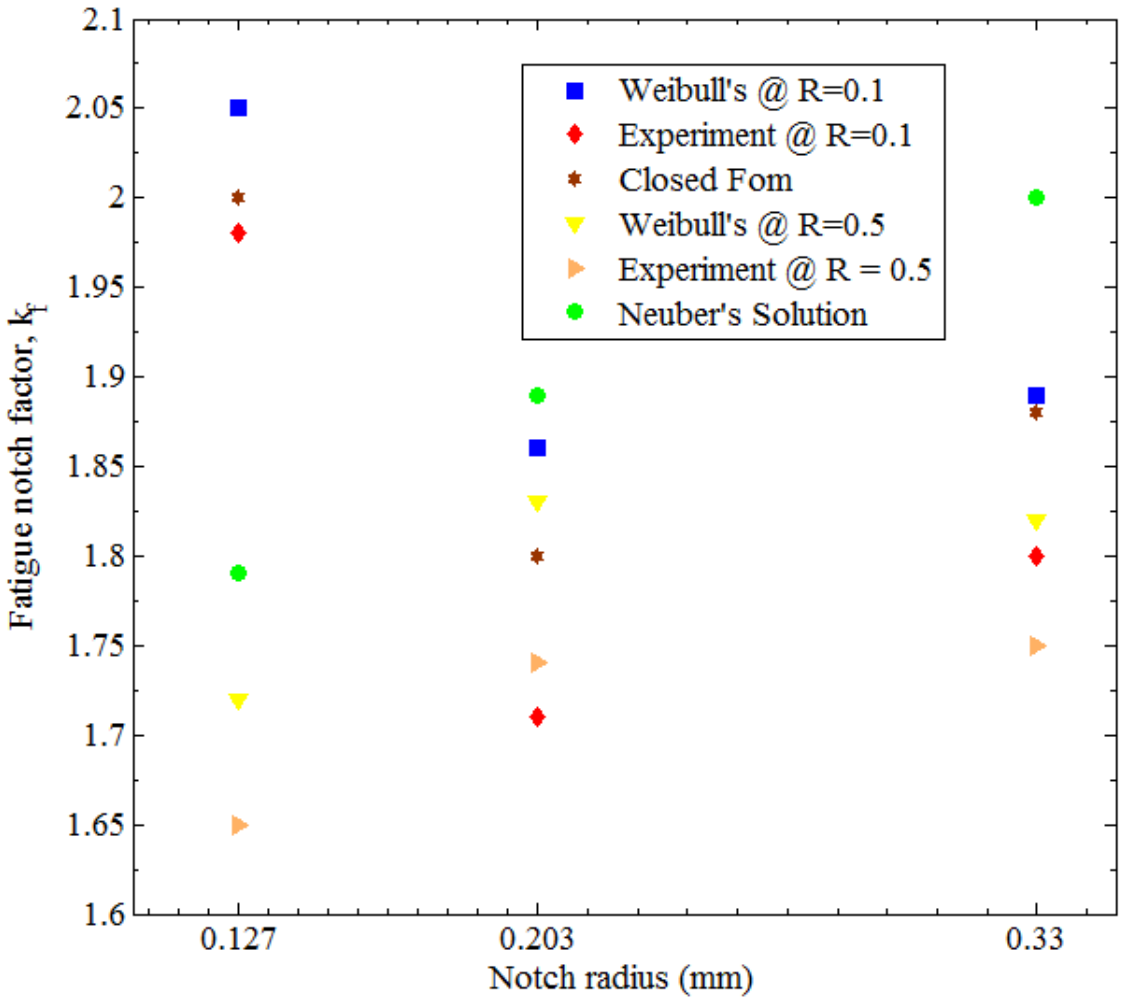

Figure 5.9. Factigue notch factor as a function notch root radius and load ratio compared to experimental values.

Table 5.3

Fatigue notch factor % variance from experimental value for Weibull, close form solution and Neuber methods

Radius	Experiment k_f		Weibull@R=0.1		Weibull@R=0.5		Neuber		Closed Form Sol.	
	R=0.1	R=0.5	K_f	% Var	k_f	% Var	k_f	% Var	k_f	% Var
0.127	1.98	1.65	2.05	-3.54	1.72	-4.24	1.79	9.60	2.00	-1.01
0.203	1.71	1.74	1.86	-8.77	1.83	-5.17	1.89	-10.53	1.80	-5.26
0.33	1.80	1.75	1.89	-5.00	1.82	-4.00	2.00	-11.11	1.88	-4.44

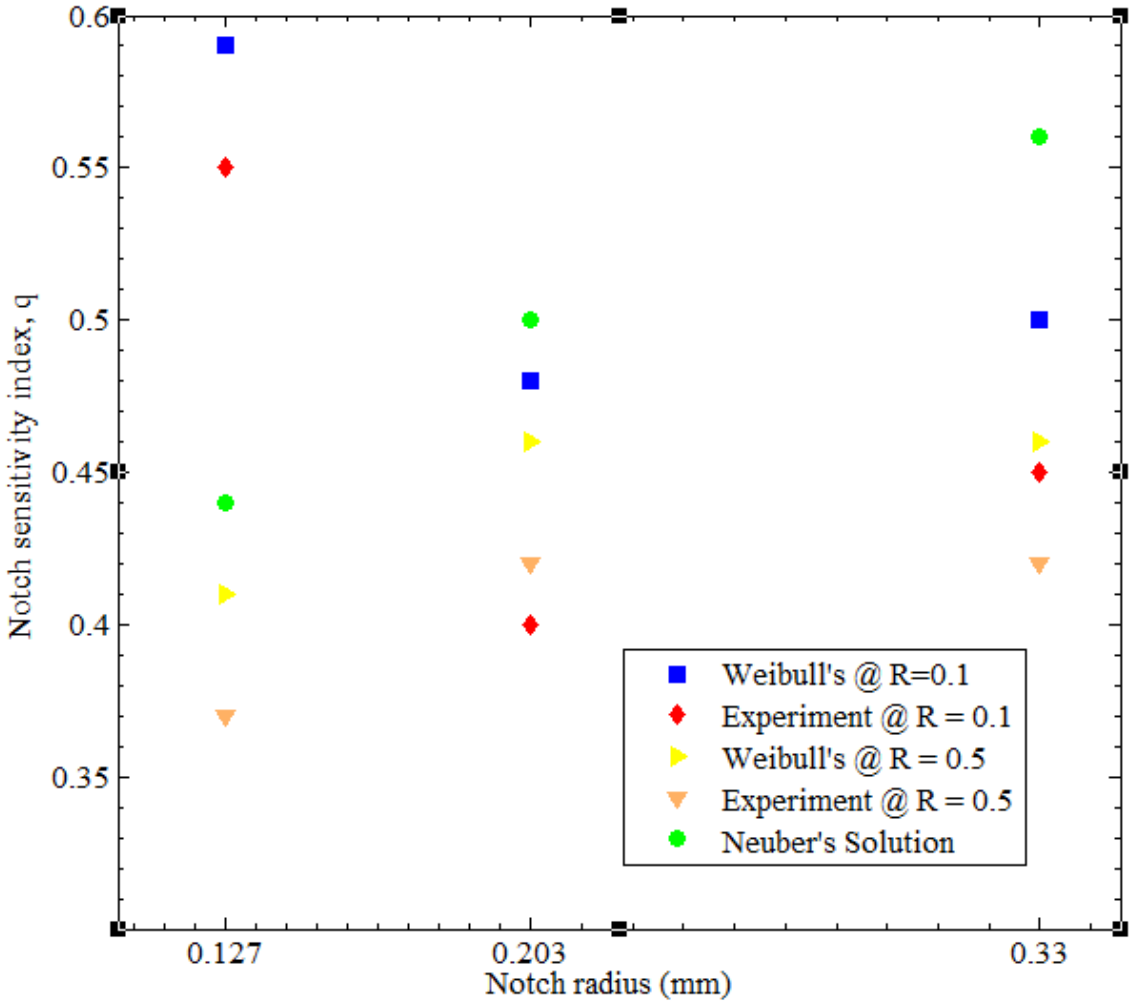

Figure 5.10. Notch sensitivity index as a function notch root radius and load ratio compared to experimental values.

It can be noted from Table 5.3 that the percentage variance for Weibull fatigue notch factor and the developed closed form solution is lower compared to Neuber's predictions. Thus, the developed probabilistic model and the close form solution are more accurate in predicting fatigue notch factor of notched titanium alloy compared to Neuber method.

The associated notch sensitivity index is also computed and compared to experimental values as shown in Figure 5.10.

5.4 Fatigue Notch Factor of IN100 with Inclusion.

To identify where the inclusion has maximum influence on the stress distribution on the specimen, the medium geometry was used. The geometry has a diameter of 5 mm, notch root radius 0.213 mm and thickness 0.267 mm with an applied stress of 568 MPa. The geometry is modeled with one Horizontal inclusion of major axis 150 um and minor axis 75 um. The inclusion is placed at varying distance from the notch root as a function of the grain size (the grain size used for nickel being 0.064mm). The maximum stress obtained for each test case is as presented in Table 5.4.

Table 5.4

Maximum stress for different inclusion distance from notch root

Distance of Inclusion	Max S22	Max Von Mises
10g	1871	1624
8g	1894	1672
6g	1885	1641
4g	1884	1650

Simulations were then conducted with inclusion placed at 8 grain distance from the notch root for the nickel base specimens. The fatigue notch factor is computed based on the stress distribution extracted from Abaqus for notch nickel base super alloy with inclusion. Table 5.5 shows how the computed fatigue notch factor compare with the fatigue notch factors of notched nickel base superalloy without inclusion. Figure 5.11 graphically shows the variation in the fatigue notch factor of notch nickel base superalloy in the presence of inclusion.

Table 5.5

Fatigue notch factor of notch nickel base superalloy with and without inclusion

Notch Radius	Fatigue Notch factor (K_f)	
	Without Inclusion	With Inclusion
0.150	1.54	2.01
0.213	1.70	2.38
0.284	1.74	2.61

Both Table 5.5 and Figure 5.11 show that the introduction of one horizontal inclusion in the matrix of the notched nickel base superalloy increases the fatigue notch factor. Thus component with inclusions of any kind will tend to have lower fatigue strength than components without inclusion. This is expected based on the fact that inclusions serve as favorable sites of premature plastic deformation due to high stress concentration in the vicinity of the inclusion curvature.

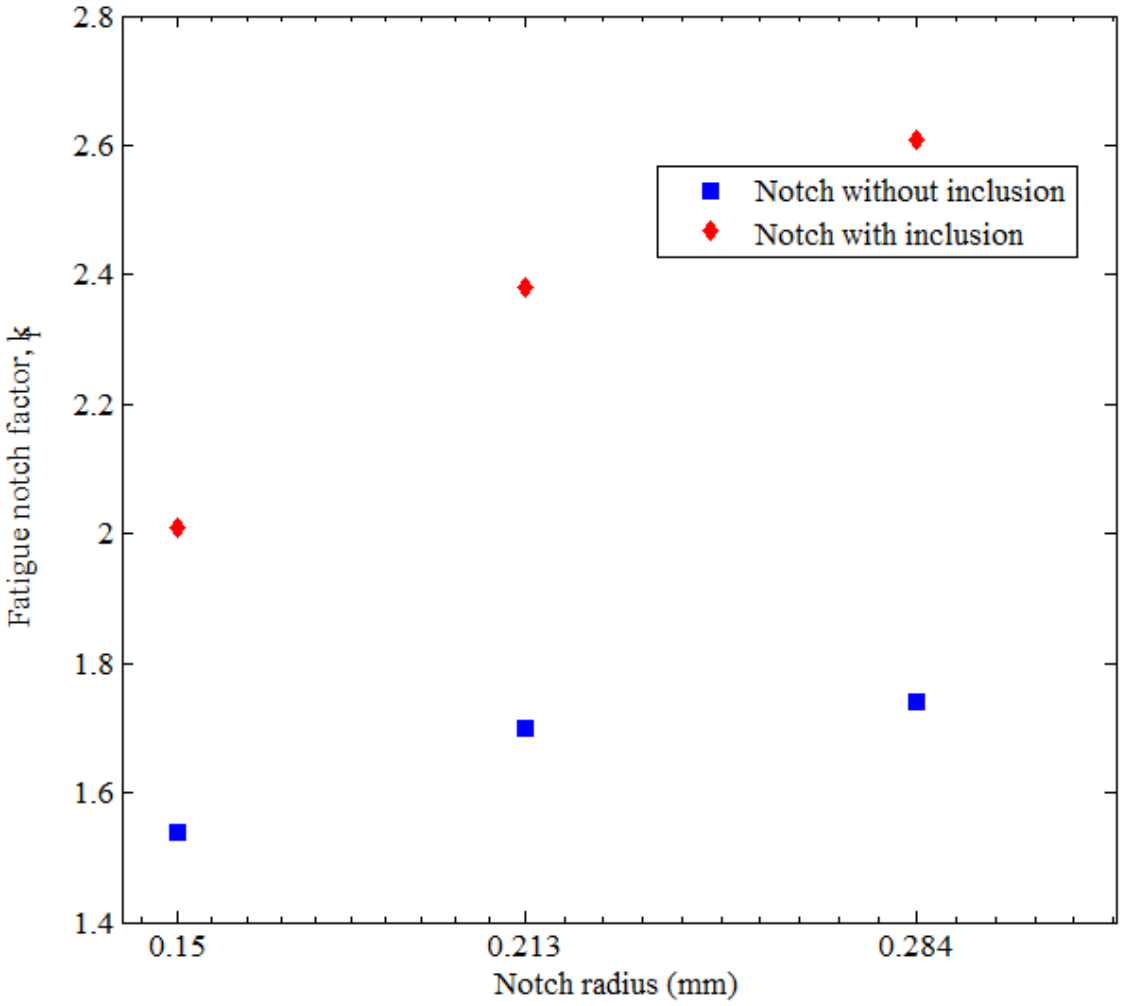

Figure 5.11. Fatigue notch factor vs. notch root radius for notched nickel base superalloy with and without inclusion.

5.5 Effects of Inclusion orientation on Fatigue Notch Factor of IN100

Here, the effect of changing the orientation of the inclusion within the matrix of a notched nickel base superalloy over its fatigue notch factor is investigated. Three different inclusion orientations (horizontal, 45^0 and 90^0) are simulated in Abaqus using the model with notch root radius 0.213 mm and the stress distributions obtained are as presented in Figure 5.12. The maximum stress in each case and the fatigue notch factor computed using the stress distribution is presented in Table 5.6.

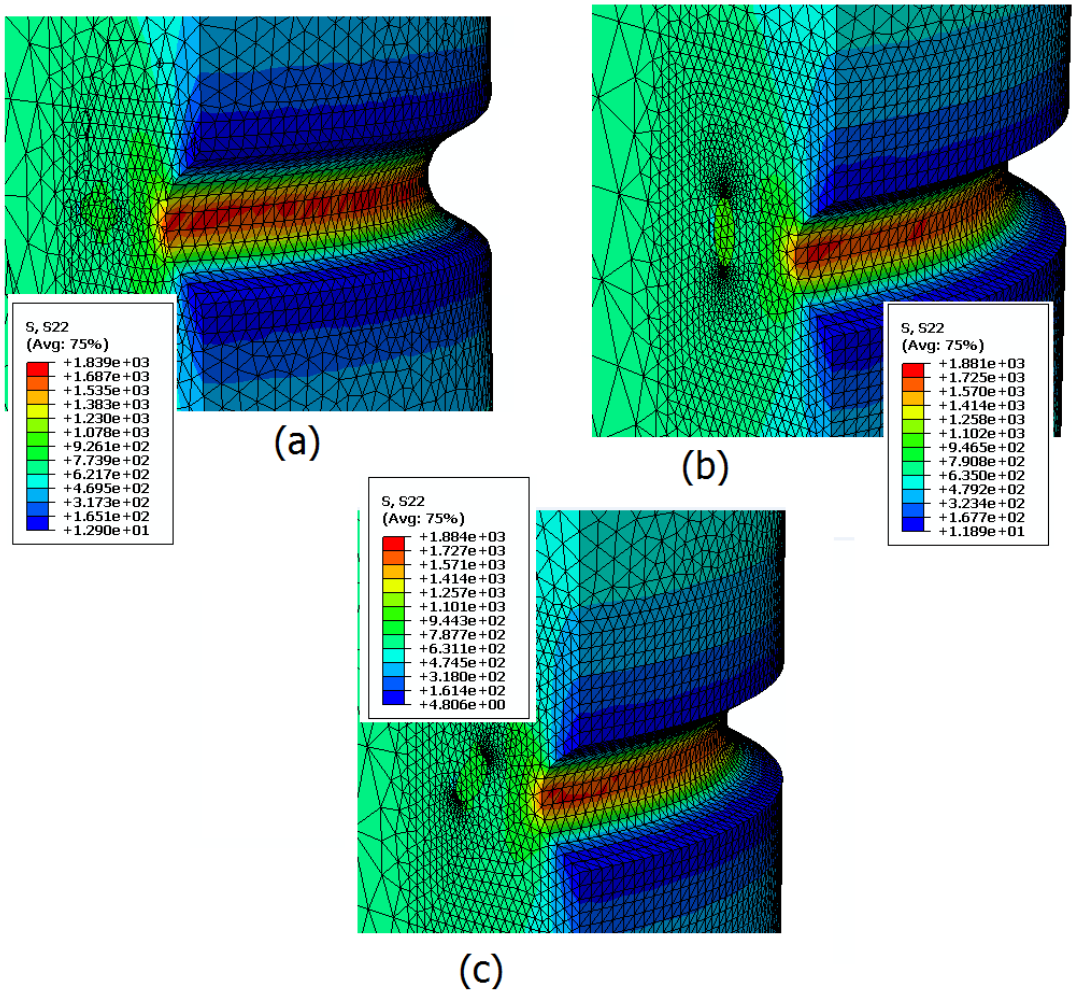

Figure 5.12. Stress distribution for different inclusion orientaton in Nickel base superalloy alloy matrix.

Table 5.6

Maximum stress and associated fatigue notch factor for three different inclusion orientations

Inclusion Orientation	S22 MPa	K_f
Horizontal	1839	2.01
Vertical (90^0)	1881	2.36
Diagonal (45^0)	1884	2.38

A significant change is noted in the maximum stress of the notched nickel base superalloy when the orientation of the inclusion is changed from horizontal to vertical. However, a minimal change is noted when the orientation is changed from vertical to

Diagonal. The changes is also reflected in the associated fatigue notch factor with horizontal orientation of inclusion having the lowest fatigue nitch factor of 2.01 and the Diagonal orientation of grain having the highest fatigue notch factor of 2.38. It can be inferred from this observation that vertical and inclined inclusion are more detrimental to fatigue failure and effort should be made to avoid them in metal forming operations of nickel based superalloy.

CHAPTER 6

CONCLUSION AND RECOMMENDATION FOR FUTURE WORK

6.1 Conclusions

A new probabilistic framework for fatigue notch factor was developed for predicting the microstructure- sensitive fatigue notch factor of aero engine materials such as titanium alloy and nickel base superalloy. The developed model make use of stress distribution result obtain from finite element crystal plasticity simulation of models in Abaqus. A number of phenomena investigated include how the notch radius, presence of inclusion, grain orientation and orientation of inclusion all influence the fatigue notch factor, probability of failure and the notch sensitivity of the material.

The result shows that the probability of failure, fatigue notch factor and notch sensitivity index all increase with increasing notch root radius. Also it is noted that the grain orientation of the material plays an important role in determining or predicting the fatigue strength of the material; the probability of failure varies at the same notch root radius for different grain orientation. Investigation of the effect of load ratio on probability of failure shows that load ratio of 0.1 is more detrimental compared to load ratio of 0.5 for component operating under fatigue loading. Lastly, it is established that vertical and diagonal orientation of inclusion within nickel base superalloy matrix gives higher fatigue notch factor and probability of failure compared to the horizontal inclusion orientation and thus if possible vertical and inclined orientation of inclusion should be avoided during metal forming of nickel base superalloy.

6.2 Recommendations for Future Work

The different areas that can be developed on to improve this research include:

1. The inclusion used in this work is assumed to be elliptical and fully bonded to the matrix. However, in real life inclusions do not have perfect shape and could exhibit different interaction with the matrix. These could be bonded, partially bonded, crack or any other form. Hence the research can be improved by modeling actual inclusion- matrix interaction as observed from a CT scan.
2. Only the presence of one inclusion has been investigated in this work, future work can consider investigating the effect of inclusion cluster on fatigue notch factor and probability of failure of materials.

REFERENCES

[1] Nicholas Theodore, High Cycle Fatigue : A Mechanics of Materials Perspective, Ohio, USA: Elsevier Ltd, 2006.

[2] "National Transportation Safety Board," [Online]. Available: http://www.ntsb.gov/investigations/summary/AAR9006.html. [Accessed 18 July 2013].

[3] Daniel J. Benac, Bryant Lee, "Failure Analysis and Life Assessment of Structural Components and Equipment," *ASM Handbook,* vol. 11, pp. 227 - 242, 2002.

[4] "Planecrashinfo," [Online]. Available: http://planecrashinfo.com/w19890719.htm. [Accessed 18 July 2013].

[5] Haritos G K, Nicholas T, & Lanning D B, "Notch Size Effects in HCF Behavior of Ti-6Al-4V," *Int. J. Fatigue,* vol. 21, pp. 643 - 652, 1999.

[6] Yoichi Yamashita, Yusuke Ueda, Hiroshi Kuroki, & Masaharu Shinozaki, "Fatigue Life Prediction of Small Notched Ti-6Al-4V Specimens Using Critical Distance," *Engineering Fracture Mechanics,* vol. 77, pp. 1439 - 1453, 2010.

[7] S.A. Padula II, A. Shyam, R.O. Ritchie, & W.W. Milligan, "High frequency fatigue crack propagation behavior of a nickel-base turbine disk alloy," *International Journal of Fatigue,* vol. 21, p. 725–731, 1999.

[8] S. Kalpakjian and S.R. Schmid, Manufacturing Processes for Engineering Materials, Pearson Education, 2008.

[9] Tim J Carter, "Common failures in gas turbine blades," *Engineering Failure Analysis,* vol. 12, p. 237–247, 2005.

[10] Shenoy M, Zhang J, & McDowell D L, "Estimating Fatigue Sensitivity to Polycrystalline Ni-base Superalloy Microstructures Using a Computational Approach," *Fatigue and Fracture of Engineering Materials & Structures,* vol. 30, no. 10, pp. 889-904, 2007.

[11] Luai M. Al-Hadhrami, S.M. Shaahid and Ali A. Al-Mubarak, "Jet Impingement Cooling in Gas Turbines for Improving Thermal Efficiency and Power Density," in *Advances in Gas Turbine Technology*, Vols. ISBN 978-953-307-611-9, In Tech, 2011, pp. 191-210.

[12] Melissa Wilcox, Richard Baldwin, Augusto Garcia-Hernandez, & Klaus Brun, "Guidline for Gas Turbine Inlet Air Filtration Systems," *Gas Machinery Research Council,* no. 1, 2010.

[13] Robert Anthony Kupkovits, "THERMOMECHANICAL FATIGUE BEHAVIOR OF THE

DIRECTIONALLY-SOLIDIFIED NICKEL-BASE SUPERALLOY CM247LC," Unpublished doctoral dissertation, Georgia Institute of Technology, 2008.

[14] H J Neuber, "Theory of Stress Concentration for Shear-Strained Prismatical Bodies with Arbitrary Nonlinear Stress-Strain Law.," *J. Appl. Mech.,* vol. 28, no. 4, pp. 544 - 550, 1961.

[15] P Kuhn; H F Hardraht, "An Engineering Method for Estimating the Notch-Size Effect in Fatigue Tests on Steel," in *NACA TN2805Langley Aeronautical Laboratory* , Washington, 1952.

[16] Peterson R E, "Notch Sensitivity," in *Metal Fatigue*, G. Sines and J. Waisman, Eds., New York, McGraw-Hill, 1959, pp. 293-306.

[17] Heywood R B, "Stress Concentration Factors," *Engineering,* vol. 179, p. 146, 1955.

[18] Heywood R E, Design Against Fatigue, London: Chapman & Hall, 1962.

[19] Buch A, "Analytical Approach to Size and Notch -Size Effect in Fatigue of Aircraft Materials Specimens," *Material Science and Engineering,* vol. 15, pp. 75 - 85, 1974.

[20] Buch A, Fatigue Strength Calculation, Switzerland: Trans Tech Publications, 1998.

[21] Siebel, E. and Stieler, M., "Significance of Dissimilar Stress Distributions for Cycling Loading," *VDI - Zeitschrift,* vol. 97, no. 5, pp. 121-126, 1955.

[22] J. C. Ting, V. Frederick and F.V. Lawrence, Jr , "Modeling the Long-Life Fatigue Behavior of a Cast Aluminum Alloy," *Fatigue Fract. Eng. Mater. Struct.,* vol. 16, pp. 631 - 647, 1993.

[23] Yu, M. T., DuQuesnay, D.L. and Tooper, T.H, *Int. J. Fatigue,* vol. 15, p. 109, 1993.

[24] Sheppard S.D, "Field Effects in Fatigue Crack Initiation Long Life Fatigue Strength," in *Failure Prevention and Reliability - 89, ASME*, New York, 1989.

[25] Adib-Ramezani H. and Jeong J., "Advanced Volumetric method for fatigue life prediction using stress gradient effects at notch root," *Computational Material Science ,* vol. 39, pp. 649 - 663, 2007.

[26] Weiju Ren, Theodore Nicholas, "Notch Size Effects on High Cycle Fatigue Limit Stress of Udimet 720," *Material Science and Engineering,* vol. A357, pp. 141-152, 2003.

[27] Owolabi G M; Prasannavenkatesan R; & McDowell DL, "Probabilistic Framework for a Microstructure - Sensitive Fatigue Notch Factor," *International Journal of Fatigue,* vol. 32, pp. 1378 - 1388, 2010.

[28] Gbadebo Owolabi, Benedict Egboiyi, Li Shi and Horace Withworth, "Microstructure-Dependent Fatigue Damage Process Zone and Notch Sensitivity Index," *International Journal of Fracture ,* pp. 159-173, 2011.

[29] Neuber H, Theory of Notch Stresses, Verlag, Berlin: Springer, 1958.

[30] Peterson R. E, Stress Concentration Factors; Charts and relations useful in making strength calculations for machine parts and structural elements, New York, NY: Wiley, 1974.

[31] Weixing Yao, X. Kaiquan, and G. Yi, "On the fatigue notch factor Kf," *Int. J. Fatigue,* vol. 17, no. 4, pp. 245-251, 1995.

[32] Dabayeh A. A, Berube A. J, & Topper T.H, "An Experimental Study of the Effect of a Flaw at a Notch Root on the Fatigue Life of Cast Al 319," *Int. J. Fatigue,* vol. 20, pp. 517 -530, 1998.

[33] Papadopoulos I V and Panoskaltsis V P , "Invariant formulation of a gradient dependent multiaxial high-cycle fatigue criterion," *Engng Fract. Mech.,* vol. 55, pp. 513-528, 1996.

[34] Papadopoulos I V and Panoskaltsis V P , "Gradient dependent multiaxial high - cycle fatigue criterion," in *Fourth International Conference on Biaxial/Multiaxial Fatigue* , France , 1994.

[35] Kristofer Karlen, Marten Olsson, Hamidreza Ahmadi, & Gunnar Harkegard, "On the Effect of Random Defects on the Fatigue Notch Factor at Different Stress Ratios," *Int. J. Fatigue,* vol. 41, pp. 179-187, 2012.

[36] Cheng Chang-Zheng, Recho Naman, Niu Zhong-Rong, & Zhou Huan-Lin, "Effect of Notch Dimension on the Fatigue Life of V-Notched Structure," *Nuclear Engineering and Design,* vol. 241, pp. 3573-3579, 2011.

[37] Benedetti M, Beghini M, & Bertini L, "Experimental Investigation on the Propagation of Fatigue Cracks Emanating from Sharp Notches," *Meccanica,* vol. 4, pp. 201 - 210, 2008.

[38] Teh L S, Love A J, & Brennan F P, "Mode 1 Stress Intensity Factors for Edge Cracks Emanating from 2-DU-Notches Using Composition of SIF Weight Functions," *Int. J. Fatigue,* vol. 28, pp. 355 - 365, 2006.

[39] Kuhn P, Hardraht H F, "An Engineering Method for Estimating the Notch-Size Effect in fatigue Tests on Steel," in *NACA TN2805*, Langley Aeronautical Laboratory Washington, 1952.

[40] Neuber H, "Theory of Stress Concentration in Shear Strained Prismatic Bodies with Arbitrary Non-Linear Stress Law," *Journal of Applied Mechnaics ,* vol. 28, pp. 544-550,

1961.

[41] Weixing Yao, "Stress field intensity approach for predicting fatigue life," *Int. J. Fatigue,* vol. 15, no. 3, pp. 243-245, 1993.

[42] Ting J C, Lawrence F V Jr, "A crack closure model for predicting threshold stress of notches," *Fatigue and Fracture of Engineering Material and Structures ,* vol. 16, no. 1, pp. 93-114, 1993.

[43] Weibull W, "A statistical theory of the strength of materials," *Royal Swed. Inst. Engng Res.,* vol. 151, 1939.

[44] Weibull W, "The phenomenom of rupture in solids," *Proc R Swed Inst Eng Res,* vol. 153, pp. 1-55, 1939.

[45] Bomas H, Linkewitz T, Mayr P, "Application of a weakest-link concept on the fatigue limit of the bearing steel SAE 52100 in a baintic condition.," *Fatigue Fract. Engng Mat. Struct.,* vol. 22, pp. 733-741, 1999.

[46] Hild F and Roux S , "Fatigue initiation in heterogenous brittle materials," *Mechanics Research Communications ,* vol. 18, pp. 409-414, 1991.

[47] Todinov M, "Probability distribution of fatigue life controlled by defects," *Computers and Structures ,* vol. 79, pp. 313-318, 2001.

[48] Todinov M, "Equations and a fast algorithm for determining the probability of failure initiated by flaws," *International Journal of Solids and Structures ,* vol. 43, pp. 5182-5195, 2006.

[49] Wormsen A, Sjodin B, Harkegard G, and Fjeldstad A, "Non-Local Stress Approach for fatigue Assessment Based on Weakest-Link Theory and Statistics of Extremes," *Fatigue & Fracture of Engineering Materials & Structures ,* vol. 30, pp. 1214-1227, 2007.

[50] Besel M, Bruckner-Foit A, Motoyashiki Y, and Schafer O, "Lifetime distribution of notched components containing void defects," *Archive of Applied Mechanics ,* vol. 76, pp. 645 - 653, 2006.

[51] Doudard C, Calloch S, Cugy P, Galtier A, and Hild F, "A probabilistic two-scale model for high fatigue life predicitons," *Fatigue & Fracture of Engineering Materials & Structures ,* vol. 28, pp. 279-288, 2005.

[52] Bazant Z P, "Size effect on structural strength : a review," *Appl Mech,* vol. 69, pp. 703-725, 1999.

[53] Freudenthal A M, "Statistical approach to brittle materials In: Liebowitz H, editor," in *Fracture, Vol 2*, New York, Academic Press, 1968, pp. 591-619.

[54] Lemaitre J, and Doghri I, "Damage 90: A post processor for crack initiation," *Comput. Methods Appl. Mech. Engng.,* vol. 115, pp. 197-232, 1994.

[55] Lemaitre J, Sermage J P, and Desmorat R, "A two scale damage concept applied to fatigue," *Int. J. Fract.,* vol. 97, pp. 67-81, 1999.

[56] Anders Wormsen and Gunner Harkegard, "A statistical investigation of fatigue behaviour according to Weibull's weakest-link theory," in *European Conference on Fracture: Advance Fracture Mechanics for Life and Safety*, Stockholm Sweden Aug 11-13, 2004.

[57] Wormsen A, Harkegard G, and Huth H J , "Probabilistic fatigue assessment of a hydro-turbine blade model.," in *The International Fatigue Congress*, Atlanta USA, 2006.

[58] De Jesus A M, Pinto H, Fernandez-Canteli A, Castillo E, and Correia J A, "Fatigue assessment of a riveted shear splice based on a probabilistic model," *International Journal of Fatigue ,* vol. 32, pp. 453-462, 2010.

[59] Iman B, "Fatigue analysis of riveted railway bridges. Ph.D Thesis, School of Engineering,," University of Surrey, UK, 2006.

[60] Neuber H, Theory of Notch Stresses: Principles for Exact Stress Calculation, Ann Abor, MI: J.W. Edwards, 1946.

[61] Molski K, and Glinka G, "A method of elastic-plastic stress and strain calculation at a notch root," *Materials Science and Engineering,* vol. 50, no. 1, pp. 93-100, 1981.

[62] Ramberg W, and Osgood W, "Description of stress-strain curves by thress paramaters," National Advisory Committee for Aeronautics , Washington D.C , 1943.

[63] Crossland B, "Effects of large hydrostatic pressure on torsional fatigue strength of an alloy steel," in *Proceedings of the international conference on fatigue of metals* , 1956.

[64] Hild F, Marquis D, "A statistical approach to the rupture of brittle materials," *Eur J Mech A/Solids,* vol. 11, pp. 753-765, 1992.

[65] Chantier I, Bobet V, Billardon R, Hild F, "A probabilistic approach to predict the very high-cycle fatigue behaviour of spheroidal graphite cast iron structures," *Fatigue Fract Eng Mater Struct,* vol. 23, pp. 173- 180, 1999.

[66] Hyzak J, and Bernstein I, "Effect of defects on the fatigue crack initiation process in two

P/M superalloys -1. Fatigue Origins," *Metallurgical transactions. A, Physical metallurgy and materials science,* vol. 13 A, no. 1, pp. 33-43, 1982.

[67] Hyzak J and Bernstein I, "Effect of defects on the fatigue crack initiation process in two P/M superalloys- 2. Surface-subsurface transition," *Metallurgical transactions. A, Physical metallurgy and materials science,* vol. 13 A , no. 1, pp. 45-52, 1982.

[68] De Bussac A, "Prediction of the competition between surface and internal fatigue crack initiation in PM alloys," *Fatigue and Fracture of Engineering Materials and Structures ,* vol. 17, no. 11, pp. 1319-1325, 1994.

[69] Deyber S, Alexandre F, Vaissaud J, and Pineau A, "Probabilistic life of DA718 for aircraft engine disks," in *Sixth International Symposium on Superalloys 718, 625, 706 and Derivatives* , Warrendale, 2006.

[70] Tomkins B, "Fatigue crack propagation- an analysis," *Philosophical Magazine,* vol. 18, pp. 1041-1066, 1968.

[71] Pineau A, "Superalloy discs durability and damage tolerance in relation to inclusions," in *Proceedings of a Conference on High Temperature Materials for Power Engineering* , 1990.

[72] Kallmeyer A R, Krgo A, and Kurath P, "Evaluation of Multiaxial Fatigue Life Prediciton Methodologies for Ti-6Al-4V," *Journal of Engineering Materials and Technology, ASME ,* vol. 124, no. 2, pp. 229-237, 2002.

[73] Doudard C, Hild F, and Calloch S, "A probabilistic model for multiaxial high cycle fatigue," *Fatigue & Fracture of Engineering Materials & Structures ,* vol. 30, pp. 107-114, 2007.

[74] Gulino, R. and Phoenix, S. L., "Weibull strength statistics for graphite fibres measured from the break progression in a model graphite/glass/epoxy microcomposite," *Journal of Material Science ,* vol. 26, p. 3107–3118, 1991.

[75] Denoual C and Hild F, "Dynamic fragmentation of brittle solids: A multi-scale model," *Eur. J. Mech. A/Solids,* vol. 21, p. 105–120, 2002.

[76] Flaceliere L and Morel F, "Probabilistic approach in high-cycle multiaxial fatigue: volume and surface effects," *Fatigue & Fracture of Engineering Materials and Structures,* vol. 27, pp. 1123-1135, 2004.

[77] Papadopoulos I V, "A high-cycle fatigue criterion applied in biaxial and triaxial out -of - phase stress conditions," *Fatigue Fract. Engng Mater. Struct.,* vol. 18, pp. 79-91, 1995.

[78] Thomas Delahay, Thierry Palin-Luc, "Estimation of the fatigue strength distribution in high-

cycle multiaxial fatigue taking into account the stress-strain gradient effect," *International Journal of Fatigue,* vol. 28, pp. 474-484, 2006.

[79] Banvillet A, Palin-Luc T, Lasserre S, "A volumetric energy based high cycle multiaxial fatigue criterion," *Int. J Fatigue,* vol. 26, no. 8, pp. 755 -769, 2003.

[80] Banvillet A, Palin-Luc T, Lasserre S, Vittori J F, "Energy based high cycle multiaxial fatigue criterion depending on stress-strain distribution.," in *Blom AF, editor. Fatigue 2002: eighth international fatigue congress, vol. 1.* , Stockholm: EMAS p. 283-290, 2002.

[81] Betteridge W and Shaw S. W. S, "Development of Superalloys," *Material Science and Technology,* vol. 3, pp. 682-694, 1987.

[82] Sims C.T., Stoloff N. S. and Hagels W.C., Superalloys II: High-temperature materials for aerospace and industrial power, New York: John Wiley and Sons , 1987.

[83] Green K.A., Pollock T.M., and Harada H, "Superalloys 2004, Proceedings of the Tenth International Symposium on Superalloys," in *The minerals, metals and materials society*, Warrendale PA, 2004.

[84] Choudhury A., Vacuum Metallurgy, Materials Park, OH: ASM International, 1990.

[85] Maurer G.E., "Primary and secondary melt processing - superalloys," in *Superalloys, supercomposites and superceramics*, San Diego, Academic Press, 1989, pp. 49-97.

[86] Reed R.C., The Superalloys; Fundamentals and Applications., Cambridge UK: University Press, 2006.

[87] De Bussac A. and Lautridou J., "A probabilistic model for prediction of LCF surface crack initiation in PM alloys," *Fatigue & Fracture of Engineering Materials & Structures,* vol. 16, no. 8, pp. 861-874, 1993.

[88] Benz M.G., "Preparation of clean superalloys," in *Impurities in Engineering Materials: Impact, Reliability and Control*, New York, Marcel Dekker Inc, 1999, pp. 31-47.

[89] Meyers M and Chawla K, Mechanical Behavior of Materials, Upper Saddle River, NJ: Prentice Hall, 1999.

[90] Gypen L A and Deruyttere A, "Multi-component solid solution hardening," *Journal of Materials Science ,* vol. 12, no. 5, pp. 1028-1033, 1977.

[91] R L Fleischer, "Substitutional solution hardening," *Acta Metallurgical ,* vol. 11, no. 3, pp. 203-209, 1963.

[92] Mott N F and Nabarro F R N, "Dislocation theory and transient creep: in 1947 Bristol Conference on Strength of Solids," in *Physical Society of London*, Bristol, 1948.

[93] Friedel J, Dislocations, Oxford, England: Pergamon Press, 1964.

[94] U F Kocks, *Metall Trans A,* vol. 16A, pp. 2109 - 2130, 1985.

[95] Huther H and Reppich B, "Interaction of Dislocations with Coherent, Stress-Free Ordered Particles," *Z. Metallkd,* vol. 19, pp. 628-634, 1978.

[96] Ducrocq C, Lasalmonie A, and Honnorat Y, "N 18, A New Damage Tolerant PM Superalloy for High Temperature Turbine Discs," *The Metallurgical Society Inc,* 1988.

[97] Caless R H and Paulonis D F , "Development of Gatorized Merl 76 for Gas Turbine Disk Applications," *The Metallurgical Society,* pp. 101 - 110, 1988.

[98] Hattori H, Takekawa M, Furrer D, and Noel R J , "Evaluation of PM U720 for Gas Turbine Engine Disk Application," *The Minerals, Metals & Materials Society,* pp. 705-711, 1996.

[99] Howson T E, Couts W H Jr, and Coyne J E, "High Temperature Deformation Behavior of PM Rene 95," *The Minerals, Metals & Materials Society 1996,* pp. 277-286, 1984.

[100] Kozar R.W., Suzuki A., Milligan W.W., Schirra J.J., Savage M.F., and Pallock T.M.,, "Strengthening mechanisms in polycrystalline multimodal nickel-base superalloys," *Metallurgical and Materials Transactions ,* vol. 40A, pp. 1588-1603, 2009.

[101] Westbrook J, Superalloys (Ni-base) and Dislocations- An Introduction, NY: Brookline Technologies , 1996.

[102] Shenoy M M , "Constitutive modeling and life prediction in Ni-base superalloys. Ph.D Thesis," Georgia Institute of Technology, 2006.

[103] Lall C, Chin S and Pope D P, "The orientation and temperature dependence of the yield stress of Ni3 (Al, Nb) single crystals," *Metallurgical Transactions A,* vol. 10, no. 9, pp. 1323-1332, 1979.

[104] Paidar V, Pope D, and Vitek V, "A theory of anomalous yield behavior in LI2 ordered alloys.," *Acta Metallurgica,* vol. 32, no. 3, pp. 435 - 448, 1984.

[105] Umakoshi Y, Pope D, Vitek V, "The asymmetry of the flow stress in Ni3 (Al, Ta) single crystals," *Acta Metallurgica,* vol. 21, no. 4, pp. 415 - 425, 1984.

[106] Jiao F, Bettge D, Osterle W and Ziebs J, "Tension-Compression asymmetry of the <001>

single crystal nickel base superalloy SC16 under cyclic loading at elevated temperatures," *Acta Materialia,* vol. 44, no. 10, pp. 3933-3942, 1996.

[107] Osterle W, Bettge D, Fedelich B, and Klingelhoffer H, "Modelling the orientation and direction dependence of the critical resolved shear stress of Nickel base superalloy single crystal," *Acta Materialia ,* vol. 48, pp. 689 - 700, 2000.

[108] Vitek V, Pope D and Bassani J, Superalloys (Ni base) and dislocations - An Introduction. Dislocations in Solids, 10: 135-186, 1996.

[109] Bilby B, Bullough R and Smith E , "Continous distributions of dislocations: A new application of the methods of non-riemannian geometry.," *Proc. Royal Soiety A231,* pp. 263 - 273, 1955.

[110] Teodosiu C, "A dynamic theory of dislocations and its applications to the theory of the elastic -plastic in fundamental aspects of dislocation theory," in *Conference proceedings, National Bureau of Standards*, 1970.

[111] Rice J, "Inelastic constitutive relations for solids: an internal variable theory and its application to metal plasticity.," *Journal of the mechanics and physics of solids ,* vol. 19, pp. 433-455, 1971.

[112] Hill R and Rice J, "Constitutive analysis of elastoplastic crystals at arbitrary strain.," *Journal of the Mechanics and Physics of Solids ,* vol. 20, pp. 401 - 413 , 1972.

[113] Mandel J, "Thermodynamics and plasticity," in *Proceedings of the international symposium on foundations of continuum thermodynamics* , Macmillan London , 1974.

[114] Asaro A, "Crystal Plasticity," *ASME J, Appl. Mech.,* vol. 50, pp. 921-934, 1983a.

[115] Asaro A , "Micromechanics of crystals and polycrystals," *Adv. Appl. Mech.,* vol. 23, pp. 1-115, 1983b.

[116] Conrad H, "Thermally activated deformation of metals," *J. Metals ,* vol. 16, pp. 582-588, 1964.

[117] Kocks U, Argon A and Ashby M, Thermodynamics and kinetics of slip. Progress in Material Science, London: Pergamon Press, 1975.

[118] Argon A, "Mechanical properties of single phase crystalline media: deformation at low temperatures.," *Pyhsical Metallurgy, Elsevier,* p. Amsterdam, 1995.

[119] Lee H, "Elastic plastic deformations at finite strains," *Journal of applied mechanics ,* vol. 36,

pp. 1-6, 1969.

[120] Orowan E, "Problems of plastic gliding," *Phil. Trans. R. Soc.,* vol. A52, pp. 8 -22, 1940.

[121] Ferney V, Hautefeuille M and Clavel M, "Multiaxial cyclic behavior in two precipitates strengthened alloys: Influence of the loading path and microstructure.," *Memoires et Etudes Scientifiques de la Revue de Metallurgie,* vol. 88, pp. 441-451, 1991.

[122] Sun Y. and Hazzleedine P, "Geometry of dislocation glide in L12- phase : TEM observations," *Dislocations in Solids ,* vol. 10, pp. 27-68, 1996.

[123] Bettge D and Osterle W, "Cube Slip in near - [111] oriented specimens of a single-crystal nickel-base superalloy.," *Scripta Materialia ,* vol. 40, no. 4, pp. 389-395, 1999.

[124] Heilmaier M, Leetz U and Reppich B, "Order strengthening in the cast nickel-based superalloy IN100 at room temperature," *Materials Science and Engineering ,* Vols. A319-321, pp. 375-378, 2001.

[125] Reppich B, Schepp P and Wehner G, "Some new aspects concerning particle hardening mechanisms in gamma prime precipitating nickel -base alloys; ii. experiments," *Acta Metallurgica ,* vol. 30, no. 1, pp. 95-104, 1982.

[126] Qin Q and Bassani J. L , "Non-schmid yield behavior in single crystals," *Journal of mechanics and physics of solids ,* vol. 40, pp. 813-833, 1992.

[127] Qin Q and Bassani J L , "Non-associated plastic flow in single crystals," *Journal of the mechanics and physics of solids ,* vol. 40, pp. 835-862, 1992.

[128] Shenoy M M, Gordon A P, Mcdowell D L and Neu R W , "Thermomechanical fatigue behavior of a directionally solidified Ni-base superallloy," *Journal of engineering materials and technology, ASME,* vol. 127, no. 3, pp. 325 - 336, 2005.

[129] Feaugas X and Haddou H, "Grain-size effects on tensile behavior of nickel and ANSI 316L stainless steel.," *Metallurgical and materials transactions A,* vol. 34, pp. 2329-2340, 2003.

[130] Przybyla C P, "Microstructure - Sensitive Extreme Value Probabilities of Fatigue in Advance Engineering Alloys PhD Thesis," Georgia Institute of Technology , 2010.

[131] Naka S, Lasalmonie A, Costa P, Kubin L P , "The low-temperature plastic deformation of alpha- titanium and the core structure of a-type screw dislocations," *Phil. Mag.,* vol. 57, pp. 717-740, 1988.

[132] Mayeur J. R and McDowell D.L, "A three-dimensional crystal plasticity model of duplex Ti-

6Al-4V.," *Int.Journal of Plasticity,* vol. 23, pp. 1457-1485, 2007.

[133] Zhang M , Zhang J and McDowell D.L, "Microstructure – based crystal plasticity modeling of cyclic deformation of Ti-6Al-4V," *Int. Journal of Plasticity,* vol. 23, pp. 1328-1348, 2007.

[134] Musinski W D, "Novel methods for microstructure - sensitive probabilistic fatigue notch factor master thesis," Georgia Institute of Technology, Atlanta , 2010.

[135] Przybyla C.P and McDowell D L, "Microstructure - sensitive extreme value probabilities for high cycle fatigue of Ni-base superalloy IN 100," *International Journal of Plasticity ,* vol. 26, pp. 372 - 394, 2010.

[136] Gayda, J. and Miner, R. V, "Fatigue crack initiation and propagation in several nickel-base superalloys at 650oc," *International Journal of Fatigue,* vol. 5, no. 3, pp. 135-143, 1983.

[137] Bridier F., McDowell D.L., Villechaise P., Mendez Jose., "Crystal plasticity modeling of slip activity in Ti-6Al-4V under high cycle fatigue loading.," *Int. J. Plasticity,* vol. 25, pp. 1066-1082, 2009.

[138] Simmons G and Wang H, Single crystal elastic constants and calculated aggregated properties: A Handbook, Cambridge M.A : MIT Press, 1971.

[139] Larson F and Zarkades A, "Properties of textured titanium alloys.," Batelle memorial institute , Columbus OH, 1974.

[140] Rajiv A. Naik, David B. Lanning, Theodore Nicholas, Alan R. Kallmeyer, "A critical plane gradient approach for the prediction of notched HCF life.," *Int. J. Fatigue,* vol. 27, pp. 481-492, 2005.

[141] Ostash O. P, Panasyuk V.V, and Kosty E.M , "A phenomenological model of fatigue macrocrack initiation near stress concentrations," *Fatigue and Fracture of Engineering Materials & Structures ,* vol. 22, no. 2, pp. 161-172, 1999.

[142] Ostash O.P, and Panasyuk V.V, "Fatigue Process Zone at Notches," *International Journal of Fatigue ,* vol. 23, pp. 627-636, 2001.

[143] Ranganathan R.M, Gu R.J, and Lee Y.L, "An Improved Automated Finite Element Analysis for Fatigue Life Predictions of Notched Components," *International Journal of Materials Product and Technology ,* vol. 21, pp. 539 - 554, 2004.

[144] Owolabi G. M, Shi L, and Whitworth H, "A Micromechanics - based Fatigue Damage Process Zone," *Procedia Engineering ,* vol. 10, pp. 496-505, 2011.

[145] Okeyoyin O.A and Owolabi G.M , "Application of Weakest Link Probabilistic Framework for Fatigue Notch Factor to Turbine Engine Materials," *World Journal of Mechanics,* vol. 5, pp. 237-244, 2013.

[146] Cohen A C and Whitten B J, Parameter Estimation in Reliability and Life Span Models, New York: Marcel Dekker, 1988.

[147] Chaboche J.L, "Constitutive equations for cyclic plasticity and cyclic viscoplasticity," *International Journal of Plasticity ,* vol. 5, no. 3, pp. 247-302, 1989.

[148] Morrissey R, Goh C H and McDowell D L, "Microstructure-scale modeling of HCF deformation," *Mech. Mater,* vol. 35, pp. 295-311, 2005.

[149] Kumar R S, Wang A J and McDowell D L, "Effects of microstructure variability on intrinsic fatigue resistance of nickel-base superalloys - a computational micromechanics approach," *Int Journal of Fracture ,* vol. 137, pp. 173-210 , 2006.

[150] McGinty R D , "Multiscale representation of polycrystaline inelasticity PhD Thesis," Georgia Institute of Technolgy , Atlanta USA , 2001.